MIT/WHOI 2005-18

Massachusetts Institute of Technology
Woods Hole Oceanographic Institution

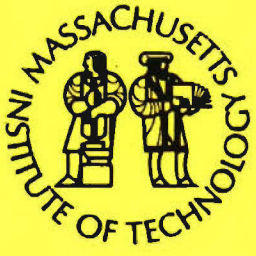

Joint Program in Oceanography/ Applied Ocean Science and Engineering

DOCTORAL DISSERTATION

Abrupt Climate Change in the Atlantic Ocean During the Last 20,000 Years: Insights from Multi-Element Analyses of Benthic and Planktic Foraminifera and a Coupled OA-GCM

by

Rosemarie Evangeline Came

September 2005

MIT/WHOI

2005-18

Abrupt Climate Change in the Atlantic Ocean During the Last 20,000 Years: Insights from Multi-Element Analyses of Benthic and Planktic Foraminifera and a Coupled OA-GCM

by

Rosemarie Evangeline Came

Massachusetts Institute of Technology
Cambridge, Massachusetts 02139

and

Woods Hole Oceanographic Institution
Woods Hole, Massachusetts 02543

September 2005

DOCTORAL DISSERTATION

Funding was provided by a John Lyons Fellowship and a WHOI Ocean and Climate Change Institute Fellowship. Analyses were funded by the Ocean and Climate Change Institute and the National Science Foundation under grants OCE98-86748, OCE02-20776, OCE96-33499, ATM05-01391, and OCE04-02565.

This thesis should be cited as: Rosemarie Evangeline Came, 2005. Abrupt Climate Change in the Atlantic Ocean During the Last 20,000 Years: Insights from Multi-Element Analyses of Benthic and Planktic Foraminifera and a Coupled OA-GCM. Ph.D. Thesis. MIT/WHOI, 2005-18.

Approved for publication; distribution unlimited.

Approved for Distribution:

Susan E. Humphris, Chair
Department of Geology and Geophysics

Paola Malanotte-Rizzoli
MIT Director of Joint Program

John W. Farrington
WHOI Dean of Graduate Studies

ABRUPT CLIMATE CHANGE IN THE ATLANTIC OCEAN DURING THE LAST 20,000 YEARS: INSIGHTS FROM MULTI-ELEMENT ANALYSES OF BENTHIC AND PLANKTIC FORAMINIFERA AND A COUPLED OA-GCM

By

Rosemarie Evangeline Came

B.S., Boston College, 1994

M.A., Boston College, 2002

Submitted in partial fulfillment of the requirements for the degree of

Doctor of Philosophy

at the

MASSACHUSETTS INSTITUTE OF TECHNOLOGY

and the

WOODS HOLE OCEANOGRAPHIC INSTITUTION

September, 2005

Signature of Author 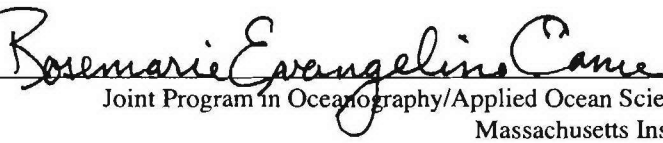

Joint Program in Oceanography/Applied Ocean Science and Engineering
Massachusetts Institute of Technology
and Woods Hole Oceanographic Institution
September 2005

Certified by 

Dr. Delia W. Oppo
Thesis Supervisor

Accepted by 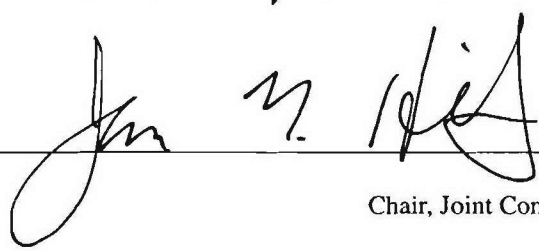

Dr. J. Gregory Hirth
Chair, Joint Committee for Marine Geology and Geophysics
Woods Hole Oceanographic Institution

Abstract (Short Version)

Minor and trace element records from planktic and benthic foraminifera from Atlantic sediment cores, as well as output from a coupled OA-GCM, were used to investigate the magnitude and distribution of the oceanic response to abrupt climate events of the past 20,000 years. The study addressed three major questions: 1) What is the magnitude of high-latitude sea surface temperature and salinity variability during abrupt climate events? 2) Does intermediate depth ventilation change in conjunction with high-latitude climate variability? 3) Are the paleoclimate data consistent with the response of a coupled OA-GCM to a freshwater perturbation? To address these questions, analytical methods were implemented for the simultaneous measurement of Mg/Ca, Zn/Ca, Cd/Ca, Mn/Ca and Al/Ca in foraminiferal samples using inductively-coupled plasma mass spectrometry.

Paired records of planktic foraminiferal $\delta^{18}O$ and Mg/Ca from the subpolar North Atlantic reveal trends of increasing temperatures (~3°C) and salinities over the course of the Holocene. The records provide the first evidence of open-ocean cooling (nearly 2°C) and freshening during the 8.2 kyr event, and suggest similar conditions at 9.3 ka.

Benthic foraminiferal Cd/Ca results from an intermediate depth, western South Atlantic core (1,268 m) are consistent with reduced export into the South Atlantic of North Atlantic Intermediate Water during the Younger Dryas.

Paired records of benthic foraminiferal Mg/Ca and $\delta^{18}O$ from two intermediate depth low latitude western Atlantic sites - one from the Florida Current (751 m) and one from the Little Bahama Bank (1,057 m) - provide insights into the spatial distribution of intermediate depth temperature and salinity variability during the Younger Dryas. The intermediate depth paleoceanographic temperature and salinity data are consistent with the results of a GFDL R30 freshwater forced model simulation, suggesting that freshwater forcing is a possible driver or amplifier for Bølling-Allerød to Younger Dryas climate variability.

Benthic foraminiferal Cd/Ca results from an intermediate depth Florida Current core (751 m) are consistent with a decrease in the northward penetration of southern source waters within the return flow of the Atlantic meridional overturning circulation (MOC) and an increase in the influence of intermediate depth northern source waters during the Younger Dryas.

Abstract (Full Version)

Minor and trace element records of planktic and benthic foraminifera from Atlantic sediment cores, as well as output from a coupled OAGCM, were used to investigate the magnitude and distribution of the oceanic response to abrupt climate events of the past 20 kyr. The study addressed three major questions: 1) What is the magnitude of high-latitude sea surface temperature and salinity variability during abrupt climate events? 2) Does intermediate depth ventilation change in conjunction with high-latitude climate variability? 3) Are the paleoclimate data consistent with the response of a coupled OAGCM to a freshwater perturbation? To address these questions, analytical methods were implemented for the simultaneous measurement of Mg/Ca, Zn/Ca, Cd/Ca, Mn/Ca and Al/Ca in foraminiferal samples using inductively-coupled plasma mass spectrometry.

Paired records of planktic foraminiferal $\delta^{18}O$ and Mg/Ca from the subpolar North Atlantic reveal trends of increasing temperatures (~3°C) and salinities over the course of the Holocene, which were punctuated by abrupt events. The variability does not appear to be periodic, but tends to recur within a broad millennial band. The records provide the first evidence of open-ocean cooling (nearly 2°C) and freshening during the 8.2 kyr event, and suggest similar conditions at 9.3 ka. However, the two largest temperature oscillations (~2°C) occurred during the last 4,000 years, suggesting a recent increase in temperature variability relative to the mid-Holocene.

Benthic foraminiferal Cd/Ca from an intermediate depth, western South Atlantic core provides insights into changes in the southward penetration of North Atlantic Intermediate Water (NAIW). Cd seawater estimates (Cd_w) for the last glacial are consistent with the production of NAIW and its export into the South Atlantic. At ~14.5 ka, the NAIW contribution to the South Atlantic began to decrease, marking a transition from a glacial subsurface geometry to a Younger Dryas geometry, which occurred concurrently with the onset of the Bølling-Allerød to Younger Dryas cooling. High Cd_w in both the deep North Atlantic and the intermediate South Atlantic imply reduced export of deep and intermediate water during the Younger Dryas, and a major decrease in northward heat transport. Modern subsurface geometry was established at ~9 ka, concurrently with the establishment of Holocene warmth in the North Atlantic region, further supporting a close linkage between subsurface circulation and North Atlantic climate.

Paired benthic foraminiferal Mg/Ca and $\delta^{18}O$ data from two intermediate depth low latitude western Atlantic sites - one from the Florida Current and one from the Little Bahama Bank – provide insights into the spatial distribution of intermediate depth temperature and salinity variability during the Younger Dryas. The Florida site lies within the deeper portion of the Florida Current; the Little Bahama Bank site lies within the deeper, unventilated portion of the North Atlantic subtropical gyre. During the Younger Dryas, temperatures increased at the Florida Current site and temperatures decreased at the Little Bahama Bank site. The temperature increase within the Florida Current is consistent with the reduced northward heat transport associated with a reduction in the Atlantic meridional overturning

circulation (MOC); the temperature decrease at Little Bahama Bank is consistent with a cooling of high latitude surface waters.

To test the possibility that a freshening of the surface North Atlantic caused the terrestrial and oceanographic changes during the Younger Dryas, the GFDL R30 coupled ocean-atmosphere general circulation model was forced using a North Atlantic freshwater perturbation of 0.1 Sv for a period of 100 years. The freshwater flux causes an overall reduction in the Atlantic overturning from 25 Sv to 13 Sv. However, at ~1,100 meters water depth, ventilation increases, causing decreases in both temperature and salinity throughout much of the intermediate depth North Atlantic. In the open North Atlantic, intermediate depth temperatures decrease by approximately 1°C; at the eastern side, intermediate depth temperatures decrease by less than 0.4°C. Intermediate depth temperatures at the western boundary, however, increase due to a reduction in northward heat transport, and also due to a shift in the location of the Intertropical Convergence Zone, which causes a reduction in surface salinity and a decrease in the upwelling of colder, deeper waters.

Benthic foraminiferal Cd/Ca from an intermediate depth Florida Current core documents the history of the northward penetration of southern source waters within the return flow of the Atlantic meridional overturning circulation (MOC). Cd seawater estimates (Cd_w) for the last glacial are consistent with the reduced influence of southern source waters at this location relative to the present. At ~18.5 ka, the southern source contribution to the Florida Current began to increase significantly, marking the onset of a transition from a glacial circulation pattern to a deglacial pattern, which lasted from ~17 ka to ~14 ka. At ~12.5 ka, following the onset of the Younger Dryas cooling in the North Atlantic and the reduction in North Atlantic Deep Water (NADW) production, the influence of southern source waters within the Florida Current decreased abruptly. A renewed influence of southern source waters occurred at ~9 ka, concurrent with the establishment of Holocene warmth in the North Atlantic region.

for my Parents and Grandparents

Acknowledgements

I'm fortunate to have an amazing group of family, friends and colleagues who have helped me through the last six years.

I owe a particular debt of gratitude to Delia Oppo. Delia has been an excellent advisor, mentor and role model. She's a generous person and scientist, and I'm grateful that she has shared her knowledge, and has encouraged those around her to do the same.

I'd like to thank my committee for their valuable input over the years, especially: Ed Boyle, for offering many excellent comments and suggestions; Bill Curry, for providing unlimited access to his sediment core collection; Lloyd Keigwin, for treating me like the trace metal expert; and Jerry McManus, for never closing his office door. I'd like to thank Sarah Das, the Chair of my committee, for cheerfully agreeing to read my thesis at the very last minute.

In addition to my committee, I've had several "advisors" outside of WHOI, each of whom has helped me without official recognition. Jean Lynch-Stieglitz of Georgia Tech provided me with access to her unpublished data. Ron Stouffer of GFDL and Tony Broccoli of Rutgers introduced me to the seemingly infinite world of model output. Yair Rosenthal of Rutgers and Tom Marchitto of UC Boulder patiently responded to my endless barrage of questions about ICP-MS methods and trace/minor element protocols. The generosity of each of these individuals is an inspiration to me.

I would like to acknowledge the tremendous support system here at WHOI. Simon Thorrold, Dave Schneider, Lary Ball, Scot Birdwhistell and Susan Brown-Leger all helped tremendously with method development and implementation. Dan McCorkle and Ellen Roosen helped with calibration work. My four WHOI "moms" - Luping, Marti, Rindy, and Rose - helped me with their words of encouragement and with a willingness to come to my rescue at a moment's notice (with things like a laptop, or a balance, or an extra pair of hands).

A significant part of a graduate education involves scientific discussions with soon-to-be colleagues. I look forward to a career that will involve continued interaction with Matt, Mea, Dave, Pete, Nathalie and Nick.

I'm grateful for the opportunity to be part of the MIT/WHOI Joint Program. I'd like to thank the folks in the Education Office - Julia Westwater, Marsha Gomes, John Farrington, and Judy McDowell - for their unwavering commitment to the Program.

And I'd like to thank the students in the Joint Program for providing a stimulating and challenging graduate school experience, in particular, my first-year house mates - Mea, Emilie, Margaret, Heidi, Rhea and Tracy.

And could I have survived in Falmouth without Julie and Mike, Julie and Brian, Kevin and Cindy, and Sara and Peter? Or without Toshi, the sushi chef at Misaki, who made my culinary life on Cape Cod tolerable?

I owe many thanks to Andrew, who has put up with me throughout this experience. And I'd like to thank my family - mom, dad, William and Peter. They taught me that true success has nothing to do with professional success, and everything to do with the way we treat the people around us.

This work was funded by a John Lyons Fellowship and a WHOI Ocean and Climate Change Institute Fellowship. Analyses were funded by the Ocean and Climate Change Institute and the following grants from the National Science Foundation: OCE98-86748, OCE02-20776, OCE96-33499, ATM05-01391, and OCE04-02565.

Contents

Figures

Figures (cont.)

Chapter 1. Introduction

Background

Millennial scale fluctuations in North Atlantic climate have been observed in many paleoceanographic and terrestrial climate proxies. Greenland ice cores, in particular, provide evidence of large amplitude, very rapid climate change during the last glacial, and also during the last deglaciation [*Grootes et al.*, 1993]. The large amplitude changes of the last glacial have received a great deal of attention within the paleoceanographic community, and until just recently, the smaller amplitude variability of the Holocene Epoch was largely ignored. However, in light of the increasing awareness within society of the potential for anthropogenic climate impact, it is critical that the scientific community develop a more thorough picture of the forcing mechanisms and climatic responses that are possible on millennial timescales, particularly during interglacial conditions, like today.

Recent paleoceanographic studies [*Bianchi and McCave*, 1999; *Bond et al.*, 1997; *Keigwin*, 1996; *O'Brien et al.*, 1995] suggest that considerable changes may have occurred in North Atlantic climate over the course of the current interglacial. For example, measurements of sea salt and terrestrial dust trapped in Greenland snow suggest significant fluctuations in atmospheric circulation over Summit Greenland [*O'Brien et al.*, 1995]; ice-rafted debris in North Atlantic sediments provide evidence of large ice-rafting events [*Bond et al.*, 1997]; and sedimentary sortable silt suggests changes in deep oceanic current speeds [*Bianchi and McCave*, 1999]. Taken together, these discoveries suggest significant millennial scale variability in the ocean-atmosphere system during the Holocene, yet the causes and potential global impacts of these events are largely unknown.

It has been suggested for some time that a large meltwater perturbation in the high latitude North Atlantic could disrupt the Atlantic meridional overturning circulation (MOC), and cause millennial scale variability in North Atlantic climate [*Broecker et al.*, 1985]. Numerical simulations have shown that even a small freshwater perturbation could cause convective instabilities that weaken or even shut down the production of deep water in the North Atlantic [*Manabe and Stouffer*, 1988, 1995; *Rahmstorf*, 1994]. A reduction in overturning could have significant implications in the northern hemisphere due to the reduction in northward heat transport via the surface return flow of the MOC. Furthermore, such a reduction may have global implications due to changes in global heat distributions and sea surface temperature gradients.

Benthic and planktic foraminiferal tests from oceanic sediment cores provide a unique opportunity to document changes in ocean properties over the course of time. Foraminiferal chemistry provides evidence of changes in sea surface and subsurface temperature, salinity and water mass origin. This evidence can then be used to make inferences about climatic forcing mechanisms and the possible amplification and propagation of climate signals throughout the ocean-atmosphere system.

Coupled ocean-atmosphere climate models can be powerful tools for enhancing our understanding of the fundamental mechanisms of the climate system. Climate models allow us to observe the response of the ocean-atmosphere system to either real or hypothesized perturbations. The results of modeling studies are especially important in the study of paleoclimate, where our understanding of the past is incredibly data limited. One useful method of utilizing climate models is to hypothesize a particular perturbation and observe the system's response. The model response can then be compared to actual paleoclimate data in order to test the validity of the hypothesis.

Paleoceanographic Questions

In the following chapters, I focus on two known North Atlantic millennial scale climate events. The first is the 8.2 kyr event, which was a brief Holocene cooling event recorded in the oxygen isotopic composition of Greenland ice. The second is the Younger Dryas cooling event, which was much larger than the 8.2 kyr event in both magnitude and duration. The Younger Dryas was not a Holocene event; it occurred on the last deglacial transition. However, it was chosen for study because its magnitude and duration make it easier to document in sediment cores. The questions I address include:

- Was there a high latitude surface freshening associated with the 8.2 kyr event? And what was the sea surface temperature response in the open-ocean, high latitude North Atlantic?

- Was there a change in the overall meridional overturning circulation associated with the Younger Dryas event?

- Was there a change in intermediate depth overturning associated with the Younger Dryas?

- Could a North Atlantic freshwater forcing scenario explain the documented climate responses of the Younger Dryas?

A Dual-Faceted Approach

I employ a dual-faceted approach of multi-element foraminiferal analyses combined with the results of a climate model simulation. The cores used in this study were taken from geographic locations that may be particularly sensitive to climatic forcings and/or responses. Among the analytical techniques employed are nutrient tracers, and tracers of sea surface and deep ocean temperature and salinity. I then compare the paleoclimate data to the results of a freshwater forced model simulation.

In Chapter 2, I present paired planktic foraminiferal Mg/Ca and $\delta^{18}O$ data from Site 984 in the high latitude North Atlantic in order to document changes in high latitude sea surface temperatures and salinities over the past 10,000 years. Site 984 is located in a sensitive region of the North Atlantic, where a surface freshwater perturbation could be associated with significant climate change.

In Chapter 3, I present foraminiferal Cd/Ca and $\delta^{13}C$ data from an intermediate depth South Atlantic core in order to document the history of southern *vs.* northern source waters at this location over the last 20,000 years. The results provide insights about intermediate depth ocean circulation and heat transport during the Younger Dryas.

In Chapter 4, I present paired, benthic foraminiferal Mg/Ca and $\delta^{18}O$ data from two intermediate depth, low latitude North Atlantic sites in order to document changes in subsurface temperatures and salinities over the past 20,000 years. I then compare the ocean's response to the response of a freshwater forced model simulation in an attempt to determine whether a freshwater perturbation is an adequate explanation for the Younger Dryas event.

In Chapter 5, I present paired benthic foraminiferal Cd/Ca and $\delta^{13}C$ data from a core within the northward return flow of the MOC in order to document the history of southern *vs.* northern source waters at this location over the last 20,000 years. This new paleo-nutrient record provides insights into changes in the MOC during the Younger Dryas.

Thesis Results

- An open-ocean, sea surface freshening did occur during the 8.2 kyr event, concurrent with the cooling already observed in the GISP2 ice core record.

- The influence of North Atlantic Intermediate Water decreased at a South Atlantic site during the Younger Dryas, consistent with a possible decrease in intermediate depth overturning and an associated reduction in northward heat transport.

- Intermediate depth temperatures and salinities during the Younger Dryas varied in a manner consistent with a freshwater forced model simulation.

- During the Younger Dryas, the influence of South Atlantic source waters decreased within the northward return flow of the MOC, consistent with a possible decrease in deep overturning and an associated reduction in northward heat transport.

Taken together, the results suggest an increase in intermediate depth ventilation in the North Atlantic during the Younger Dryas relative to today, but with no associated increase in the export of North Atlantic Intermediate Water into the South Atlantic (Figure 1c). A vigorous but shallow ventilation in the North Atlantic may have caused an increase in the influence of North Atlantic source waters within the northward return flow of the MOC and a decrease in the influence of North Atlantic Intermediate Water in the South Atlantic during the Younger Dryas.

Figure 1. Holocene, Glacial and Younger Dryas subsurface geometries for the western Atlantic Ocean. **a.)** distribution of $\delta^{13}C$ in the modern western Atlantic [*Kroopnick*, 1985]; **b.)** glacial $\delta^{13}C$ [*Curry and Oppo*, 2005]; **c.)** schematic of a possible Younger Dryas subsurface geometry based on the trace and minor element data presented in the following chapters.

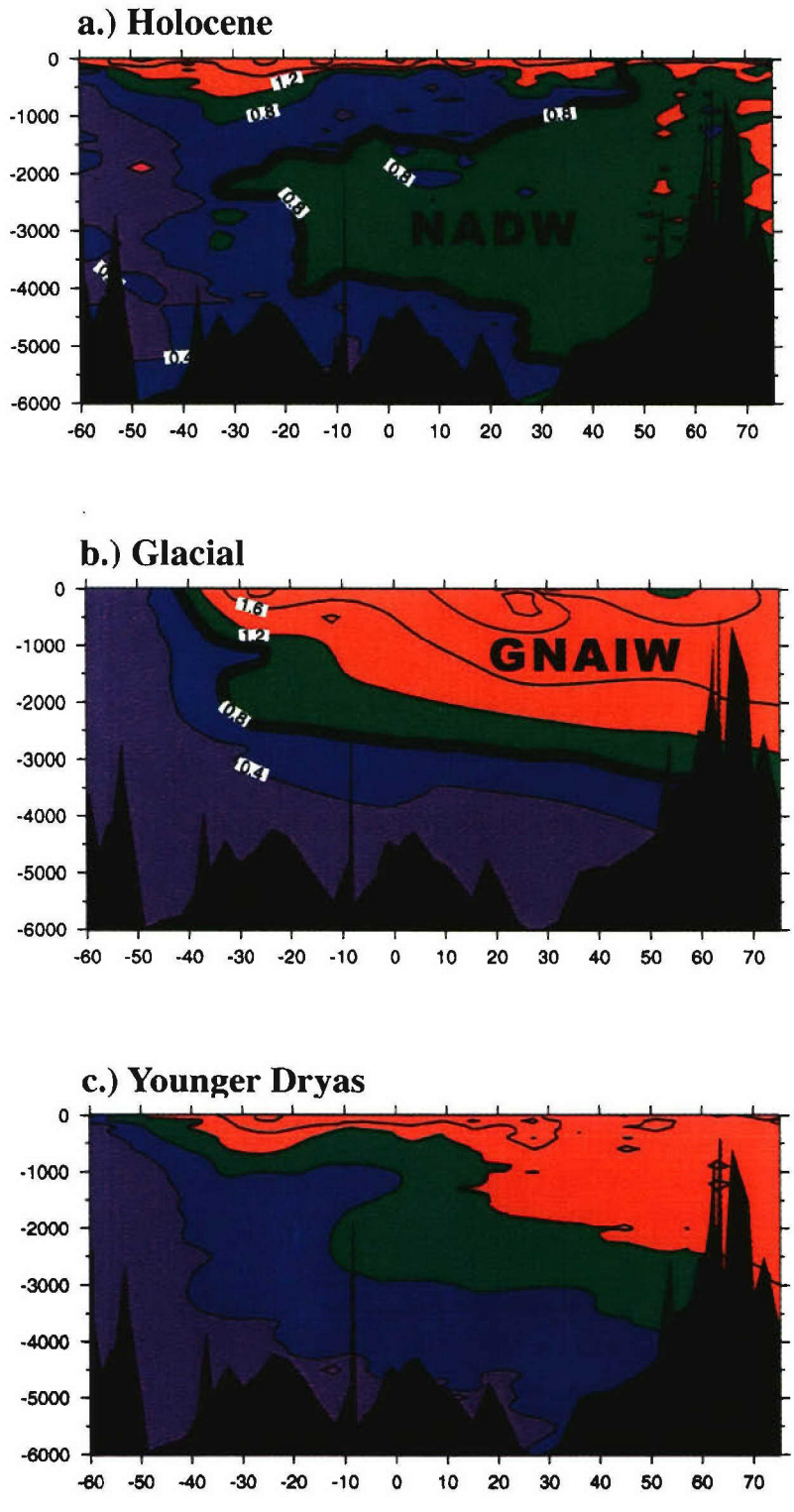
a.) Holocene
NADW
b.) Glacial
GNAIW
c.) Younger Dryas
0
-1000
-2000
-3000
-4000
-5000
-6000
-60 -50 -40 -30 -20 -10 0 10 20 30 40 50 60 70
Latitude

References

Bianchi, G. G., and I. N. McCave (1999), Holocene periodicity in North Atlantic climate and deep-ocean flow south of Iceland, *Nature*, *397*, 515-517.

Bond, G., W. Showers, M. Cheseby, R. Lotti, P. Almasi, P. B. deMenocal, P. Priore, H. Cullen, I. Hajdas, and G. Bonani (1997), A pervasive millennial-scale cycle in North Atlantic Holocene and glacial climates, *Science*, *278*, 1257-1266.

Broecker, W. S., D. M. Peteet, and D. Rind (1985), Does the ocean-atmosphere system have more than one stable mode of operation? *Nature*, *315*, 21-25.

Curry, W. B., and D. W. Oppo (20050, Glacial water mass geometry and the distribution of $\delta^{13}C$ of ΣCO_2 in the western Atlantic Ocean, *Paleoceanography, 20*, doi:10.1029/2004PA001021.

Grootes, P. M., M. Stuiver, J. W. C. White, S. J. Johnsen, and J. Jouzel (1993), Comparison of oxygen-isotope records from the GISP2 and GRIP Greenland ice cores, *Nature*, *366*, 552-554.

Keigwin, L. D. (1996), The Little Ice Age and the Medieval Warm Period in the Sargasso Sea, *Science*, *274*, 1504-1508.

Kroopnick, P. M. (1985), The distribution of $\delta^{13}C$ of ΣCO_2 in the world oceans, *Deep Sea Res. Part A*, 32, 57– 84.

Manabe, S., and R. J. Stouffer (1988), Two stable equilibria of a coupled ocean-atmosphere model, *J. Clim.*, *1*, 841-866.

Manabe, S., and R. J. Stouffer (1995), Simulation of abrupt climate change induced by freshwater input to the North Atlantic Ocean, *Nature*, *378*, 165-167.

O'Brien, S. R., P. A. Mayewski, L. D. Meeker, D. A. Meese, M. S. Twickler, and S. I. Whitlow (1995), Complexity of Holocene climate as reconstructed from a Greenland ice core, *Science*, *270*, 1962-1964.

Rahmstorf, S. (1994), Rapid climate transitions in a coupled ocean-atmosphere model, *Nature*, *372*, 82-85.

Chapter 2. Amplitude and Timing of Salinity and Temperature Variability in the High Latitude North Atlantic

Abstract

Paired records of planktic foraminiferal $\delta^{18}O$ and Mg/Ca from the subpolar North Atlantic reveal trends of increasing temperatures (~3°C) and salinities over the course of the Holocene, which were punctuated by abrupt events. The variability does not appear to be periodic, but tends to recur within a broad millennial band. The records provide the first evidence of open-ocean cooling (nearly 2°C) and freshening during the 8.2 kyr event, and suggest similar conditions at 9.3 ka. However, the two largest temperature oscillations (~2°C) occurred during the last 4,000 years, suggesting a recent increase in temperature variability relative to the mid-Holocene.

Introduction

The Holocene epoch is a time of relative climate stability when viewed within the context of the large amplitude, millennial scale fluctuations observed in the colder sections of the Greenland ice core records [*Dansgaard et al.*, 1993; *Grootes and Stuiver*, 1997]. Recent studies, however, confirm an earlier work [*Denton and Karlén*, 1973] suggesting that smaller, suborbital scale variability did occur throughout the last 10,000 years [*Bianchi and McCave*, 1999; *Bond et al.*, 1997; *deMenocal et al.*, 2000; *O'Brien et al.*, 1995]. At present, Holocene climate variability is poorly characterized and the forcing mechanisms are not well constrained. It has been argued that the same mechanisms that drive millennial scale variability during glacial periods also drive Holocene variability, causing a pervasive 1,500-year cyclicity in sea surface temperature, sea surface salinity, and subsurface processes [*Bianchi and McCave*, 1999; *Bond et al.*, 1997]. It has also been argued that solar forcing underlies the Holocene portion of the 1,500-year cycle, causing surface hydrographic changes that may have affected North Atlantic Deep Water formation, thereby amplifying the solar signal [*Bond et al.*, 2001], although recent work [*Marchal*, 2005] indicates that a solar forcing mechanism for millennial scale variability is unlikely.

Of the Holocene climate events, the 8.2 kyr event has received the most attention because it is the largest Holocene excursion in the GISP2 $\delta^{18}O$ record [*Alley et al.*, 1997]. Multiple proxies in Greenland ice reveal a pattern at 8.2 ka of reduced air temperatures, drier conditions, stronger winds over the North Atlantic, and low atmospheric methane [*Alley et al.*, 1997]. Evidence of climatic excursions at 8.2 ka are also present in regional

and global records, suggesting a widespread climatic event: European lake sediments [*von Grafenstein et al.*, 1998] and tree ring data [*Klitgaard-Kristensen et al.*, 1998]; North Sea foraminiferal abundances [*Klitgaard-Kristensen et al.*, 1998]; African lake level records [*Gasse*, 2000]; and Cariaco Basin sediments [*Hughen et al.*, 1996]. The spatial pattern of climate variability at ~8.2 ka is similar to that of the Younger Dryas [*Alley et al.*, 1997], and is consistent with model responses to a reduction in the North Atlantic meridional overturning circulation (MOC) [*Manabe and Stouffer*, 1988]. A reduction in MOC is often attributed to an increase in freshwater supply to the sea surface in the high latitude North Atlantic [*Broecker et al.*, 1985], and a freshwater forcing hypothesis has been proposed for the 8.2 kyr event [*Barber et al.*, 1999].

Oxygen isotopes in planktic foraminifera are often used as a tracer of freshwater in the surface North Atlantic [*Bond et al.*, 2001; *Keigwin et al.*, 2005]. One complication with this approach, however, is that both seawater $\delta^{18}O$ ($\delta^{18}O_{sw}$) and calcification temperature influence the $\delta^{18}O$ of foraminifera, making it difficult to disentangle the temperature and salinity signals. For example, oxygen isotopic variability in subpolar North Atlantic planktic foraminifera may not be robust indicators of surface variability because the effects of cooling and freshening could cancel each other out in the foraminiferal $\delta^{18}O$ [*Bond et al.*, 1997]. Both temperature and salinity can be estimated by obtaining paired Mg/Ca and $\delta^{18}O$ measurements in planktic foraminifera [*Mashiotta et al.*, 1999]. An exponential relationship exists between calcification temperature and the Mg/Ca of planktic foraminifera [*Nürnberg et al.*, 1996], so Mg/Ca can be used to determine temperature independently of $\delta^{18}O$. Using Mg/Ca-derived temperatures, the foraminiferal $\delta^{18}O$, and a correction for ice volume, the $\delta^{18}O_{sw}$ can be calculated, and salinity can be estimated using a regional $\delta^{18}O$-salinity relationship.

In this study, we present the first open-ocean, subpolar North Atlantic record of near surface temperature and salinity variability during the Holocene using this method. We measured Mg/Ca and $\delta^{18}O$ in the tests of the planktic foraminifer *N. pachyderma* (d.), which calcifies throughout the year, and at a depth of 30 to 40 meters [*Ostermann et al.*, 2001]. Our records were generated using sediment from Ocean Drilling Project Site 984, located on the Bjorn Drift, on the eastern flank of the Reykjanes Ridge (61°N, 25°W, 1,648 m). A near constant elevated sedimentation rate of ~29 cm/kyr in this core during the last 10 kyr makes it ideal for the study of suborbital climate variability (see supplementary material). Today, surface waters at Site 984 are dominated by the warm salty North Atlantic Current; however, colder fresher water may enter the study area from the northwest, making it

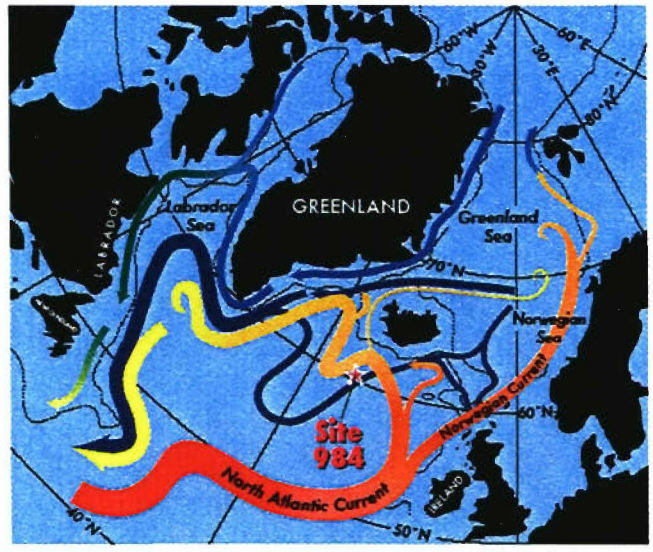

Figure 1. Map of the North Atlantic showing ODP Site 984 (61°N, 25°W, 1,648 m).

an ideal location to study variability in surface temperatures and salinities that may be associated with changes in the vigor of the MOC. Seasonal temperatures at 30 meters depth range from 7.3°C to 11.2°C, and salinities are nearly constant at 35.1 to 35.2 p.s.u. [*Levitus and Boyer*, 1994]. Modern thermocline $\delta^{18}O_{sw}$ in this region of the North Atlantic lie between 0 and 0.3‰ [*Schmidt et al.*, 1999], in agreement with core top calculations. A conservative estimate using available near surface data [*Schmidt et al.*, 1999] indicates that today a change of 0.1‰ in $\delta^{18}O_{sw}$ is equivalent to ~0.2 p.s.u. salinity change. However, the presence of glacial meltwater would cause a different relationship: a change of 0.1‰ in $\delta^{18}O_{sw}$ would be equivalent to ~0.1 p.s.u. salinity change.

Results and Discussion

The Site 984 Mg/Ca and $\delta^{18}O$ records reveal trends of increasing temperatures (~3°C) and increasing $\delta^{18}O_{sw}$ (~1.0‰) from the early Holocene to 4 ka (Figure 2b-d). Superimposed on the Holocene trend are suborbital scale oscillations. At 9.3 ka, Mg/Ca-derived near surface temperatures decreased by 1-2°C, and $\delta^{18}O_{sw}$ decreased by ~0.3‰. Similarly, at 8.2 ka, near surface temperatures decreased by ~2°C, and $\delta^{18}O_{sw}$ decreased by ~0.3‰. The records do not reveal significant suborbital variability from 8 to 4 ka, but they do reveal variability in the later Holocene. After 4 ka, two 2°C temperature oscillations

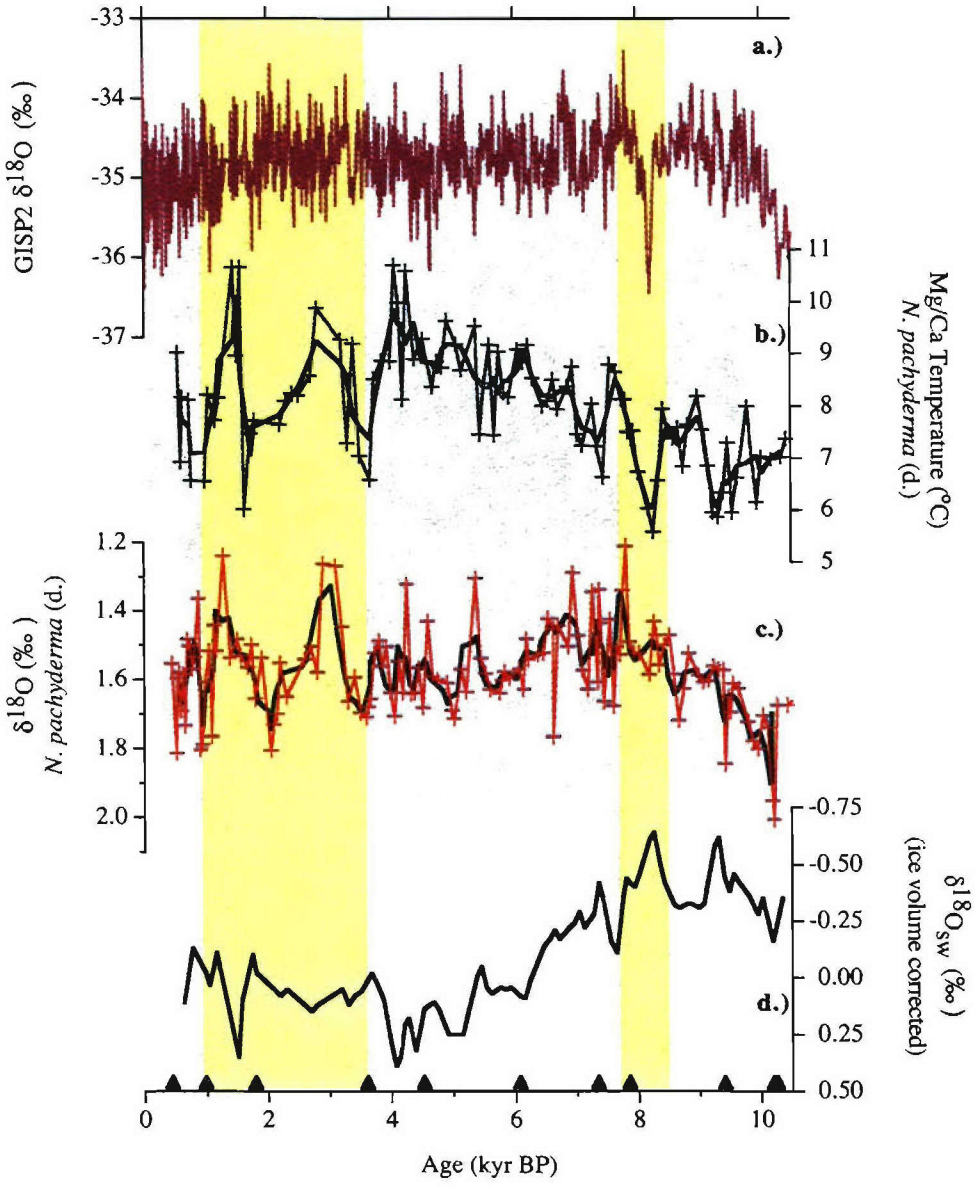

Figure 2. Planktic data from ODP Site 984 (61°N, 25°W, 1,648 m). **a.)** GISP2 $\delta^{18}O$ (purple) [*Grootes et al.*, 1993]. **b.)** Average Mg/Ca-derived temperature estimates (blue), with a 3-point running mean (black). Mg/Ca converted to temperature using the Elderfield and Ganssen [2000] relationship. **c.)** Average $\delta^{18}O$ (red), with a 3-point running mean (black). **d.)** Seawater $\delta^{18}O$ (black), calculated using 3-point smoothed Mg/Ca temperatures, 3-point smoothed foraminiferal $\delta^{18}O$, an ice volume correction [*Waelbroeck et al.*, 2002], and the $\delta^{18}O$ temperature equation for *N. pachyderma* (d.) [*von Langen*, 2001]. AMS radiocarbon dates converted to calendar age (green) using CALIB 5.01 [*Stuiver and Reimer*, 1993] and the calibration dataset [*Hughen et al.*, 2004]. Yellow shading denotes suborbital oscillations discussed in text.

occurred, with cold events at 3.7, 1.8, and 0.9 ka, and relative warming at 3 and 1.5 ka. The late Holocene oscillations are also present in the foraminiferal $\delta^{18}O$, suggesting relatively little change in $\delta^{18}O_{sw}$ after 3.7 ka.

The overall warming trend observed in the Mg/Ca data from Site 984 is consistent with the Holocene trend observed in high latitude North Atlantic foraminiferal-based proxies such as modern analogue technique [*Marchal et al.*, 2002; *Risebrobakken et al.*, 2003], but contradicts alkenone- and diatom-based proxies [*Keigwin et al.*, 2005; *Koç and Jansen*, 1994; *Marchal et al.*, 2002; *Moros et al.*, 2004], which reveal a cooling trend. This discrepancy can be explained by differences in depth habitat [*Moros et al.*, 2004]. Diatoms and alkenones record summer temperatures in the shallow euphotic zone. Foraminifera, living deeper in the water column, record thermocline temperatures, which are set by ventilation during the winter months. Thus, alkenones and diatoms may record the oceanographic response to changes in summer insolation, which decreased over the course of the Holocene, while foraminifera may record the oceanographic response to changes in winter insolation, which increased over the course of the Holocene. This interpretation is supported by model simulations [*Liu et al.*, 2003], which predict a Holocene cooling trend in the surface North Atlantic and a warming trend in the subsurface due to the decreasing summer insolation and increasing winter insolation.

The $\delta^{18}O_{sw}$ record suggests that wintertime salinities increased steadily at Site 984 from a minimum value at 8.2 ka to a maximum at 4 ka. The low salinities in the earlier part of the Holocene may partially reflect the presence of light deglacial surface waters. The subsequent gradual increase in salinity must reflect either a trend of increasing advection of high salinity waters relative to fresher polar waters, or a change in evaporation minus precipitation, since deglaciation was largely over by 8 ka. A change in the Atlantic-Pacific freshwater contrast, which may accompany a southward migration of the Intertropical Convergence Zone [*Haug et al.*, 2001], is one possible explanation for increasing salinities over the course of the Holocene. Alternatively, a gradual redistribution of freshwater within the Atlantic, as has occurred in recent decades [*Curry et al.*, 2003], may have led to increasing salinities at high latitudes and associated freshening at low latitudes. Such a redistribution may have been associated with intensification in the MOC, which would lead to a greater influence at Site 984 of warm salty surface waters from the south relative to the cold fresh waters from the north. After 4 ka, the $\delta^{18}O_{sw}$ suggests that salinities rapidly decreased by as much as 0.8 p.s.u., and remained at or near modern values for the remainder of the record.

The Mg/Ca-derived temperature data also reveal very well defined suborbital variability. At 8.2 ka, temperatures decreased by ~2°C, coincident with the cooling recorded in the GISP2 ice core. Concurrently with that cooling, there was no significant change in the planktic foraminiferal $\delta^{18}O$, suggesting a 0.3‰ $\delta^{18}O_{sw}$ decrease. (Using our modern estimate, a decrease of 0.3‰ equals a freshening of ~0.6 p.s.u.; using a glacial meltwater estimate, a decrease of 0.3‰ equals a freshening of ~0.3 p.s.u.) The data strongly suggest the presence of freshwater along with the 2°C cooling at 8.2 ka, although we cannot rule out the possibility of a change in the $\delta^{18}O$ of precipitation source waters. A freshwater induced reduction in MOC has been proposed as a mechanism of high latitude cooling during the 8.2 kyr event. Barber *et al.* [1999] suggest that a catastrophic drainage of Laurentide lakes caused a surface ocean stability in the Labrador Sea that disrupted the formation of Labrador Sea Water (LSW), and caused the cooling over central Greenland [*Barber et al.*, 1999]. While planktic foraminiferal $\delta^{18}O$ records from the active convection region of the Labrador Sea do not suggest a freshening during this interval [*Hillaire-Marcel et al.*, 1994], a record from the Laurentian Fan, located south of the Labrador Sea, does show a significant freshening at 8.2 ka [*Keigwin et al.*, 2005]. The lack of a surface freshening signal in the central Labrador Sea, and the existence of this signal at the Laurentian Fan may suggest an alternate freshwater drainage route, or it may suggest that the pulse of freshwater stayed close to the coast without influencing the $\delta^{18}O$ signal in the central Labrador Sea [*Keigwin et al.*, 2005]. In either case, the freshwater may have mixed with waters of the North Atlantic Current, carrying the freshwater signal to the high latitudes. Alternatively, the freshwater signal may have arrived at Site 984 from the north, associated with a decrease in MOC.

Similar temperature and salinity decreases occurred at 9.3 ka, although the magnitude of the temperature change was smaller (1-2°C), and the existence of the excursion in the GISP2 $\delta^{18}O$ record is less evident. However, the cooling and freshening occurred concurrently with an excursion in the GISP2 terrestrial dust concentration, indicating increased windiness over Greenland [*O'Brien et al.*, 1995], and is consistent with detrital evidence of an ice rafting event in the North Atlantic at 9.3 ka [*Bond et al.*, 2001].

Suborbital variability also occurred in the later Holocene. The ~2°C temperature oscillations recorded in the most recent 4,000 years of the record occurred without large episodic increases and decreases in freshwater; only at 8.2 and 9.3 ka were temperature oscillations associated with large changes in local salinity. However, the temperature minima and maxima of the last 4,000 years may have coincided with neoglacial advances

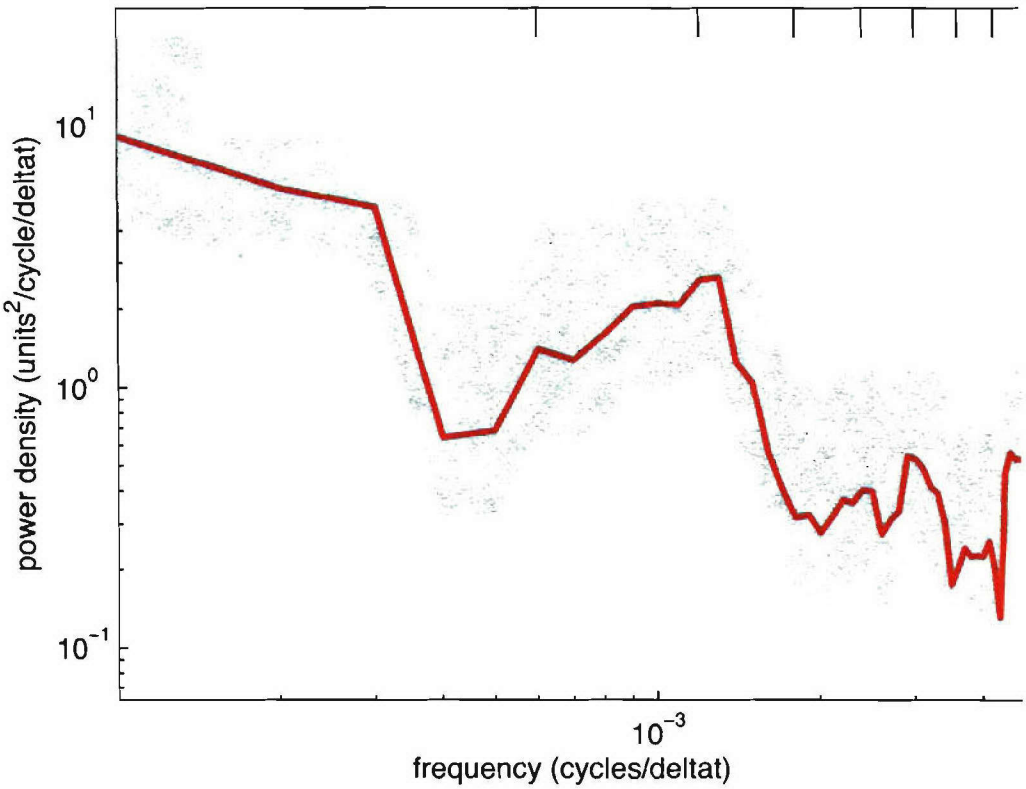

Figure 3. Multi-taper spectral analysis for Mg/Ca temperatures. 554-10,423 years BP. Mean time step = 107.3 years, with linear interpolation of temperature data. Time-bandwidth product = 3. Shading denotes the 95% confidence interval. Matlab code courtesy of Peter Huybers.

and retreats. Maximum advances on Baffin Island at approximately 1,000, 1,900, and 3,000 ^{14}C years BP [*Davis*, 1985], or at approximately 0.9, 1.8, and 3.2 kyr BP, roughly correspond to the temperature minima in the most recent 4,000 years of our record, suggesting the possibility that these temperature changes reflect regional high latitude North Atlantic climate variations.

Bond *et al.* [1997] suggest that synchronous surface cooling and freshening events occurred throughout the Holocene with a cyclicity of 1.5 kyr. Our records do not confirm a persistent 1.5 kyr cyclicity throughout the Holocene. Instead, they suggest suborbital variability in the early Holocene, relative stability in the mid-Holocene, and renewed variability in the late Holocene. Furthermore, multi-taper spectral analysis of our Mg/Ca temperatures does not yield a peak at 1.5 kyr. Rather, it suggests variance in a broad millennial band spanning frequencies from approximately 1/0.5 kyr to 1/1.5 kyr, indicating

a preference for millennial variability. We also generated multi-taper coherence estimates using our Mg/Ca data set and the atmospheric $\Delta^{14}C$ data set of Stuiver *et al.* [*Stuiver et al.*, 1998] in order to assess the influence of solar variability (see supplementary material). However, the results are inconclusive because the coherence changes significantly when age control points are altered within the 2σ range of calibrated radiocarbon ages.

Summary

In summary, our new Mg/Ca and $\delta^{18}O$ records from Site 984 reveal long-term Holocene trends of increasing temperatures and salinities. Further investigations at lower latitudes are necessary in order to determine whether there has been an overall shift in the Atlantic-Pacific freshwater contrast, or whether there has been a redistribution of freshwater within the Atlantic. In addition, our records do not confirm a 1.5 kyr cyclicity during the Holocene, but do suggest a preference for millennial variability. The new records provide the first open ocean confirmation of temperature and salinity decreases during the 8.2 kyr event, consistent with the hypothesis of a reduced MOC. However, the 8.2 kyr event is not the only large temperature event of the Holocene; our new records reveal temperature excursions during the last 4,000 years that are the largest oscillations of the Holocene, underscoring the need to better understand the forcing mechanisms for millennial climate change.

Acknowlegements

Thanks to D. Schneider, S. Birdwhistell, D. Ostermann, M. Jeglinski and L. Zou for laboratory assistance; and to L. Keigwin, J. Sachs, Y. Rosenthal, E. Boyle, S. Thorrold, W. Curry, and P. Huybers for helpful discussions. Work supported by the WHOI Ocean and Climate Change Institute, and by NSF OCE02-20776 and OCE04-02565. This is WHOI contribution number *****.

References

Alley, R. B., P. A. Mayewski, T. Sowers, M. Stuiver, K. C. Taylor, and P. U. Clark (1997), Holocene climatic instability: A prominent, widespread event 8200 yr ago, *Geology*, *25*, 483-486.

Barber, D. C., et al. (1999), Forcing of the cold event 8,200 years ago by catastrophic drainage of Laurentide lakes, *Nature*, *400*, 344-348.

Bianchi, G. G., and I. N. McCave (1999), Holocene periodicity in North Atlantic climate and deep-ocean flow south of Iceland, *Nature*, *397*, 515-517.

Bond, G., B. Kromer, J. Beer, R. Muscheler, M. N. Evans, W. Showers, S. Hoffmann, R. Lotti-Bond, I. Hajdas, and G. Bonani (2001), Persistent solar Influence on North Atlantic climate during the Holocene, *Science*, *294*, 2130-2136.

Bond, G., W. Showers, M. Cheseby, R. Lotti, P. Almasi, P. B. deMenocal, P. Priore, H. Cullen, I. Hajdas, and G. Bonani (1997), A pervasive millennial-scale cycle in North Atlantic Holocene and glacial climates, *Science*, *278*, 1257-1266.

Broecker, W. S., D. M. Peteet, and D. Rind (1985), Does the ocean-atmosphere system have more than one stable mode of operation? *Nature*, *315*, 21-25.

Curry, R., B. Dickson, and I. Yashayaev (2003), A change in the freshwater balance of the Atlantic Ocean over the past four decades, *Nature*, *426*, 826-829.

Dansgaard, W., et al. (1993), Evidence for general instability of past climate from a 250-kyr ice core record, *Nature*, *364*, 218-220.

Davis, P. T. (1985), Neoglacial moraines on Baffin Island, in *Quaternary Environments: Eastern Canadian Arctic, Baffin Bay and Western Greenland*, edited by J. T. A. Andrews, pp. 682-718, Allen & Unwin, Boston.

deMenocal, P. B., J. Ortiz, T. Guilderson, and M. Sarnthein (2000), Coherent high- and low-latitude climate variability during the Holocene Warm Period, *Science*, *288*, 2198-2202.

Denton, G. H., and W. Karlén (1973), Holocene climate variations - their pattern and possible cause, *Quat. Res.*, *3*, 155-205.

Elderfield, H., and G. Ganssen (2000), Past temperature and $\delta^{18}O$ of surface ocean waters inferred from foraminiferal Mg/Ca ratios, *Nature*, *405*, 442-445.

Gasse, F. (2000), Hydrological changes in the African tropics since the Last Glacial Maximum, *Quat. Sci. Rev.*, *19*, 189-211.

Grootes, P. M., and M. Stuiver (1997), Oxygen 18/16 variability in Greenland snow and ice with 10(-3)- to 10(5) -year time resolution, *J. Geophys. Res.*, *102*, 26455-26470.

Grootes, P. M., M. Stuiver, J. W. C. White, S. J. Johnsen, and J. Jouzel (1993), Comparison of oxygen-isotope records from the GISP2 and GRIP Greenland ice cores, *Nature*, *366*, 552-554.

Haug, G. H., K. A. Hughen, D. M. Sigman, L. C. Peterson, and U. Röhl (2001), Southward migration of the Intertropical Convergence Zone through the Holocene, *Science*, *294*, 1304-1308.

Hillaire-Marcel, C., A. de Vernal, G. Bilodeau, and G. Wu (1994), Isotope stratigraphy,

sedimentation rates, deep circulation, and carbonate events in the Labrador Sea during the last ~200 ka, *Can. J. Earth Sci.*, *31*, 63-89.

Hughen, K. A., et al. (2004), Marine04 marine radiocarbon age calibration, 0–26 cal kyr BP, *Radiocarbon*, *46*, 1059-1086.

Hughen, K. A., J. T. Overpeck, L. C. Peterson, and S. Trumbore (1996), Rapid climate changes in the tropical Atlantic region during the last deglaciation, *Nature*, *380*, 51-54.

Keigwin, L. D., J. P. Sachs, Y. Rosenthal, and E. A. Boyle (2005), The 8200 year B.P. event in the slope water system, western subpolar North Atlantic, *Paleoceanography*, *20*, 10.1029/2004PA001074.

Klitgaard-Kristensen, D., H. P. Sejrup, H. Haflidason, S. J. Johnsen, and M. Spurk (1998), A regional 8200 cal. yr BP cooling event in northwest Europe, induced by final stages of the Laurentide ice-sheet deglaciation? *J. Quat. Sci.*, *13*, 165-169.

Koç, N., and E. Jansen (1994), Response of the high-latitude Northern Hemisphere to orbital climate forcing: Evidence from the Nordic Seas, *Geology*, *22*, 523-526.

Levitus, S., and T. Boyer (1994), *World Ocean Atlas 1994 Volume 4: Temperature. NOAA Atlas NESDIS 4*, U.S. Department of Commerce, Washington, D.C.

Liu, Z., E. Brady, and J. Lynch-Stieglitz (2003), Global ocean response to orbital forcing in the Holocene, *Paleoceanography*, *18*, 10.1029/2002PA000819.

Manabe, S., and R. J. Stouffer (1988), Two stable equilibria of a coupled ocean-atmosphere model, *J. Clim.*, *1*, 841-866.

Marchal, O. (2005), Optimal estimation of atmospheric ^{14}C production over the Holocene: paleoclimate implications, *Clim. Dyn.*, *24*, 71-88.

Marchal, O., et al. (2002), Apparent long-term cooling of the sea surface in the northeast Atlantic and Mediterranean during the Holocene, *Quat. Sci. Rev.*, *21*, 455–483.

Mashiotta, T. A., D. W. Lea, and H. Spero (1999), Glacial–interglacial changes in Subantarctic sea surface temperature and $\delta^{18}O$-water using foraminiferal Mg, *Earth Planet. Sci. Lett.*, *170*, 417-432.

Moros, M., K. Emeis, B. Risebrobakken, I. Snowball, A. Kuijpers, J. F. McManus, and E. Jansen (2004), Sea surface temperatures and ice rafting in the Holocene North Atlantic: climate influences on northern Europe and Greenland, *Quat. Sci. Rev.*, *23*, 2113–2126.

Nürnberg, D., J. Bijma, and C. Hemleben (1996), Assessing the reliability of magnesium in foraminiferal calcite as a proxy for water mass temperature, *Geochim. Cosmochim. Acta*, *60*, 803-814.

Ostermann, D. R., J. Olafsson, S. Manganini, W. B. Curry, and S. Honjo (2001), A dramatic increase in particle flux in the Iceland Sea since 1997, results from a 15-year time series, poster presented at 7th International Conference on Paleoceanography, Sapporo, Japan.

O'Brien, S. R., P. A. Mayewski, L. D. Meeker, D. A. Meese, M. S. Twickler, and S. I. Whitlow (1995), Complexity of Holocene climate as reconstructed from a Greenland ice core, *Science*, *270*, 1962-1964.

Risebrobakken, B., E. Jansen, C. Andersson, E. Mjelde, and K. Hevrøy (2003), A high-resolution study of Holocene paleoclimatic and paleoceanographic changes in the Nordic Seas, *Paleoceanography, 18(1)*, 10.1029/2002PA000764.

Schmidt, G. A., G. R. Bigg, and E. J. Rohling (1999), Global Seawater Oxygen-18 Database, edited, available at http://data.giss.nasa.gov/data/.

Stuiver, M., and P. J. Reimer (1993), Extended ^{14}C database and revised CALIB radiocarbon calibration program, *Radiocarbon, 35*, 215-230.

Stuiver, M., P. J. Reimer, and T. F. Braziunas (1998), High-precision radiocarbon age calibration for terrestrial and marine samples, *Radiocarbon, 40*, 1127-1151.

von Grafenstein, U., H. Erlenkeuser, J. Müller, J. Jouzel, and S. J. Johnsen (1998), The cold event 8200 years ago documented in oxygen isotope records of precipitation in Europe and Greenland, *Clim. Dyn., 14*, 73-81.

von Langen, P. (2001), Non-spinose planktonic foraminifera (*Neogloboquadrina pachyderma*) cultured for geochemical and paleoceanographic applications, Ph.D. Thesis, Univ. of Calif. at Santa Barbara, Santa Barbara.

Waelbroeck, C., L. Labeyrie, E. Michel, J.-C. Duplessy, J. F. McManus, K. Lambeckd, E. Balbona, and M. Labracherie (2002), Sea-level and deep water temperature changes derived from benthic foraminifera isotopic records, *Quat. Sci. Rev., 21*, 295-305.

Supplementary Material

Methods

The age model for Site 984 is based on linear interpolation between 11 *G. bulloides* accelerator mass spectrometer radiocarbon dates which were converted to calendar age using CALIB 5.01 [*Stuiver and Reimer*, 1993], the Marine04 calibration dataset [*Hughen et al.*, 2004], and a reservoir correction of 400 years (Table 1 and Figure S-1a). The converted ages reveal a near constant elevated sedimentation rate of approximately 29 cm/kyr, making it an ideal core for the study of suborbital climate variability.

Mg/Ca and $\delta^{18}O$ were measured in the tests of the planktic foraminifer *N. pachyderma* (d.), which were picked from the narrow size fraction of 150-212 microns. Each Mg/Ca sample consisted of approximately 50 individuals, which were crushed and cleaned using the full trace metal method, with a reversal of the oxidative and reductive steps [*Boyle and Keigwin*, 1985/6; *Boyle and Rosenthal*, 1996]. Each stable isotope sample consisted of 7-10 individuals.

Mg/Ca data were generated using a Thermo-Finnigan Element2 sector field single collector ICP-MS, following the protocol of Rosenthal *et al.* [1999]. In order to assess the precision of measurements on the ICP-MS, three consistency standards were treated as samples in each of 9 runs (including the two runs in which the data were generated). Mean Mg/Ca for the three consistency standards were 1.7 mmol mol^{-1}, 3.3 mmol mol^{-1} and 5.0 mmol mol^{-1}. Standard deviations were ±0.02 mmol mol^{-1} (n=9), ±0.03 mmol mol^{-1} (n=9), and ±0.04 mmol mol^{-1} (n=9), respectively. Average Mg/Ca in our samples range from 0.91 to 2.31 mmol mol^{-1}. Using the Mg/Ca-temperature relationship [Mg/Ca] = 0.52 exp 0.10 T [*Elderfield and Ganssen*, 2000], the resulting temperature errors range from ±0.2°C at our highest Mg/Ca values, to ±0.4°C at our lowest values. Stable isotope data were generated using a Finnegan-MAT 253. Calibration to the VPDB scale was made using NBS-19 ($\delta^{18}O$ = -2.20‰). Long-term reproducibility (1σ; n=461) of NBS-19 for this mass spectrometer is ±0.08‰.

Very good agreement exists between most replicate analyses, especially at the interval around 150 cm, which corresponds to the 8.2 kyr event (Figure S-1b). Post-depositional dissolution is a potential problem [*Brown and Elderfield*, 1996] because Mg is preferentially removed from carbonates [*Lorens et al.*, 1977; *Rosenthal and Boyle*, 1993]. To monitor dissolution, we weighed each sample of 50 individual foraminiferal tests and obtained average foraminiferal weights (Figure S-1c). Low foraminiferal weights do not

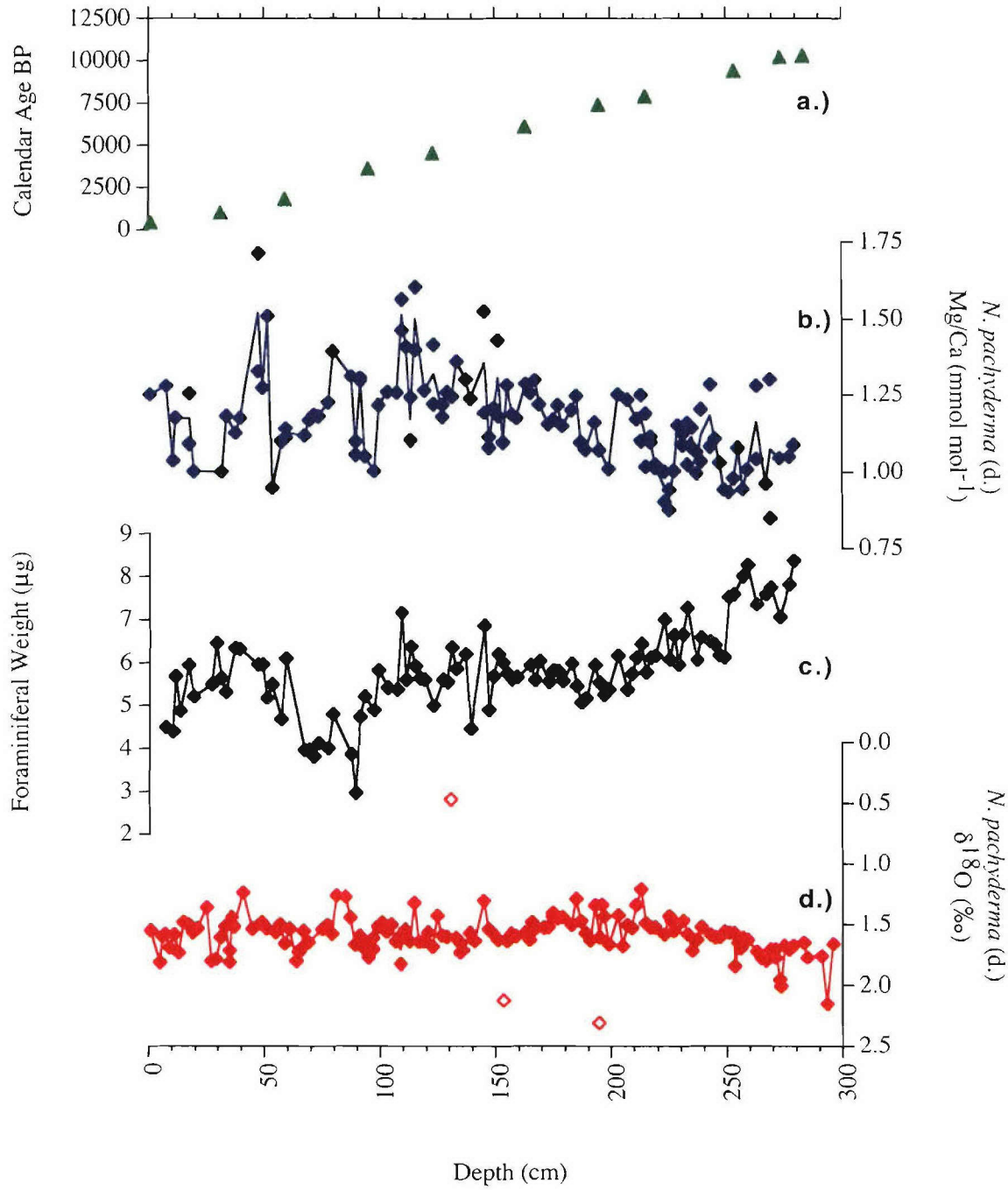

Figure S-1. Planktic data from ODP Site 984 *vs.* depth. **a.)** Accelerator mass spectrometer radiocarbon dates (green triangles). **b.)** All Mg/Ca data (blue diamonds), with average Mg/Ca where replicates exist (solid blue line). **c.)** Average test weight (black diamonds). **d.)** All $\delta^{18}O$ data (red diamonds), with average $\delta^{18}O$ where replicates exist (solid red line), and omitted data (open red diamonds).

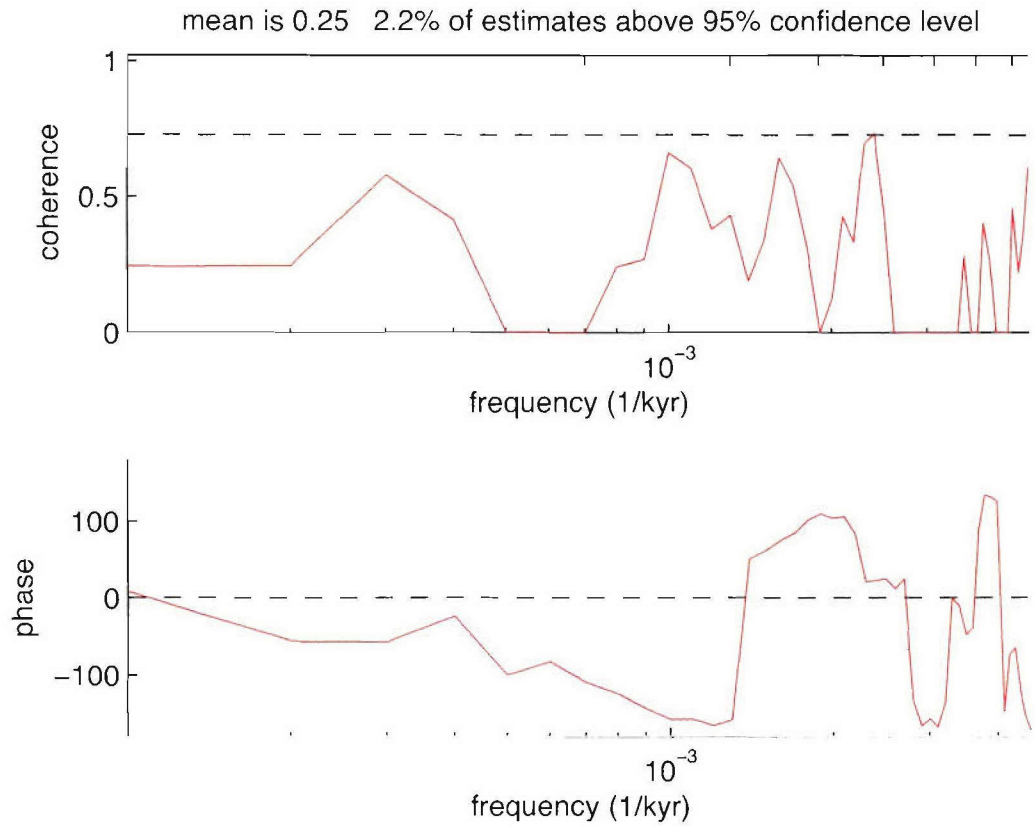

Figure S-2. Multi-taper coherence for Mg/Ca-derived temperatures and atmospheric $\Delta^{14}C$. **a.)** 554-10,423 years BP. Atmospheric $\Delta^{14}C$ linearly de-trended. Mean time step = 107.3 years, with linear interpolation of temperature and atmospheric $\Delta^{14}C$ data. Time-bandwidth product = 3. Dashed line denotes the 95% confidence interval.

coincide with low Mg/Ca values, making it unlikely that carbonate dissolution drives the Mg/Ca variability at this site. Since we do not believe that dissolution is a significant problem at this site, we chose the conservative approach of not applying a dissolution correction based on foraminiferal weights [*Rosenthal and Lohmann*, 2002], which would only exaggerate the Mg/Ca-derived temperature signal.

Coherence Estimates

In order to assess the influence of solar variability, we generated coherence estimates for our Mg/Ca temperature data and the atmospheric $\Delta^{14}C$ data of Stuiver *et al.* [1998]. While coherence within a broad millennial band does exist between Mg/Ca-

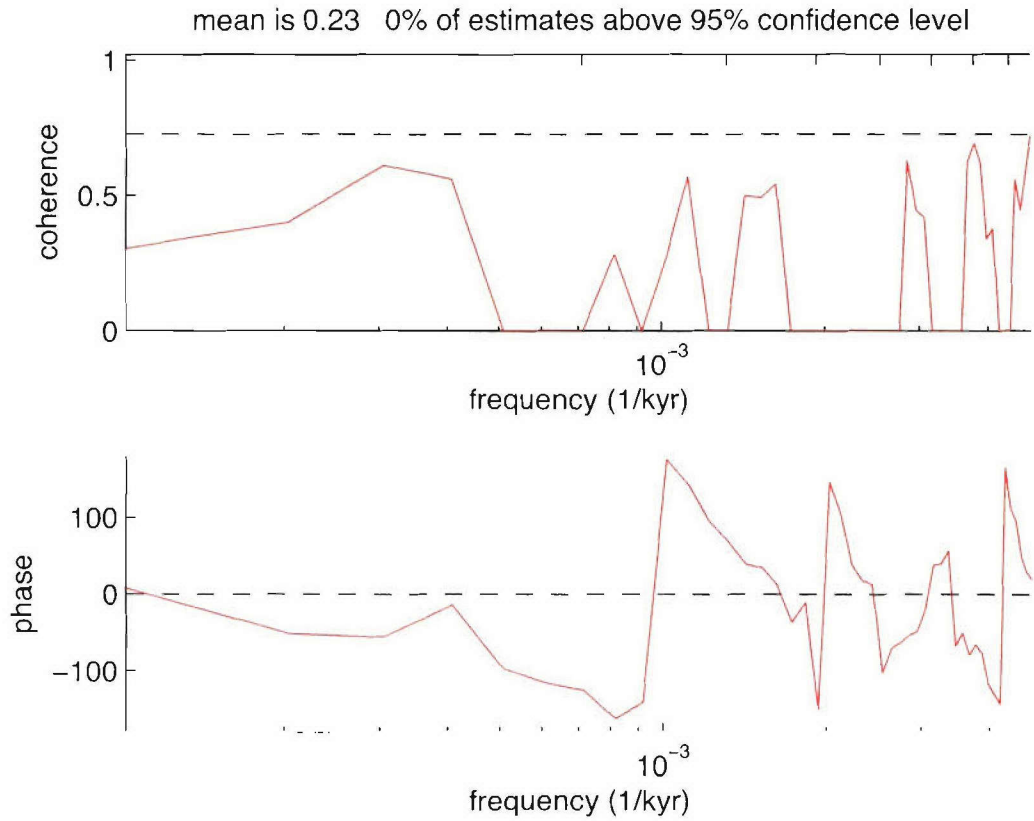

Figure S-2b.) Same as in **a.)**, except using a different age model for the Mg/Ca time series, which was based on randomly selected age control points from within the 2σ range of calibrated radiocarbon dates. Matlab code courtesy of Peter Huybers.

derived temperatures and atmospheric $\Delta^{14}C$, it lies well below the 95% confidence limits (Figure S-2a). In addition, we generated several age models for Site 984, using randomly selected age control points from within the 2σ range of calibrated radiocarbon dates, and a linear interpolation between those control points. The different age models yield radically different coherence estimates, making it difficult to draw conclusions about the influence of solar variability on the temperatures at our site (Figure S-2b).

References for Supplementary Material

Boyle, E. A., and L. D. Keigwin (1985/6), Comparison of Atlantic and Pacific paleochemical records for the last 215,000 years: changes in deep ocean circulation and chemical inventories, *Earth Planet. Sci. Lett.*, *76*, 135-150.

Boyle, E. A., and Y. Rosenthal (1996), Chemical hydrography of the South Atlantic during the Last Glacial Maximum: Cd and $\delta^{13}C$, in *The South Atlantic: Present and Past Circulation*, edited by G. Wefer, pp. 423-443, Springer-Verlag, Berlin.

Brown, S. J., and H. Elderfield (1996), Variations in Mg/Ca and Sr/Ca ratios of planktonic foraminifera caused by postdepositional dissolution: Evidence of shallow Mg-dependent dissolution, *Paleoceanography*, *11*, 543-551.

Elderfield, H., and G. Ganssen (2000), Past temperature and $\delta^{18}O$ of surface ocean waters inferred from foraminiferal Mg/Ca ratios, *Nature*, *405*, 442-445.

Hughen, K. A., S. J. Lehman, J. Southon, J. T. Overpeck, O. Marchal, C. Herring, and J. Turnbull (2004), ^{14}C Activity and global carbon cycle changes over the past 50,000 years, *Science*, *303*, 202-207.

Lorens, R. B., D. F. Williams, and M. L. Bender (1977), The early nonstructural chemical diagenesis of foraminiferal calcite, *J. Sediment. Petrol.*, *42*, 1602-1609.

Rosenthal, Y., and E. A. Boyle (1993), The factors controlling the flouride content of planktonic foraminifera -- an evaluation of its paleoceanographic applicability, *Geochim. Cosmochim. Acta*, *57*, 335-346.

Rosenthal, Y., M. P. Field, and R. M. Sherrell (1999), Precise determination of element/calcium ratios in calcareous samples using sector field inductively coupled plasma mass spectrometry, *Anal. Chem.*, *71*, 3248-3253.

Rosenthal, Y., and G. P. Lohmann (2002), Accurate estimation of sea surface temperatures using dissolution corrected calibrations for Mg/Ca paleothermometry, *Paleoceanography*, *17*, 10.1029/2001PA000749.

Stuiver, M., and P. J. Reimer (1993), Extended ^{14}C database and revised CALIB radiocarbon calibration program, *Radiocarbon*, *35*, 215-230.

Stuiver, M., P. J. Reimer, and T. F. Braziunas (1998), High-precision radiocarbon age calibration for terrestrial and marine samples, *Radiocarbon*, *40*, 1127-1151.

Tables

Table 1. AMS dates and calendar ages*.

Depth (cm)	MCD (cm)	Species	NOSAMS ID	AMS Date	AMS Error	1 or 2 σ	Age Lower (yrs BP)	Age Upper (yrs BP)	Age (yrs BP)
ODP Site 984C 1H-01(A)									
0-2	1	*G. bulloides*	OS-19325	805	40	1	415	489	446
						2	333	506	
30-32	31	*G. bulloides*	OS-36742	1,440	35	1	940	1,029	985
						2	906	1,072	
58-60	59	*G. bulloides*	OS-36743	2,200	40	1	1,743	1,854	1,798
						2	1,689	1,900	
94-96	95	*G. bulloides*	OS-19326	3,690	40	1	3,550	3,667	3,604
						2	3,470	3,716	
122-124	123	*G. bulloides*	OS-36744	4,380	40	1	4,441	4,576	4,524
						2	4,406	4,655	
ODP Site 984C 1H-02(A)									
12-14	163	*G. bulloides*	OS-36745	5,670	45	1	6,009	6,148	6,075
						2	5,942	6,190	
44-46	195	*G. bulloides*	OS-19322	6,830	65	1	7,293	7,412	7,350
						2	7,228	7,471	
64-66	215	*G. bulloides*	OS-36746	7,390	50	1	7,808	7,919	7,857
						2	7,733	7,956	
103-104	253.5	*G. bulloides*	OS-22738	8,730	55	1	9,354	9,473	9,408
						2	9,276	9,508	
123-124	273.5	*G. bulloides*	OS-22943	9,360	45	1	10,161	10,237	10,204
						2	10,116	10,326	
133-134	283.5	*G. bulloides*	OS-22740	9,410	55	1	10,187	10,319	10,259
						2	10,152	10,407	

* AMS radiocarbon dates were converted to calendar age using CALIB 5.01 [*Stuiver and Reimer,* 1993], the Marine04 dataset [*Hughen et al.,* 2004], and a reservoir correction of 400 years.

Table 2. ODP Site 984 *N. pachyderma* (d.) Mg/Ca data.

Depth (cm)	Composite Depth (cm)	Age (yrs BP)	Mean Test Weight (µg)	[Ca] ppm	Mg/Ca (mmol mol^{-1})	Mean Mg/Ca (mmol mol^{-1})	Temperature (°C; EG*)
984C 1H-01(A)							
7	7	554	4.5	38	1.28	1.28	9.0
9	10	608	4.4	31	1.04	1.04	6.9
11	11	626	5.7	29	1.18	1.18	8.2
17	17	733	5.9	44	1.09	1.17	8.1
17	17	733	5.9	33	1.26		
19	19	769	5.2	49	1.00	1.00	6.6
31	31	985	5.6	42	1.00	1.00	6.6
33	33	1,043	5.3	37	1.18	1.18	8.2
37	37	1,159	6.3	53	1.13	1.13	7.7
39	39	1,217	6.3	51	1.18	1.18	8.2
47	47	1,450	6.0	55	1.33	1.52	10.7
47	47	1,450	6.0	37	1.71		
49	49	1,508	6.0	36	1.27	1.27	9.0
51	51	1,566	5.2	42	1.51	1.51	10.7
53	53	1,624	5.5	37	0.95	0.95	6.0
57	57	1,740	4.7	38	1.10	1.10	7.5
59	59	1,798	6.1	43	1.14	1.13	7.7
59	59	1,798	6.1	68	1.11		
67	67	2,199	4.0	56	1.12	1.12	7.6
69	69	2,300	4.0	63	1.17	1.17	8.1
71	71	2,400	3.8	54	1.18	1.18	8.2
73	73	2,500	4.1	56	1.18	1.18	8.2
77	77	2,701	4.0	34	1.23	1.23	8.6
79	79	2,801	4.8	29	1.39	1.39	9.9
87	87	3,203	3.9	40	1.31	1.31	9.3
89	89	3,303	3.0	44	1.10	1.08	7.3
89	89	3,303	3.0	34	1.06		
91	91	3,403	4.7	37	1.31	1.30	9.2
91	91	3,403	4.7	30	1.30		
93	93	3,504	5.2	41	1.05	1.05	7.0
97	97	3,670	4.9	33	1.00	1.00	6.6
99	99	3,735	5.8	40	1.22	1.22	8.5
103	103	3,867	5.4	45	1.26	1.26	8.8
107	107	3,998	5.4	46	1.26	1.26	8.8
109	109	4,064	7.2	61	1.46	1.51	10.7
109	109	4,064	7.2	36	1.56		
111	111	4,130	5.6	32	1.41	1.41	10.0
113	113	4,195	6.4	58	1.24	1.17	8.1
113	113	4,195	6.4	32	1.10		
115	115	4,261	5.9	56	1.40	1.50	10.6
115	115	4,261	5.9	28	1.60		
119	119	4,393	5.6	33	1.26	1.26	8.9
123	123	4,524	5.0	46	1.22	1.32	9.3
123	123	4,524	5.0	34	1.42		
127	127	4,679	5.6	40	1.22	1.20	8.4

Table 2 (cont.).

Depth (cm)	Composite Depth (cm)	Age (yrs BP)	Mean Test Weight (µg)	[Ca] ppm	Mg/Ca (mmol mol^{-1})	Mean Mg/Ca (mmol mol^{-1})	Temperature (°C; EG*)
984C 1H-01(A)							
127	127	4,679	5.6	41	1.18		
129	129	4,757	5.6	43	1.26	1.26	8.8
131	131	4,834	6.4	36	1.25	1.25	8.7
133	133	4,912	5.9	36	1.36	1.36	9.6
137	137	5,067	6.2	37	1.30	1.30	9.2
139	139	5,144	4.5	36	1.24	1.24	8.7
145	145	5,377	6.9	36	1.19	1.36	9.6
145	145	5,377	6.9	50	1.52		
147	147	5,455	4.9	70	1.08	1.09	7.4
147	147	5,455	4.9	50	1.11		
149	149	5,532	5.7	57	1.21	1.21	8.4
984C 1H-02(A)							
1	151	5,610	6.2	68	1.18	1.31	9.2
1	151	5,610	6.2	30	1.43		
3	153	5,687	6.0	36	1.09	1.09	7.4
5	155	5,765	5.7	29	1.28	1.28	9.0
7	157	5,842	5.6	27	1.19	1.19	8.2
9	159	5,920	5.7	54	1.18	1.18	8.2
13	163	6,075		40	1.29	1.29	9.1
15	165	6,155	5.9	39	1.26	1.26	8.8
17	167	6,234	5.6	41	1.30	1.30	9.2
19	169	6,314	6.0	29	1.22	1.22	8.5
23	173	6,473	5.6	59	1.16	1.16	8.0
25	175	6,553	5.8	47	1.17	1.17	8.1
25	175	6,553	5.8	62	1.17		
27	177	6,633	5.8	64	1.22	1.22	8.5
29	179	6,713	5.6	44	1.15	1.15	7.9
33	183	6,872	6.0	55	1.20	1.20	8.4
35	185	6,952	5.5	55	1.25	1.25	8.7
37	187	7,031	5.1	31	1.10	1.10	7.5
39	189	7,111	5.2	44	1.07	1.07	7.2
43	193	7,270	5.9	44	1.16	1.16	8.0
45	195	7,350	5.5	30	1.07	1.07	7.2
49	199	7,451	5.4	55	1.01	1.01	6.6
53	203	7,553	6.2	55	1.25	1.25	8.8
57	207	7,654	5.4	44	1.23	1.23	8.6
61	211	7,756	6.1	26	1.17	1.17	8.1
63	213	7,806	6.4	28	1.25	1.17	8.1
63	213	7,806		65	1.10		
65	215	7,857	5.8	62	1.19	1.10	7.5
65	215	7,857	5.8	32	1.02		
67	217	7,938	6.1	43	1.10	1.10	7.5

Table 2 (cont.).

Depth (cm)	Composite Depth (cm)	Age (yrs BP)	Mean Test Weight (µg)	[Ca] ppm	Mg/Ca (mmol mol^{-1})	Mean Mg/Ca (mmol mol^{-1})	Temperature (°C; EG*)
984C 1H-02(A)							
67	217	7,938	6.1	45	1.11		
69	219	8,018	6.2	51	1.01	1.02	6.7
69	219	8,018	6.2	37	1.02		
73	223	8,179	7.0	52	1.00	0.95	6.0
73	223	8,179	7.0	50	0.90		
75	225	8,260	6.1	56	0.94	0.91	5.6
75	225	8,260	6.1	44	0.88		
77	227	8,340	6.6	51	1.00	1.00	6.6
77	227	8,340	6.6	34	1.00		
79	229	8,421	5.9	57	1.15	1.15	7.9
81	231	8,502	6.7	43	1.09	1.10	7.5
81	231	8,502	6.7	38	1.12		
83	233	8,582	7.3	49	1.16	1.09	7.4
83	233	8,582	7.3	51	1.02		
85	235	8,663		54	1.14	1.11	7.6
85	235	8,663		52	1.08		
87	237	8,743	6.1	61	1.00	1.03	6.8
87	237	8,743	6.1	46	1.07		
89	239	8,824	6.6	63	1.04	1.12	7.7
89	239	8,824	6.6	52	1.20		
93	243	8,985	6.5	51	1.08	1.18	8.2
93	243	8,985	6.5	45	1.28		
95	245	9,066	6.4	48	1.11	1.11	7.6
97	247	9,146	6.2	43	1.03	1.03	6.8
99	249	9,227	6.1	53	0.94	0.94	6.0
101	251	9,307	7.5	65	0.93	0.93	5.9
103	253	9,388	7.6	50	0.98	0.98	6.3
105	255	9,468		74	1.08	1.08	7.3
107	257	9,547	8.0	52	0.94	0.94	5.9
109	259	9,627	8.3	64	1.01	1.01	6.6
113	263	9,786	7.4	65	1.04	1.16	8.0
113	263	9,786	7.4	36	1.28		
117	267	9,945	7.6	44	0.96	0.96	6.1
119	269	10,025	7.8	52	1.30	1.07	7.3
119	269	10,025	7.8	65	0.85		
123	273	10,184	7.1	60	1.04	1.04	7.0
127	277	10,343	7.8	60	1.05	1.05	7.0
129	279	10,423	8.4	63	1.09	1.09	7.4

* Temperatures were calculated using the equation of Elderfield and Ganssen [2000].

Table 3. ODP Site 984 *N. pachyderma* (d.) $\delta^{18}O$ data.

Depth (cm)	Composite Depth (cm)	Age (yrs BP)	$\delta^{18}O$ (‰)	Mean $\delta^{18}O$ (‰)
984C 1H-01(A)				
1	1	446	1.55	1.55
5	5	518	1.81	1.81
6	6	536	1.60	1.60
7	7	554	1.58	1.58
9	9	590	1.69	1.69
11	11	626	1.58	1.58
13	13	662	1.73	1.73
15	15	698	1.48	1.48
17	17	733	1.50	1.50
19	19	769	1.57	1.57
21	21	805	1.54	1.54
25	25	877	1.36	1.36
27	27	913	1.80	1.80
29	29	949	1.79	1.79
31	31	985	1.61	1.61
33	33	1,043	1.52	1.52
35	35	1,101	1.81	
35	35	1,101	1.72	1.76
36	36	1,130	1.44	1.44
37	37	1,159	1.52	1.52
41	41	1,275	1.24	1.24
45	45	1,392	1.54	1.54
49	49	1,508	1.48	1.48
51	51	1,566	1.53	1.53
55	55	1,682	1.56	1.56
57	57	1,740	1.50	1.50
59	59	1,798	1.66	1.66
61	61	1,898	1.54	1.54
64	64	2,049	1.81	1.81
65	65	2,099	1.73	1.73
66	66	2,149	1.70	1.70
67	67	2,199	1.55	1.55
69	69	2,300	1.65	1.65
75	75	2,601	1.54	1.54
77	77	2,701	1.51	1.51
79	79	2,801	1.58	1.58
81	81	2,902	1.26	1.26
85	85	3,102	1.27	1.27
87	87	3,203	1.45	1.45
89	89	3,303	1.67	1.67
91	91	3,403	1.59	1.59
93	93	3,504	1.70	1.70
95	95	3,604	1.77	
95	95	3,604	1.65	1.71
96	96	3,637	1.68	1.68
97	97	3,670	1.61	

Table 3 (cont.).

Depth (cm)	Composite Depth (cm)	Age (yrs BP)	$\delta^{18}O$ (‰)	Mean $\delta^{18}O$ (‰)
984C 1H-01(A)				
97	97	3,670	1.71	1.66
99	99	3,735	1.52	1.52
101	101	3,801	1.49	1.49
103	103	3,867	1.56	1.56
105	105	3,933	1.50	1.50
107	107	3,998	1.64	1.64
109	109	4,064	1.83	
109	109	4,064	1.59	1.71
111	111	4,130	1.55	1.55
113	113	4,195	1.64	1.64
115	115	4,261	1.32	1.32
117	117	4,327	1.64	1.64
119	119	4,393	1.64	1.64
121	121	4,458	1.57	1.57
123	123	4,524	1.68	1.68
125	125	4,602	1.43	1.43
127	127	4,679	1.59	1.59
129	129	4,757	1.60	1.60
131	131	4,834	0.47	0.47
133	133	4,912	1.61	1.61
135	135	4,989	1.65	
135	135	4,989	1.73	1.69
136	136	5,028	1.72	1.72
139	139	5,144	1.57	1.57
141	141	5,222	1.64	1.64
145	145	5,377	1.31	1.31
147	147	5,455	1.54	1.54
149	149	5,532	1.58	1.58
984C 1H-02(A)				
1	151	5,610	1.63	1.63
3.5	153.5	5,707	2.12	2.12
5	155	5,765	1.64	1.64
6	156	5,804	1.60	1.60
7	157	5,842	1.58	1.58
9	159	5,920	1.60	1.60
13	163	6,075	1.57	1.57
15	165	6,155	1.63	1.63
16	166	6,195	1.48	1.48
17	167	6,234	1.54	1.54
21	171	6,394	1.53	1.53
23	173	6,473	1.52	1.52
25	175	6,553	1.44	
25	175	6,553	1.40	1.42

Table 3 (cont.).

Depth (cm)	Composite Depth (cm)	Age (yrs BP)	$\delta^{18}O$ (‰)	Mean $\delta^{18}O$ (‰)
984C 1H-02(A)				
27	177	6,633	1.45	1.45
29	179	6,713	1.44	1.44
33	183	6,872	1.50	1.50
35	185	6,952	1.29	1.29
37	187	7,031	1.47	1.47
39	189	7,111	1.57	1.57
41	191	7,191	1.63	1.63
43	193	7,270	1.34	1.34
45	195	7,350	2.31	
45	195	7,350	1.61	1.96
46	196	7,375	1.34	1.34
47	197	7,401	1.44	1.44
49	199	7,451	1.66	1.66
53	203	7,553	1.43	1.43
55	205	7,604	1.68	1.68
57	207	7,654	1.51	1.51
59	209	7,705	1.53	1.53
61	211	7,756	1.34	1.34
63	213	7,806	1.21	1.21
65	215	7,857	1.49	1.49
67	217	7,938	1.53	1.53
69	219	8,018	1.52	1.52
73	223	8,179	1.58	1.58
75	225	8,260	1.43	1.43
76	226	8,300	1.47	1.47
77	227	8,340	1.56	1.56
79	229	8,421	1.50	1.50
81	231	8,502	1.47	1.47
83	233	8,582	1.58	1.58
85	235	8,663	1.72	1.72
87	237	8,743	1.63	1.63
89	239	8,824	1.52	1.52
93	243	8,985	1.59	1.59
95	245	9,066	1.61	1.61
97	247	9,146	1.60	1.60
99	249	9,227	1.56	1.56
101	251	9,307	1.57	1.57
103	253	9,388	1.57	1.57
103.5	253.5	9,408	1.84	1.84
105	255	9,468	1.65	1.65
106	256	9,508	1.69	1.69
107	257	9,547	1.61	1.61
109	259	9,627	1.63	1.63
113	263	9,786	1.72	1.72
115	265	9,866	1.78	1.78
117	267	9,945	1.80	1.80

Table 3 (cont.).

Depth (cm)	Composite Depth (cm)	Age (yrs BP)	$\delta^{18}O$ (‰)	Mean $\delta^{18}O$ (‰)
984C 1H-02(A)				
119	269	10,025	1.71	1.71
121	271	10,105	1.77	
121	271	10,105	1.70	1.74
123	273	10,184	1.95	1.95
123.5	273.5	10,204	2.01	2.01
125	275	10,264	1.68	1.68
129	279	10,423	1.68	1.68
133.5	283.5	10,602	1.65	1.65
135	285	10,662	1.78	1.78
141	291	10,901	1.77	1.77
143.5	293.5	11,000	2.16	2.16
146	296	11,100	1.66	1.66

Table 4. ODP Site 984 residual seawater $\delta^{18}O$.

Composite Depth (cm)	Age (yrs BP)	Smoothed Temp (°C)	Smoothed $\delta^{18}O_C$ Uncorrected (‰)	Ice Volume Correction* (‰)	Smoothed $\delta^{18}O_C$ Corrected (‰)	$\delta^{18}O_{SW}$** Corrected (‰)
984C 1H-01(A)						
1	446					
5	518		1.65	-0.01	1.66	
6	536		1.66	-0.01	1.67	
7	554		1.62	-0.01	1.63	
9	590		1.62	-0.01	1.63	
10	608	8.0				
11	626	7.7	1.67	-0.01	1.68	0.11
13	662		1.60	-0.01	1.61	
15	698		1.57	-0.01	1.59	
17	733	7.6	1.52	-0.02	1.53	-0.06
19	769	7.1	1.54	-0.02	1.55	-0.13
21	805		1.49	-0.02	1.50	
25	877		1.57	-0.02	1.58	
27	913		1.65	-0.02	1.67	
29	949		1.73	-0.02	1.75	
31	985	7.1	1.64	-0.02	1.66	-0.02
33	1,043	7.5	1.63	-0.02	1.65	0.03
35	1,101		1.57	-0.02	1.59	
36	1,130		1.57	-0.02	1.59	
37	1,159	8.0	1.40	-0.02	1.42	-0.11
39	1,217	8.9				
41	1,275		1.43	-0.02	1.45	
45	1,392		1.42	-0.02	1.44	
47	1,450	9.3				
49	1,508	10.1	1.52	-0.02	1.53	0.35
51	1,566	8.5	1.53	-0.02	1.54	0.10
53	1,624	8.0				
55	1,682		1.53	-0.01	1.54	
57	1,740	7.1	1.57	-0.01	1.59	-0.10
59	1,798	7.6	1.56	-0.01	1.58	-0.02
61	1,898		1.67	-0.01	1.68	
64	2,049		1.69	-0.01	1.70	
65	2,099		1.75	-0.01	1.75	
66	2,149		1.66	-0.01	1.67	
67	2,199	7.8	1.63	-0.01	1.64	0.08
69	2,300	8.0	1.58	-0.01	1.59	0.05
71	2,400	8.2				
73	2,500	8.3				
75	2,601		1.57	0.00	1.57	
77	2,701	8.9	1.54	0.00	1.54	0.15
79	2,801	9.2	1.45	0.00	1.45	0.12
81	2,902		1.37	0.01	1.36	
85	3,102		1.33	0.01	1.32	
87	3,203	8.8	1.46	0.01	1.45	0.05
89	3,303	8.6	1.57	0.01	1.56	0.12

Table 4 (cont.).

Composite Depth (cm)	Age (yrs BP)	Smoothed Temp (°C)	Smoothed $\delta^{18}O_c$ Uncorrected (‰)	Ice Volume Correction* (‰)	Smoothed $\delta^{18}O_c$ Corrected (‰)	$\delta^{18}O_{sw}$** Corrected (‰)
984C 1H-01(A)						
91	3,403	7.8	1.65	0.01	1.64	0.08
93	3,504	7.6	1.67	0.01	1.66	0.06
95	3,604		1.70	0.01	1.69	
96	3,637		1.68	0.01	1.67	
97	3,670	7.4	1.62	0.01	1.61	-0.02
99	3,735	8.0	1.56	0.01	1.55	0.01
101	3,801		1.52	0.01	1.51	
103	3,867	8.7	1.52	0.01	1.51	0.10
105	3,933		1.57	0.01	1.56	
107	3,998	9.5	1.62	0.01	1.61	0.31
109	4,064	9.8	1.63	0.01	1.62	0.39
111	4,130	9.6	1.63	0.01	1.62	0.35
113	4,195	9.6	1.50	0.01	1.49	0.21
115	4,261	9.2	1.54	0.02	1.52	0.18
117	4,327		1.54	0.02	1.52	
119	4,393	9.6	1.62	0.02	1.59	0.32
121	4,458		1.63	0.03	1.60	
123	4,524	8.8	1.56	0.03	1.53	0.14
125	4,602		1.57	0.03	1.54	
127	4,679	8.8	1.54	0.03	1.51	0.11
129	4,757	8.6	1.60	0.03	1.57	0.14
131	4,834	9.1				
133	4,912	9.2	1.63	0.04	1.59	0.25
135	4,989		1.67	0.04	1.63	
136	5,028		1.66	0.05	1.61	
137	5,067	9.2				
139	5,144	9.2	1.64	0.05	1.59	0.25
141	5,222		1.50	0.06	1.45	
145	5,377	8.6	1.49	0.07	1.43	-0.01
147	5,455	8.5	1.48	0.07	1.41	-0.05
149	5,532	8.4	1.58	0.07	1.51	0.04
984C 1H-02(A)						
151	5,610	8.4	1.62	0.08	1.54	0.07
153	5,687	8.6				
155	5,765	8.2	1.62	0.09	1.54	0.04
156	5,804		1.61	0.09	1.52	
157	5,842	8.5	1.59	0.09	1.50	0.05
159	5,920	8.5	1.58	0.09	1.49	0.04
163	6,075	8.7	1.60	0.10	1.50	0.08
165	6,155	9.0	1.56	0.11	1.45	0.09
166	6,195		1.55	0.11	1.44	
167	6,234	8.8	1.52	0.11	1.40	0.01

Table 4 (cont.).

Composite Depth (cm)	Age (yrs BP)	Smoothed Temp (°C)	Smoothed $\delta^{18}O_c$ Uncorrected (‰)	Ice Volume Correction* (‰)	Smoothed $\delta^{18}O_c$ Corrected (‰)	$\delta^{18}O_{sw}$** Corrected (‰)
984C 1H-02(A)						
169	6,314	8.6				
171	6,394		1.53	0.13	1.40	
173	6,473	8.2	1.49	0.13	1.36	-0.14
175	6,553	8.2	1.46	0.14	1.33	-0.17
177	6,633	8.2	1.44	0.14	1.30	-0.21
179	6,713	8.3	1.47	0.15	1.32	-0.17
183	6,872	8.3	1.41	0.16	1.26	-0.22
185	6,952	8.2	1.42	0.16	1.26	-0.24
187	7,031	7.8	1.44	0.17	1.27	-0.29
189	7,111	7.6	1.56	0.18	1.38	-0.22
191	7,191		1.51	0.19	1.32	
193	7,270	7.5	1.53	0.20	1.33	-0.28
195	7,350	7.3	1.43	0.20	1.23	-0.42
196	7,375		1.46	0.21	1.26	
197	7,401		1.48	0.21	1.27	
199	7,451	7.5	1.51	0.21	1.30	-0.31
203	7,553	8.0	1.59	0.22	1.37	-0.16
205	7,604		1.54	0.22	1.32	
207	7,654	8.5	1.57	0.23	1.34	-0.11
209	7,705		1.46	0.24	1.22	
211	7,756	8.3	1.36	0.24	1.12	-0.36
213	7,806	7.9	1.35	0.25	1.10	-0.44
215	7,857	7.7	1.41	0.25	1.16	-0.42
217	7,938	7.3	1.51	0.26	1.26	-0.40
219	8,018	6.8	1.54	0.26	1.28	-0.46
223	8,179	6.1	1.51	0.28	1.24	-0.61
225	8,260	6.1	1.50	0.28	1.22	-0.64
226	8,300		1.49	0.28	1.21	
227	8,340	6.7	1.51	0.29	1.22	-0.52
229	8,421	7.3	1.51	0.29	1.22	-0.42
231	8,502	7.6	1.52	0.29	1.23	-0.37
233	8,582	7.5	1.59	0.30	1.30	-0.32
235	8,663	7.3	1.64	0.30	1.34	-0.31
237	8,743	7.4	1.62	0.31	1.32	-0.32
239	8,824	7.6	1.58	0.31	1.27	-0.33
243	8,985	7.8	1.57	0.32	1.26	-0.31
245	9,066	7.5	1.60	0.32	1.28	-0.33
247	9,146	6.8	1.59	0.32	1.27	-0.46
249	9,227	6.2	1.58	0.33	1.25	-0.58
251	9,307	6.0	1.57	0.33	1.24	-0.62
253	9,388	6.5	1.66	0.34	1.33	-0.45
253.5	9,408		1.69	0.34	1.35	
255	9,468	6.5	1.73	0.34	1.39	-0.38
256	9,508		1.65	0.34	1.31	
257	9,547	6.6	1.64	0.35	1.30	-0.46

Table 4 (cont.).

Composite Depth (cm)	Age (yrs BP)	Smoothed Temp (°C)	Smoothed $\delta^{18}O_c$ Uncorrected (‰)	Ice Volume Correction* (‰)	Smoothed $\delta^{18}O_c$ Corrected (‰)	$\delta^{18}O_{sw}$** Corrected (‰)
984C 1H-02(A)						
259	9,627	6.9	1.65	0.35	1.30	-0.42
263	9,786	6.9	1.71	0.36	1.35	-0.36
265	9,866		1.77	0.36	1.41	
267	9,945	7.1	1.76	0.37	1.40	-0.28
269	10,025	6.8	1.75	0.37	1.38	-0.35
271	10,105		1.80	0.37	1.43	
273	10,184	7.1	1.90	0.38	1.52	-0.16
273.5	10,204		1.88	0.38	1.50	
275	10,264		1.82	0.38	1.44	
277	10,343	7.1	1.71	0.38	1.33	-0.35
279	10,423		1.70	0.38	1.32	

* Ice volume correction is from Waelbroeck *et al.* [2002].

** Seawater $\delta^{18}O$ was calculated using the equation of von Langen [2001].

Chapter 3. Atlantic Ocean circulation during the Younger Dryas: Insights from a new Cd/Ca record from the western subtropical South Atlantic

(Reprinted with permission from *Paleoceanography*)

Rosemarie E. Came
Massachusetts Institute of Technology/Woods Hole Oceanographic Institution Joint Program in Oceanography, Woods Hole, Massachusetts

Delia W. Oppo, and William B. Curry
Department of Geology and Geophysics, Woods Hole Oceanographic Institution, Woods Hole, Massachusetts

Abstract

Benthic foraminiferal Cd/Ca from an intermediate depth, western South Atlantic core documents the history of southward penetration of North Atlantic Intermediate Water (NAIW). Cd seawater estimates (Cd_w) for the last glacial are consistent with the production of NAIW and its export into the South Atlantic. At ~14.5 kyr, the NAIW contribution to the South Atlantic began to decrease, marking a transition from a glacial circulation pattern to a Younger Dryas circulation, which occurred concurrently with the onset of the Bølling-Allerød to Younger Dryas cooling. High Cd_w in both the deep North Atlantic and the intermediate South Atlantic imply reduced export of deep and intermediate water during the Younger Dryas, and a significant decrease in northward oceanic heat transport. A modern circulation was reached at ~9 kyr, concurrently with the establishment of Holocene warmth in the North Atlantic region, further supporting a close linkage between deepwater variability and North Atlantic climate.

PALEOCEANOGRAPHY, VOL. 18, NO. 4, 1086, doi:10.1029/2003PA000888, 2003

Atlantic Ocean circulation during the Younger Dryas: Insights from a new Cd/Ca record from the western subtropical South Atlantic

Rosemarie E. Came

Massachusetts Institute of Technology/Woods Hole Oceanographic Institution Joint Program in Oceanography, Woods Hole, Massachusetts, USA

Delia W. Oppo and William B. Curry

Department of Geology and Geophysics, Woods Hole Oceanographic Institution, Woods Hole, Massachusetts, USA

Received 31 January 2003; revised 14 June 2003; accepted 15 August 2003; published 25 November 2003.

[1] Benthic foraminiferal Cd/Ca from an intermediate depth, western South Atlantic core documents the history of southward penetration of North Atlantic Intermediate Water (NAIW). Cd seawater estimates (Cd_W) for the last glacial are consistent with the production of NAIW and its export into the South Atlantic. At ~14.5 ka concurrently with the onset of the Bølling-Allerød to Younger Dryas cooling, the NAIW contribution to the South Atlantic began to decrease, marking the transition from a glacial circulation pattern to a Younger Dryas circulation. High Cd_W in both the deep North Atlantic and the intermediate South Atlantic imply reduced export of deep and intermediate water during the Younger Dryas and a significant decrease in northward oceanic heat transport. A modern circulation was achieved at ~9 ka, concurrently with the establishment of Holocene warmth in the North Atlantic region, further supporting a close linkage between deepwater variability and North Atlantic climate. *INDEX TERMS:* 4267 Oceanography: General: Paleoceanography; 4875 Oceanography: Biological and Chemical: Trace elements; 4870 Oceanography: Biological and Chemical: Stable isotopes; *KEYWORDS:* Cd/Ca, $\delta^{13}C$, Younger Dryas, intermediate water, foraminifera

Citation: Came, R. E., D. W. Oppo, and W. B. Curry, Atlantic Ocean circulation during the Younger Dryas: Insights from a new Cd/Ca record from the western subtropical South Atlantic, *Paleoceanography, 18*(4), 1086, doi:10.1029/2003PA000888, 2003.

1. Introduction

[2] A large body of evidence suggests that several abrupt millennial-scale climate changes occurred during the last deglaciation [*Dansgaard et al.*, 1993; *Bond et al.*, 1993; *Lehman and Keigwin*, 1992]. The most notable of these deglacial climate events was the Younger Dryas, a brief return to near-glacial temperatures in the North Atlantic that began ~13,000 years ago and lasted ~1500 years. The Younger Dryas cooling has been observed in many North Atlantic climate proxies, including oxygen isotopes in Greenland ice cores [*Dansgaard*, 1984] and the faunal assemblages of planktonic foraminifera in the North Atlantic [*Ruddiman and McIntyre*, 1981].

[3] Major changes in the Atlantic Ocean's meridional overturning cell (MOC) may amplify millennial-scale climate variations in the North Atlantic. A decrease in the strength of the MOC would cause a reduction in the amount of heat transported by the upper ocean to the North Atlantic and therefore would cool the northern high latitudes [*Broecker et al.*, 1985a]. Models predict that a large decrease in the strength of the MOC also warms the surface and thermocline of the lower latitudes as a result of the reduced northward export of heat [*Manabe and Stouffer*, 1997; *Rahmstorf*, 1994; *Marchal et al.*, 1999]. Alkenone-derived temperature estimates from the tropics suggest that such a warming did occur during the Younger Dryas, with sea surface temperatures increasing by 1.2°C [*Rühlemann et al.*, 1999]. However, recent modeling studies [*Manabe and Stouffer*, 1997; *Marchal et al.*, 1999] suggest that only dramatic reductions in MOC could cause tropical warming. Thus a very large reduction in MOC would be consistent with the evidence suggesting a warming of the tropics during the Younger Dryas.

[4] Nutrient proxies may be used to trace changes in ocean water mass geometry. In the modern ocean, North Atlantic Deep Water (NADW) forms in the northern Atlantic Ocean when surface water loses heat, becomes extremely dense, and sinks to great depths. Because surface water is relatively nutrient depleted, the NADW that originates from it is also nutrient depleted, causing a southward penetrating tongue of nutrient-depleted deep water. By contrast, Circumpolar Deep Water forms in the Southern Ocean from relatively nutrient enriched waters that upwell from great depth [e.g., *Broecker et al.*, 1985b]. Thus the pattern of nutrient distributions in the Atlantic Ocean reflects deepwater circulation patterns.

[5] Cd and $\delta^{13}C$ are two nutrient proxies used to trace deepwater circulation [*Boyle and Keigwin*, 1982; *Curry and Lohman*, 1982; *Boyle*, 1988; *Curry et al.*, 1988; *Duplessy et al.*, 1988]. Cd is a trace metal incorporated into organisms proportionately to other nutrients, resulting in a positive

0883-8305/03/2003PA000888$12.00

correlation between Cd seawater (Cd_W) concentrations and oceanic PO_4 concentrations. Benthic foraminifera incorporate Cd into their $CaCO_3$ tests in direct proportion to the Cd concentration in the water in which they calcify. Thus the Cd/Ca ratio of the tests can be used as an indicator of the concentration of Cd (and thus PO_4) in the water at the time the foraminifera tests formed [*Hester and Boyle*, 1982]. The $\delta^{13}C$ distribution is the result of the isotopic fractionation of carbon associated with photosynthesis, which favors ^{12}C over ^{13}C. The remineralization at depth of low-$\delta^{13}C$ organic material produces a negative correlation between the $\delta^{13}C$ of dissolved inorganic carbon ($\delta^{13}C_{DIC}$) and PO_4 [e.g., *Kroopnick*, 1985]. Like Cd_W, the oceanic $\delta^{13}C_{DIC}$ signal is recorded in the tests of benthic foraminifera. Thus benthic foraminifera can be used to infer past water mass geometry: Low Cd and high $\delta^{13}C$ are indicative of a nutrient-depleted northern source, while high Cd and low $\delta^{13}C$ are indicative of a nutrient-enriched southern source.

[6] The $\delta^{13}C$ distribution, however, is complicated by the influence of the $\delta^{13}C$ air-sea exchange signature ($\delta^{13}C_{AS}$). When ocean water has contact with the atmosphere, a temperature-dependent fractionation of the carbon isotopes in CO_2 occurs [*Mook et al.*, 1974]. For a given atmospheric $\delta^{13}C$, colder temperatures result in higher $\delta^{13}C_{DIC}$. However, since different parcels of water spend varying amounts of time in contact with the atmosphere, the degree to which a parcel equilibrates with the atmosphere also varies. High wind speeds increase exchange rates, bringing the $\delta^{13}C_{DIC}$ closer to equilibrium with the atmosphere [*Liss and Merlivat*, 1986; *Broecker and Maier-Reimer*, 1992].

[7] Changes in Cd/Ca and $\delta^{13}C$ have been used to trace the past changes in the ocean's subsurface geometry. During the last glacial, deep waters of the North Atlantic were nutrient enriched relative to the present, and intermediate waters were nutrient depleted, suggesting a reduction in NADW formation and an increase in Glacial North Atlantic Intermediate Water (GNAIW) formation [*Boyle and Keigwin*, 1987]. Many studies have confirmed this glacial subsurface geometry of GNAIW overlying waters of southern origin [*Duplessy et al.*, 1988; *Oppo and Lehman*, 1993; *Marchitto et al.*, 2002]. There are conflicting interpretations for the subsurface geometry during the Younger Dryas. It has been suggested that deepwater formation decreased [*Boyle and Keigwin*, 1987] and intermediate water formation increased, signifying a glacial-like stratification for the Younger Dryas [*Marchitto et al.*, 1998; *Zahn and Stüber*, 2002]. Alternatively, *Sarnthein et al.* [2001] have suggested that MOC during the early Younger Dryas was similar to the modern mode, with significant NADW formation and little NAIW formation. They suggest that deepwater reduction occurred late, near the end of the Younger Dryas. Because the production of NADW at high latitudes results in greater heat loss to the atmosphere than the production of intermediate water at lower latitudes, the above interpretations predict very different roles of the MOC in cooling the North Atlantic during the Younger Dryas. Thus it is clear that a better understanding of changes in subsurface geometries is necessary in order to understand how oceanic heat transport changes on millennial timescales. In this study, we present a new record of intermediate depth variability using Cd/Ca data from a South Atlantic core to determine the response of North Atlantic Intermediate Water during the Younger Dryas.

2. Study Area

[8] Sediment core KNR159-5-36GGC (36GGC) was taken from the Brazilian margin at 27°31′S and 46°28′W, 1268 m (Figure 1). Today, the core site lies within waters that are a mixture of Upper Circumpolar Deep Water, Antarctic Intermediate Water (AAIW), and Labrador Sea Water [*Oppo and Horowitz*, 2000]. During the last glacial, water at this location consisted of at least one-third GNAIW but may have been entirely GNAIW (aged) [*Oppo and Horowitz*, 2000]. This core is ideally situated: It is directly in the flow path of GNAIW if this water mass exits the North Atlantic.

3. Methods

[9] Cd, Mn, and Ca concentrations were measured in the shells of the benthic foraminifera *Hoeglundina elegans*. This aragonitic species faithfully records bottom water Cd concentrations with a partition coefficient $D_P = [(Cd/Ca)_{foram}/(Cd/Ca)_{water}] \approx 1.0$ [*Boyle et al.*, 1995]. The partition coefficient of the aragonitic *H. elegans* is constant with depth, unlike the partition coefficients of calcitic foraminifera, which are depth dependent [*Boyle*, 1992]. A constant seawater Ca concentration of 0.01 mol kg^{-1} was assumed to estimate Cd seawater concentrations.

[10] Each sample consisted of approximately five individuals and was cleaned according to the methods of *Boyle and Keigwin* [1985] with a reversal of the oxidative and reductive steps to improve the removal of authigenic Cd deposits [*Boyle and Rosenthal*, 1996; *Rosenthal*, 1994; *Rosenthal et al.*, 1995]. Measurements were made using a Hitachi Z8200 atomic absorption spectrophotometer (AAS) tandem flame and graphite furnace. Cd and Mn were measured using graphite furnace AAS, and Ca was measured using flame AAS. Mn/Ca ratios were measured when possible in order to verify that manganese carbonate overgrowths are not a source of contamination at this site. Manganese carbonate overgrowths are a potential source of contamination in many species of benthic foraminifera [*Boyle*, 1983]. However, the species *H. elegans* was chosen for this study because it does not suffer from the contamination caused by such overgrowths [*Boyle et al.*, 1995].

[11] In order to assess the precision of measurements on the AAS, three consistency standards were treated as samples in each of the six runs in which the data were generated. Mean Cd/Ca values for the three consistency standards were 0.037, 0.089, and 0.127 μmol mol^{-1}. Standard deviations were 0.005, 0.004, and 0.007 μmol mol^{-1}, respectively. For *H. elegans*, which has a partition coefficient of 1, the resulting Cd_W errors range from 0.04 to 0.07 nmol kg^{-1}. Consistency standard data and sample data are available electronically.[1]

[1] Auxiliary consistency standard data and sample data are available electronicallly at World Data Center-A for Paleoclimatology, NOAA/NGDC, 325 Broadway, Boulder, CO 80303, USA. (paleo@mail.ngdc.noaa.gov; URL: http://www.ngdc.noaa.gov/paleo)

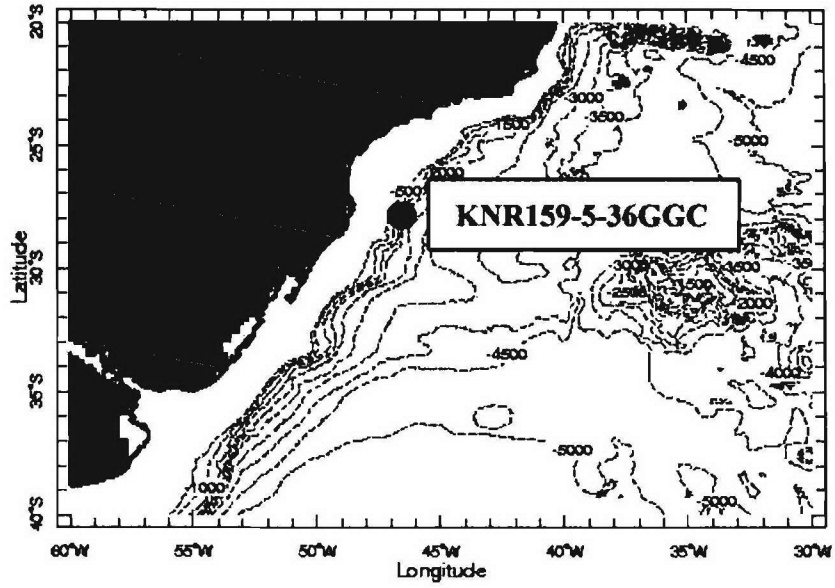

Figure 1. Map of the study area showing the location of core KNR159-5-36GGC (27°31′S, 46°28′W; 1268 m).

[12] For $\delta^{13}C$ determinations, *Oppo and Horowitz* [2000] used the species *Cibicidoides pachyderma* and a species that closely resembles *C. wuellerstorfi*. At one depth interval in this core (4 cm), $\delta^{13}C$ values were determined for both *C. wuellerstorfi* and the species that resembles it, and these values were found to be the same [*Oppo and Horowitz*, 2000]. In the western subtropical Atlantic, *C. pachyderma* and *C. wuellerstorfi* have the same $\delta^{13}C$ values as well [*Slowey and Curry*, 1995]. *Oppo and Horowitz* [2000] therefore concluded that the two species used for $\delta^{13}C$ measurements in this core are equivalent.

[13] Accelerator mass spectrometer (AMS) radiocarbon dates were obtained for 17 samples of the planktonic foraminifer *Globigerinoides ruber* and 1 sample of the benthic foraminifer *C. pachyderma*. AMS radiocarbon dates were converted to calendar age using the calibration program of *Stuiver and Reimer* [1993] (Table 1 and Figure 2). Overall, the data indicate a relatively constant sedimentation rate of slightly greater than 6 cm kyr^{-1} at this location, which is sufficient for resolution of the Younger Dryas. There is an age reversal in the chronology at 148 cm, where the age of the planktonic foraminifer *G. ruber* is ~14 kyr. However, the age of the benthic foraminifer *C. pachyderma* from the same sample (148 cm) is glacial, in close agreement with neighboring AMS dates. Benthic $\delta^{18}O$ and $\delta^{13}C$ values at this core depth are also typical of the last glacial and are distinctly different from those at ~14 kyr age (~90 cm) (Figure 2). Hence, while the benthic AMS date is not included in the determination of the age model, we proceed under the assumption that the *C. pachyderma* date more closely approximates the age of the sediment at this core level. We also note that the age reversal does not affect the deglacial portion of this core and hence our conclusions of the Younger Dryas.

[14] Additional AMS radiocarbon dates were obtained for deep North Atlantic core EN120-GGC1 (33°40′N, 57°37′W; 4450 m) and intermediate depth North Atlantic core OC205-2-103GGC (26°04′N, 78°03′W; 965 m) (Table 1). A new age model was developed for OC205-2-103GGC using the new and previously published dates [*Marchitto et al.*, 1998; *Curry et al.*, 1999]. The ages at 99.5 and 100 cm were averaged for the age model calculation.

4. Results and Discussion

[15] Average Cd_W values in core 36GGC range from a minimum value of 0.26 nmol kg^{-1} at 160 cm (19.4 kyr) to a maximum of 1.02 nmol kg^{-1} at 14 cm (2.9 kyr) (Figure 2). We have no explanation for the three anomalously high values that occur in the upper portion of the core, and a lack of sufficient *H. elegans* in this portion prevents further analysis. If the anomalously high values are removed, a maximum value of 0.64 nmol kg^{-1} is observed at 25.5 cm (4.3 kyr). Average glacial (0.40 nmol kg^{-1}) and Holocene (0.55 nmol kg^{-1}) Cd_W values determined using *H. elegans* are consistent with the previously published glacial *Uvigerina* spp. estimate of 0.43 nmol kg^{-1} and the modern seawater estimate of 0.67 nmol kg^{-1} [*Oppo and Horowitz*, 2000].

[16] The Cd_W data from Brazilian margin core 36GGC reveal an overall glacial-interglacial trend of increasing Cd_W values (Figures 2 and 3). The increase in Cd_W values at this intermediate depth site is indicative of increased nutrient concentrations and thus an overall decrease in the relative influence of northern source waters since the last glacial. These data are consistent with the work of *Boyle and Keigwin* [1987], who suggested that intermediate

Table 1. Accelerator Mass Spectrometer (AMS) Dates and Calendar Ages

Depth, cm	NOSAMS Number[a]	AMS Date	AMS Error	Calendar Age B.P.	Species	Source
				KNR159-5-36GGC		
1	OS-22674	1,740	30	1,283	*G. ruber*	this study
16	OS-25478	3,170	60	2,946	*G. ruber*	this study
28	OS-22675	4,450	40	4,606	*G. ruber*	this study
28	OS-22681	4,480	55	4,647	*G. ruber*	this study
40	OS-23216	6,000	35	6,402	*G. ruber*	this study
56	OS-22676	8,510	50	8,965	*G. ruber*	this study
60	OS-27350	9,450	50	10,262	*G. ruber*	this study
64	OS-25479	10,750	90	12,047	*G. ruber*	this study
68	OS-23210	10,600	45	11,683	*G. ruber*	this study
80	OS-23211	11,400	50	12,945	*G. ruber*	this study
88	OS-23212	12,200	50	13,674	*G. ruber*	this study
92	OS-22677	12,450	60	13,927	*G. ruber*	this study
104	OS-23318	13,550	60	15,691	*G. ruber*	this study
112	OS-23317	13,650	60	15,808	*G. ruber*	this study
141	OS-23213	14,850	120	17,192	*G. ruber*	this study
148	OS-22678	12,350	65	13,832	*G. ruber*	this study
148	OS-23214	16,050	65	18,573	*C. pachyderma*	this study
200	OS-22679	19,300	95	22,313	*G. ruber*	this study
				EN120-GGC1		
93	OS-33623	9,040	50	9,694	*G. ruber*	this study
107	OS-33624	10,850	60	12,212	*G. ruber*	this study
115	OS-33625	11,250	60	12,874	*G. ruber*	this study
115	OS-33626	11,200	65	12,838	*G. ruber*	this study
				OC205-2-103GGC		
10	OS-10523	920	35	518	*G. sacculifer*	*Marchitto et al.* [1998]
28	OS-26154	2,970	50	2,739	*G. sacculifer*	this study
42	OS-26155	3,850	35	3,815	*G. sacculifer*	this study
61	OS-26785	5,280	45	5,622	*G. sacculifer*	this study
62	OS-10524	5,290	45	5,636	*G. sacculifer*	*Marchitto et al.* [1998]
73	OS-26786	6,500	45	6,988	*G. sacculifer*	this study
88	OS-15376	7,630	45	8,073	*G. sacculifer*	*Curry et al.* [1999]
90	OS-33629	7,890	45	8,350	*G. ruber*	J. F. McManus, unpublished data, 2003
95.5	OS-33630	9,260	60	9,842	*G. ruber*	J. F. McManus, unpublished data, 2003
99.5	OS-33631	9,800	60	10,456	*G. ruber*	J. F. McManus, unpublished data, 2003
100	OS-26787	9,410	50	10,218	*G. sacculifer*	this study
105.5	OS-33632	10,400	55	11,334	*G. ruber*	J. F. McManus, unpublished data, 2003
113	OS-10526	11,000	50	12,472	*G. sacculifer*	*Marchitto et al.* [1998]
121	OS-10525	12,200	55	13,674	*G. sacculifer*	*Marchitto et al.* [1998]
134	OS-10527	17,100	100	19,781	*G. sacculifer*	*Marchitto et al.* [1998]

[a]NOSAMS is the National Ocean Sciences Accelerator Mass Spectrometer facility.

water formation was greater during the last glacial than it is today.

[17] Millennial-scale oscillations are superimposed on the glacial-interglacial trend. At ~14.5 ka, Cd_W values began to increase in concert with the gradual cooling observed in the Greenland Ice Sheet Project 2 (GISP2) ice core record (Figure 3). At ~12.8 ka a sharp depletion in the $\delta^{18}O$ of Greenland ice marks the rapid Northern Hemisphere cooling of the Younger Dryas. Concurrently, a more gradual increase is seen in the Cd_W concentration recorded in core 36GGC, culminating in peak values of 0.55 nmol kg^{-1} during the Younger Dryas, almost as high as interglacial values. These high values suggest an increase in nutrient concentrations at this intermediate depth site during the Younger Dryas, consistent with a decrease in the influence of northern source waters. Following the Younger Dryas, one lower Cd_W value at 36GGC suggests a possible resumption of northern source ventilation. Cd_W values soon increased, indicating a Holocene-like circulation with the contribution of nutrient-rich southern source waters.

[18] Comparison of the new Cd_W data with published data from the intermediate depth North Atlantic [*Marchitto et al.*, 1998] and from a deep North Atlantic site [*Boyle and Keigwin*, 1987] provides additional insight into the evolution of deep water since the last glacial. Figure 3 reveals three separate water mass geometries. During the period 14–20 ka both intermediate water sites were lower in Cd_W (and hence nutrients) than the deep North Atlantic, consistent with the interpretation of decreased NADW formation and increased GNAIW formation during the last glacial [*Boyle and Keigwin*, 1987]. At ~14 ka the deep North Atlantic became more nutrient depleted than the intermediate depth South Atlantic, marking an important transition between glacial and interglacial circulation. From ~9 to 14 ka, highest Cd_W values occurred in the intermediate depth South Atlantic, intermediate values occurred in the deep North Atlantic, and the lowest values occurred in the intermediate depth North Atlantic. At ~9 ka the modern geometry was firmly established: The North Atlantic deep and intermediate sites were both nutrient depleted, while the

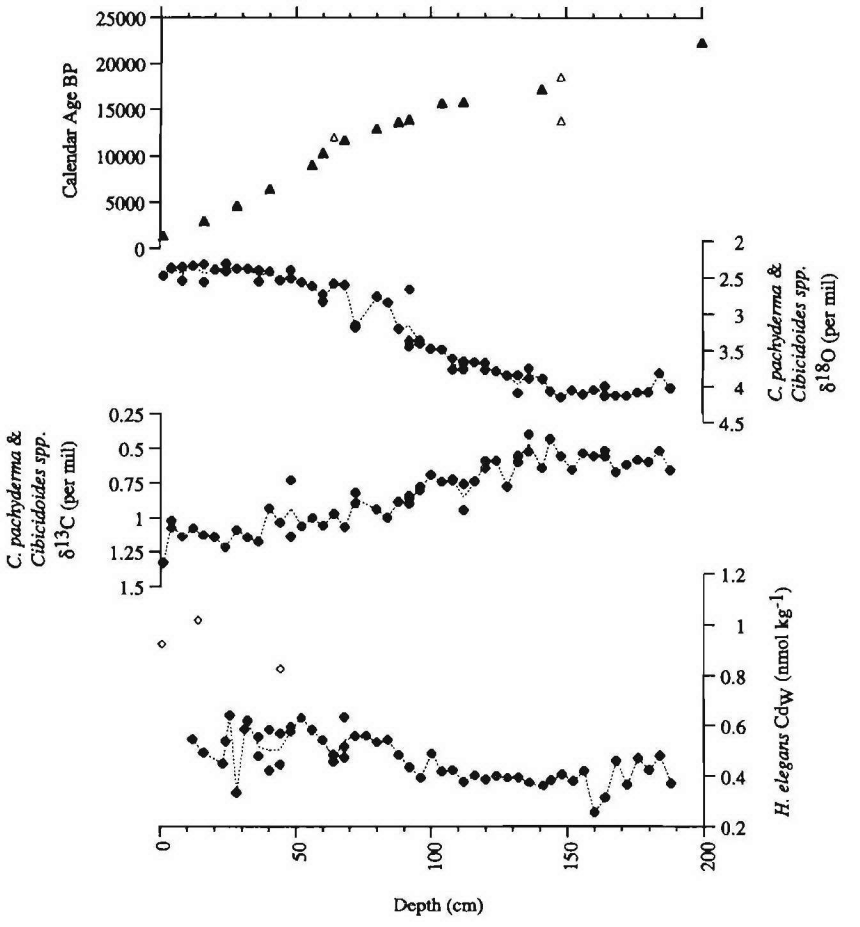

Figure 2. Data from core KNR159-5-36GGC (27°31′S, 46°28′W; 1268 m). At 148 cm a calendar age was obtained using the benthic foraminifer *C. pachyderma*; the rejected ages are open symbols (see text). Benthic foraminiferal $\delta^{18}O$ and $\delta^{13}C$ were obtained previously by *Oppo and Horowitz* [2000]. Benthic foraminiferal Cd seawater (Cd_W) estimates were obtained using the benthic foraminifer *H. elegans*. Rejected Cd_W values are open symbols.

intermediate South Atlantic remained high in nutrient concentrations (like today).

[19] Both North Atlantic sites show Cd_W increases at ~16.5 ka that may be associated with Heinrich event 1, an episode of massive iceberg discharge into the North Atlantic. This event is not clearly expressed in core 36GGC. As noted above, nutrients began to increase in the intermediate depth South Atlantic synchronously with the depletion in GISP2 $\delta^{18}O$ leading from the Bølling-Allerød into the Younger Dryas (Figure 3). A marked nutrient increase at the deep North Atlantic site began later, after the onset of GISP2 depletion in $\delta^{18}O$ but synchronously with the abrupt depletion in $\delta^{18}O$ at the onset of the Younger Dryas. Maximum Cd_W values were reached at both these sites during the Younger Dryas, suggesting a dramatic reduction in southward penetration of both deep and intermediate northern source waters. Cd_W data from the intermediate depth North Atlantic site are consistent with this interpretation. However, lower Cd_W values in the North Atlantic than in the South Atlantic indicate that NAIW continued to form, although it was less influential at the southern site. The early reduction in NAIW may indicate that intermediate waters are more sensitive to surface perturbation than deep waters, which appear closely linked with the rapid Younger Dryas temperature decreases over Greenland.

[20] The reduction in both NAIW and NADW during the Younger Dryas suggests a stronger decrease in northward heat transport than would a reduction in NADW alone. Although the deep North Atlantic core did not penetrate glacial sediments, data from IOS82 PC SO1 (42.38°N, 23.52°W; 3540 m) [*Boyle*, 1992] can be used to estimate glacial values (Figure 3, blue bars). For the deep North Atlantic, glacial Cd_W values are similar to Younger Dryas values. At both intermediate depth sites, Cd_W values are

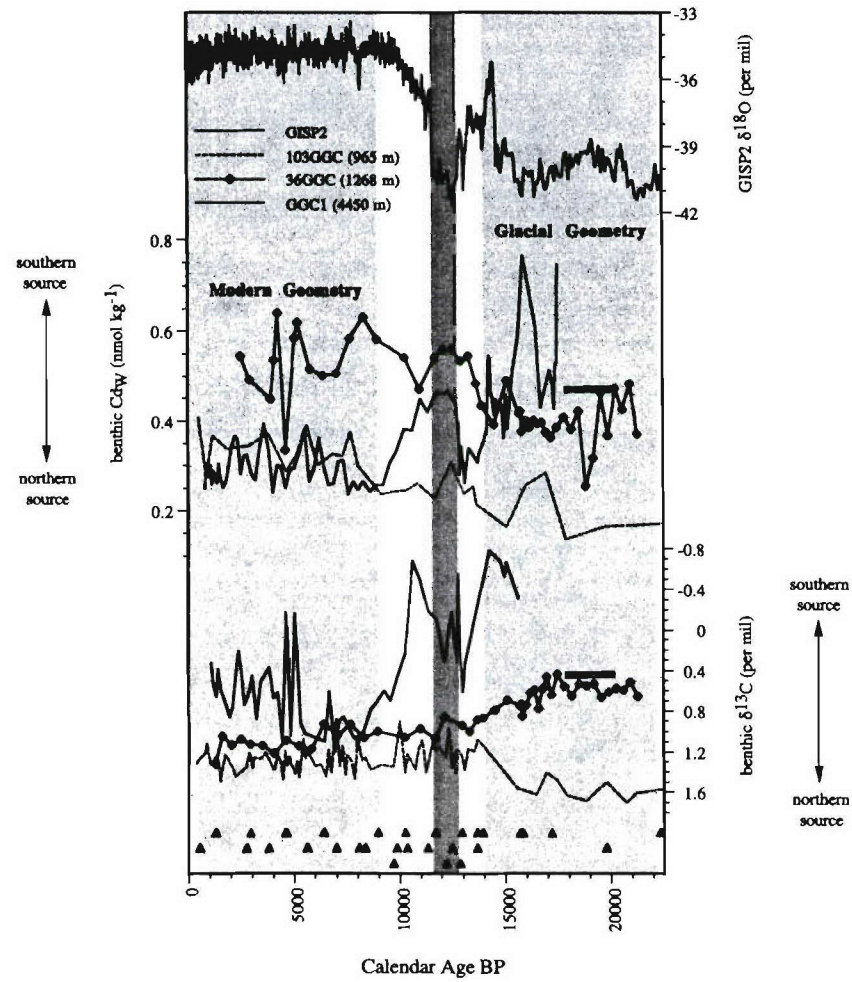

Figure 3. Cd_W and $\delta^{13}C$ data. Data shown are (1) GISP2 $\delta^{18}O$ (pink) [*Grootes et al.*, 1993]; (2) mean Cd_W from KNR159-5-36GGC (27°31′S, 46°28′W; 1268 m; red), OC205-2-103GGC (26°04′N, 78°03′W; 965 m; green) [*Marchitto et al.*, 1998], and EN120-GGC1 (33°40′N, 57°37′W; 4450 m; blue) [*Boyle and Keigwin*, 1987]; (3) mean $\delta^{13}C$ 36GGC (red) [*Oppo and Horowitz*, 2000], 103GGC (green) [*Slowey and Curry*, 1995; *Marchitto et al.*, 1998; *Curry et al.*, 1999], and EN120-GGC1 (blue) [*Boyle and Keigwin*, 1987]. Glacial Cd_W and $\delta^{13}C$ estimates for the deep North Atlantic (blue bars) are based on data from IOS82 PC SO1 (42.38°N, 23.52°W; 3540 m) [*Boyle*, 1992]. Accelerator mass spectrometer (AMS) radiocarbon dates for 103GGC were obtained in this study and previously [*Marchitto et al.*, 1998; *Curry et al.*, 1999; J. F. McManus, unpublished data, 2003]. The age models for 103GGC and 36GGC are based on AMS radiocarbon dates converted to calendar age (green triangles for 103GGC and red triangles for 36GGC) and linear interpolation between points. The age model for GGC1 is based on cross correlation with features that have been radiocarbon dated in nearby cores [*Boyle and Keigwin*, 1987]. Newly obtained ages for GGC1 (blue triangles) support the model of *Boyle and Keigwin* [1987]. Yellow shading indicates the Younger Dryas interval. See color version of this figure at back of this issue.

higher during the Younger Dryas than during the glacial. These results suggest a weaker overall North Atlantic MOC during the Younger Dryas than during the last glacial, which may imply less northward heat transport during the Younger Dryas than during the Last Glacial Maximum.

[21] At the end of the Younger Dryas cold period, one low Cd_W value at the Brazilian margin site suggests a possible increase in the influence of nutrient-depleted northern source water. By 9 ka, Cd_W values at all sites reached Holocene levels, suggesting that the modern deepwater

configuration was finally established at this time. The GISP2 $\delta^{18}O$ record suggests that Holocene warmth was also reached at ~9 ka, providing further evidence for a close link between the MOC, heat transport, and North Atlantic temperatures.

[22] Glacial-interglacial circulation changes suggested by the $\delta^{13}C$ trends from EN120-GGC1 [*Boyle and Keigwin*, 1987], OC205-2-103GGC [*Slowey and Curry*, 1995; *Marchitto et al.*, 1998; *Curry et al.*, 1999], and KNR159-5-36GGC [*Oppo and Horowitz*, 2000] are similar to those suggested by the Cd_W data (Figure 3). For the last glacial the $\delta^{13}C$ data suggest that the deep North Atlantic was the most nutrient rich of the three sites and the intermediate depth North Atlantic was the most nutrient depleted, in agreement with the Cd_W data. Similarly, the overall glacial-interglacial trends of decreasing nutrients in the deep North Atlantic and increasing nutrients in the intermediate depth North Atlantic also agree with the Cd_W data. However, the intermediate depth South Atlantic $\delta^{13}C$ data obtained by *Oppo and Horowitz* [2000] exhibit an overall trend of increasing $\delta^{13}C$ since the last glacial. As discussed above, the trend of increasing Cd_W values at the South Atlantic site indicates increasing nutrients on glacial-interglacial timescales. Therefore the glacial-interglacial $\delta^{13}C$ trend was not driven by decreasing nutrients. Rather, increasing $\delta^{13}C$ in parallel with the Cd_W increase suggests that the $\delta^{13}C_{AS}$ signature changed on glacial-interglacial timescales.

[23] During the last glacial, water at the Brazilian margin site had a low $\delta^{13}C_{AS}$ exchange signature of 0–0.3‰, while today it has a very high $\delta^{13}C_{AS}$ exchange signature of 0.5‰ [*Oppo and Horowitz*, 2000]. During the glacial the low-$\delta^{13}C_{AS}$ signature at the Brazilian margin site is similar to that of GNAIW, so waters at this site may be the result of GNAIW aging along its flow path from the North Atlantic to the South Atlantic. Today, the very high $\delta^{13}C_{AS}$ signature observed at this location could not result from aging of a low-$\delta^{13}C_{AS}$ exchange signature water mass like NAIW since the $\delta^{13}C_{AS}$ is a conservative property of a water mass. Instead, water at this location and depth is more influenced by AAIW, which has a very high $\delta^{13}C_{AS}$ signature [*Oppo and Horowitz*, 2000]. Thus the nearly constant north-south gradient in Cd_W between the intermediate depth North Atlantic and the intermediate depth South Atlantic could be viewed as simple aging of northern source waters during the glacial but not during the Holocene.

[24] The increase in glacial $\delta^{13}C$ values began at ~17 ka, but it is not possible to separate the contributions of the increase in the mean ocean $\delta^{13}C$ value that resulted from the increase in the size of the terrestrial biosphere from the increase because of the changes in the $\delta^{13}C_{AS}$ exchange signature. These complicating effects may also explain why the Younger Dryas is not clearly expressed in the $\delta^{13}C$ of the intermediate depth North Atlantic or the intermediate depth South Atlantic.

5. Conclusion

[25] New Cd_W data from an intermediate depth southwestern Atlantic core clarify the response of NAIW since the last glacial. During the last glacial, deep, nutrient-rich Southern Ocean water was overlain by nutrient-depleted NAIW [*Boyle and Keigwin*, 1987], and NAIW penetrated farther into the South Atlantic than it does today [*Oppo and Horowitz*, 2000]. The new data suggest a trend of decreasing southward penetration of NAIW that began with the gradual cooling leading to the Younger Dryas and culminating during the event. Lower Cd_W values in the intermediate depth North Atlantic [*Marchitto et al.*, 1998] than in the intermediate depth South Atlantic, however, indicate that NAIW continued to form. Data from a previous study suggest that a dramatic reduction in NADW contribution to the deep North Atlantic occurred later and more abruptly, synchronously with the rapid cooling that marked the beginning of the Younger Dryas [*Boyle and Keigwin*, 1987]. The similar timing of surface cooling in the North Atlantic region and changes in intermediate and deep circulation confirm a close link between the MOC and North Atlantic climate. This linkage is further bolstered by our observation that deepwater geometry reached its modern configuration at about the same time that deglacial warming of the North Atlantic was complete, ~9 kyr.

[26] **Acknowledgments.** We would like to thank L. Zou and S. Trimarchi for their assistance with sample preparation and the members of the NOSAMS/NSF facility at WHOI for generating the AMS radiocarbon dates. We would also like to thank Ed Boyle and Tom Marchitto for their constructive comments and suggestions as well as Jerry McManus for use of his unpublished radiocarbon data. We are grateful for the help provided by the WHOI Core Laboratory and the captain and crew of the R/V *Knorr*. This work was supported by an MIT John Lyons Fellowship, a WHOI Ocean and Climate Change Institute Fellowship, and NSF grant OCE96-33499. This is WHOI contribution 10954.

References

Bond, G., W. Broecker, S. Johnson, J. McManus, L. Labeyrie, J. Jouzel, and G. Bonani, Correlations between climate records from North Atlantic sediments and Greenland ice, *Nature*, *365*, 143–147, 1993.

Boyle, E. A., Manganese carbonate overgrowths on foraminifera tests, *Geochim. Cosmochim. Acta*, *47*, 1815–1819, 1983.

Boyle, E. A., Cadmium: Chemical tracer of deep water paleoceanography, *Paleoceanography*, *3*, 471–489, 1988.

Boyle, E. A., Cadmium and $\delta^{13}C$ paleochemical ocean distributions during the stage 2 glacial maximum, *Annu. Rev. Earth Planet. Sci.*, *20*, 245–287, 1992.

Boyle, E. A., and L. D. Keigwin, Deep circulation of the North Atlantic over the last 200,000 years: Geochemical evidence, *Science*, *218*, 784–787, 1982.

Boyle, E. A., and L. D. Keigwin, Comparison of Atlantic and Pacific paleochemical records for the last 215,000 years: Changes in deep ocean circulation and chemical inventories, *Earth Planet. Sci. Lett.*, *76*, 135–150, 1985.

Boyle, E. A., and L. D. Keigwin, North Atlantic thermohaline circulation during the past 20,000 years linked to high-latitude surface temperature, *Nature*, *330*, 35–40, 1987.

Boyle, E. A., and Y. Rosenthal, Chemical hydrography of the South Atlantic during the Last Glacial Maximum: $\delta^{13}C$ versus Cd, in *The South Atlantic: Present and Past Circulation*, edited by G. Wefer et al., pp. 423–443, Springer-Verlag, New York, 1996.

Boyle, E. A., L. Labeyrie, and J.-C. Duplessy, Calcitic foraminiferal data confirmed by cadmium in aragonitic *Hoeglundina*: Application to the Last Glacial Maximum in the northern Indian Ocean, *Paleoceanography*, *10*, 881–900, 1995.

Broecker, W. S., and E. Maier-Reimer, The influence of air-sea exchange on the carbon isotope distribution in the sea, *Global Biogeochem. Cycles*, *6*, 315–320, 1992.

Broecker, W. S., D. M. Peteet, and D. Rind, Does the ocean-atmosphere system have more than one stable mode of operation?, *Nature*, *315*, 21–26, 1985a.

Broecker, W. S., T. Takahashi, and T. Takahashi, Sources and flow patterns of deep-ocean waters as deduced from potential temperature, salinity, and initial phosphate concentration, *J. Geophys. Res.*, *90*, 6925–6939, 1985b.

Curry, W. B., and G. P. Lohman, Carbon isotopic changes in benthic foraminifera from the western South Atlantic: Reconstruction of glacial abyssal circulation patterns, *Quat. Res.*, *18*, 218–235, 1982.

Curry, W. B., J. C. Duplessy, L. D. Labeyrie, and N. J. Shackleton, Changes in the distribution of $\delta^{13}C$ of deep water ΣCO_2 between the last glaciation and the Holocene, *Paleoceanography*, *3*, 317–341, 1988.

Curry, W. B., T. M. Marchitto, J. F. McManus, D. W. Oppo, and K. Laarkamp, Millennial-scale changes in ventilation of the thermocline, intermediate, and deep waters of the glacial North Atlantic, in *Mechanisms of Global Climate Change at Millennial Time Scales*, *Geophys. Monogr. Ser.*, vol. 112, edited by P. U. Clark, R. S. Webb, and L. D. Keigwin, pp. 59–76, AGU, Washington, D. C., 1999.

Dansgaard, W., North Atlantic climate oscillations revealed by deep Greenland ice cores, in *Climate Processes and Climate Sensitivity*, *Geophys. Monogr. Ser.*, vol. 29, edited by J. E. Hanson and T. Takahashi, pp. 288–298, AGU, Washington, D. C., 1984.

Dansgaard, W., et al., Evidence for general instability of past climate from a 250-kyr ice core record, *Nature*, *364*, 218–220, 1993.

Duplessy, J. C., N. J. Shackleton, R. G. Fairbanks, L. Labeyrie, D. Oppo, and N. Kallel, Deepwater source variations during the last climatic cycle and their impact on the global deepwater circulation, *Paleoceanography*, *3*, 343–360, 1988.

Grootes, P. M., M. Stuiver, J. W. C. White, S. Johnsen, and J. Jouzel, Comparison of oxygen isotope records from the GISP2 and GRIP Greenland ice cores, *Nature*, *336*, 552–554, 1993.

Hester, K., and E. A. Boyle, Water chemistry control of cadmium content in recent benthic foraminifera, *Nature*, *298*, 260–262, 1982.

Kroopnick, P. M., The distribution of $\delta^{13}C$ of ΣCO_2 in the world oceans, *Deep Sea Res., Part A*, *32*, 57–84, 1985.

Lehman, S. J., and L. D. Keigwin, Sudden changes in North Atlantic circulation during the last glaciation, *Nature*, *356*, 757–762, 1992.

Liss, P. S., and L. Merlivat, Air-sea gas exchange rates: Introduction and synthesis, in *The Role of Air-Sea Exchange in Geochemical Cycling*, edited by P. Buat-Menard, pp. 113–127, D. Reidel, Norwell, Mass., 1986.

Manabe, S., and R. J. Stouffer, Coupled ocean-atmosphere response to freshwater input: Comparison to Younger Dryas event, *Paleoceanography*, *12*, 321–336, 1997.

Marchal, O., T. F. Stocker, and F. Joos, Physical and biogeochemical responses to freshwater-induced thermohaline variability in a zonally averaged ocean model, in *Mechanisms of Global Climate Change at Millennial Time Scales*, *Geophys. Monogr. Ser.*, vol. 112, edited by P. U. Clark, R. S. Webb, and L. D. Keigwin, pp. 263–284, AGU, Washington, D. C., 1999.

Marchitto, T. M., Jr., D. W. Oppo, and W. B. Curry, Millennial-scale changes in North Atlantic circulation since the last glaciation, *Nature*, *393*, 557–561, 1998.

Marchitto, T. M., Jr., D. W. Oppo, and W. B. Curry, Paired benthic foraminiferal Cd/Ca and Zn/Ca evidence for a greatly increased presence of Southern Ocean Water in the glacial North Atlantic, *Paleoceanography*, *17*(3), 1038, doi:10.1029/2000PA000598, 2002.

Mook, W. G., J. C. Bommerson, and W. H. Staverman, Carbon isotope fractionation between dissolved bicarbonate and gaseous carbon dioxide, *Earth Planet. Sci. Lett.*, *22*, 169–176, 1974.

Oppo, D. W., and M. Horowitz, Glacial deep water geometry: South Atlantic benthic foraminiferal Cd/Ca and $\delta^{13}C$ evidence, *Paleoceanography*, *15*, 147–160, 2000.

Oppo, D. W., and S. J. Lehman, Mid-depth circulation of the subpolar North Atlantic during the Last Glacial Maximum, *Science*, *259*, 1148–1152, 1993.

Rahmstorf, S., Rapid climate transitions in a coupled ocean-atmosphere model, *Nature*, *372*, 82–85, 1994.

Rosenthal, Y., Late Quaternary paleochemistry of the Southern Ocean: Evidence from cadmium variability in sediments and foraminifera, Ph.D. thesis, Mass. Inst. of Technol./Woods Hole Oceanogr. Inst. Joint Program, Woods Hole, 1994.

Rosenthal, Y., P. Lam, E. A. Boyle, and J. Thomson, Authigenic cadmium enrichments in suboxic sediments: Precipitation and postdepositional mobility, *Earth Planet. Sci. Lett.*, *132*, 99–111, 1995.

Ruddiman, W. F., and A. McIntyre, The North Atlantic Ocean during the last deglaciation, *Palaeogeogr. Palaeoclimatol. Palaeoecol.*, *35*, 145–214, 1981.

Rühlemann, C., S. Mulitza, P. Müller, G. Wefer, and R. Zahn, Warming of the tropical Atlantic Ocean and slowdown of thermohaline circulation during the last deglaciation, *Nature*, *402*, 511–514, 1999.

Sarnthein, M., et al., Fundamental modes and abrupt changes in North Atlantic circulation and climate over the last 60 kyr—Concepts, reconstruction and numerical modeling, in *The Northern North Atlantic: A Changing Environment*, edited by P. Schafer et al., pp. 365–410, Springer-Verlag, New York, 2001.

Slowey, N. C., and W. B. Curry, Glacial-interglacial differences in circulation and carbon cycling within the upper western Atlantic, *Paleoceanography*, *10*, 715–732, 1995.

Stuiver, M., and P. J. Reimer, Extended ^{14}C database and revised CALIB radiocarbon calibration program, *Radiocarbon*, *35*, 215–230, 1993.

Zahn, R., and A. Stüber, Suborbital intermediate water variability inferred from paired benthic foraminiferal Cd/Ca and $\delta^{13}C$ in the tropical west Atlantic and linking with North Atlantic climates, *Earth Planet. Sci. Lett.*, *200*, 191–205, 2002.

R. E. Came, Massachusetts Institute of Technology/Woods Hole Oceanographic Institution Joint Program in Oceanography, Woods Hole, MA 02543, USA. (rcame@whoi.edu)

W. B. Curry and D. W. Oppo, Department of Geology and Geophysics, Woods Hole Oceanographic Institution, Woods Hole, MA 02543, USA. (wcurry@whoi.edu; doppo@whoi.edu)

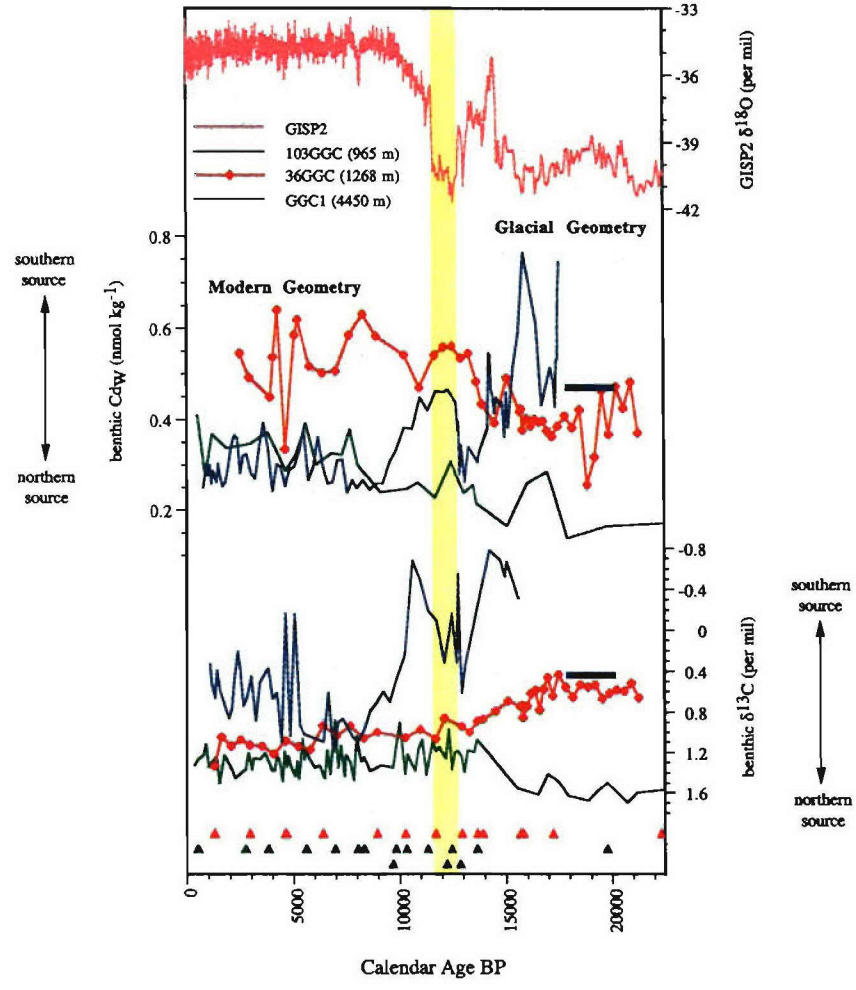

Figure 3. Cd_W and $\delta^{13}C$ data. Data shown are (1) GISP2 $\delta^{18}O$ (pink) [*Grootes et al.*, 1993]; (2) mean Cd_W from KNR159-5-36GGC (27°31′S, 46°28′W; 1268 m; red), OC205-2-103GGC (26°04′N, 78°03′W; 965 m; green) [*Marchitto et al.*, 1998], and EN120-GGC1 (33°40′N, 57°37′W; 4450 m; blue) [*Boyle and Keigwin*, 1987]; (3) mean $\delta^{13}C$ 36GGC (red) [*Oppo and Horowitz*, 2000], 103GGC (green) [*Slowey and Curry*, 1995; *Marchitto et al.*, 1998; *Curry et al.*, 1999], and EN120-GGC1 (blue) [*Boyle and Keigwin*, 1987]. Glacial Cd_W and $\delta^{13}C$ estimates for the deep North Atlantic (blue bars) are based on data from IOS82 PC SO1 (42.38°N, 23.52°W; 3540 m) [*Boyle*, 1992]. Accelerator mass spectrometer (AMS) radiocarbon dates for 103GGC were obtained in this study and previously [*Marchitto et al.*, 1998; *Curry et al.*, 1999; J. F. McManus, unpublished data, 2003]. The age models for 103GGC and 36GGC are based on AMS radiocarbon dates converted to calendar age (green triangles for 103GGC and red triangles for 36GGC) and linear interpolation between points. The age model for GGC1 is based on cross correlation with features that have been radiocarbon dated in nearby cores [*Boyle and Keigwin*, 1987]. Newly obtained ages for GGC1 (blue triangles) support the model of *Boyle and Keigwin* [1987]. Yellow shading indicates the Younger Dryas interval.

Tables

Table 2. KNR159-5-36GGC *H. elegans* Cd/Ca data.

Depth (cm)	CALIB 4 Age (yrs BP)	CALIB 5.01 Age (yrs BP)	Cd/Ca (μmol mol^{-1})	Mean Cd/Ca (μmol mol^{-1})	Cd_w (nmol kg^{-1})	Mean Cd_w (nmol kg^{-1})
KNR159-5-36GGC						
0.5	642	645	(0.092)		(0.92)	
12	2,503	2,521	0.054	0.054	0.54	0.54
14	2,724	2,744	(0.102)		(1.02)	
16	2,946	2,968	0.049	0.049	0.49	0.49
23	3,926	3,951	0.045	0.045	0.45	0.45
24	4,066	4,091	0.054	0.054	0.54	0.54
25.5	4,276	4,302	0.064	0.064	0.64	0.64
28	4,627	4,653	0.033	0.033	0.33	0.33
31	5,070	5,092	0.058	0.058	0.58	0.58
32	5,218	5,239	0.062	0.062	0.62	0.62
36	5,810	5,826	0.048	0.052	0.48	0.52
36	5,810	5,826	0.055		0.55	
40	6,402	6,412	0.042	0.050	0.42	0.50
40	6,402	6,412	0.058		0.58	
44	7,043	7,094	0.057	0.051	0.57	0.51
44	7,043	7,094	0.045		0.45	
44	7,043	7,094	(0.083)		(0.83)	
48	7,684	7,777	0.059	0.058	0.59	0.58
48	7,684	7,777	0.058		0.58	
52	8,324	8,459	0.063	0.063	0.63	0.63
56	8,965	9,141	0.058	0.058	0.58	0.58
60	10,262	10,301	0.054	0.054	0.54	0.54
64	10,973	11,092	0.048	0.047	0.48	0.47
64	10,973	11,092	0.046		0.46	
68	11,683	11,884	0.063	0.054	0.63	0.54
68	11,683	11,884	0.047		0.47	
68	11,683	11,884	0.052		0.52	
72	12,104	12,231	0.056	0.056	0.56	0.56
76	12,524	12,577	0.056	0.056	0.56	0.56
80	12,945	12,924	0.053	0.053	0.53	0.53
84	13,310	13,294	0.054	0.054	0.54	0.54
88	13,674	13,665	0.048	0.048	0.48	0.48
92	13,927	13,900	0.043	0.043	0.43	0.43
96	14,515	14,451	0.039	0.039	0.39	0.39
100	15,103	15,002	0.049	0.049	0.49	0.49
104	15,691	15,553	0.042	0.042	0.42	0.42
108	15,750	15,624	0.042	0.042	0.42	0.42
112	15,808	15,695	0.038	0.038	0.38	0.38
116	15,999	15,926	0.040	0.040	0.40	0.40
120	16,190	16,157	0.039	0.039	0.39	0.39

Table 2 (cont.).

Depth (cm)	CALIB 4 Age (yrs BP)	CALIB 5.01 Age (yrs BP)	Cd/Ca (μmol mol^{-1})	Mean Cd/Ca (μmol mol^{-1})	Cd_w (nmol kg^{-1})	Mean Cd_w (nmol kg^{-1})
KNR159-5-36GGC						
124	16,381	16,389	0.040	0.040	0.40	0.40
128	16,572	16,620	0.039	0.039	0.39	0.39
132	16,762	16,851	0.040	0.040	0.40	0.40
136	16,953	17,082	0.038	0.038	0.38	0.38
141	17,192	17,371	0.036	0.036	0.36	0.36
144	17,452	17,628	0.039	0.039	0.39	0.39
148	17,800	17,970	0.041	0.041	0.41	0.41
152	18,147	18,312	0.038	0.038	0.38	0.38
156	18,494	18,654	0.042	0.042	0.42	0.42
160	18,841	18,996	0.026	0.026	0.26	0.26
164	19,188	19,338	0.032	0.032	0.32	0.32
168	19,536	19,680	0.046	0.046	0.46	0.46
172	19,883	20,022	0.037	0.037	0.37	0.37
176	20,230	20,364	0.047	0.047	0.47	0.47
180	20,577	20,706	0.043	0.043	0.43	0.43
184	20,924	21,048	0.048	0.048	0.48	0.48
188	21,271	21,390	0.037	0.037	0.37	0.37

Values in parentheses were omitted.
* D_P = 1 [*Boyle et al.,* 1995].

Chapter 4. North Atlantic Intermediate Depth Variability During the Younger Dryas: Evidence from Benthic Foraminiferal Mg/Ca and the GFDL R30 Coupled OA-GCM

Abstract

Benthic foraminiferal Mg/Ca data from two intermediate depth low-latitude western Atlantic sites - one from the Florida Current and one from the Little Bahama Bank – provide insights into the spatial distribution of intermediate depth temperature variability during the Younger Dryas. The Florida site lies within the deeper portion of the Florida Current; the Little Bahama Bank site lies within the deeper, unventilated portion of the North Atlantic subtropical gyre. During the Younger Dryas, temperatures increased at the Florida Current site and temperatures decreased at the Little Bahama Bank site. The temperature increase within the Florida Current is consistent with the reduced northward heat transport associated with a reduction in the Atlantic meridional overturning circulation (MOC); the temperature decrease at Little Bahama Bank is consistent with a cooling of high latitude surface waters.

To test the possibility that a freshening of the surface North Atlantic caused the terrestrial and oceanographic changes during the Younger Dryas, the GFDL R30 coupled ocean-atmosphere general circulation model was forced using a North Atlantic freshwater perturbation of 0.1 Sv for a period of 100 years. The freshwater flux causes an overall reduction in the Atlantic overturning from 25 Sv to 13 Sv. However, at ~1,100 meters water depth, ventilation increases, causing decreases in both temperature and salinity throughout much of the intermediate depth North Atlantic. In the open North Atlantic, intermediate depth temperatures decrease by approximately 1°C; at the eastern side, intermediate depth temperatures decrease by less than 0.4°C. Intermediate depth temperatures at the western boundary, however, increase due to a reduction in northward heat transport, and also due to a shift in the location of the Intertropical Convergence Zone, which causes a reduction in surface salinity and a decrease in the upwelling of colder, deeper waters.

Introduction

The transition from the most recent glaciation to the Holocene interglacial was punctuated by several millennial-scale climate oscillations [*Bond et al.*, 1993; *Dansgaard et al.*, 1993; *Lehman and Keigwin*, 1992]. The most notable of these oscillations was the Younger Dryas, a brief return to near-glacial temperatures in the North Atlantic that began approximately 13,000 years ago and lasted about 1,500 years. The Younger Dryas cooling event has been observed in many high latitude North Atlantic climate proxies, including oxygen isotopes in Greenland ice cores [*Dansgaard*, 1984] and the faunal assemblages

of planktic foraminifera in the North Atlantic [*Ruddiman and McIntyre*, 1981]. More recently, however, the widespread nature of the event has been revealed in paleoclimate records from around the globe, including sea surface temperatures in the Cariaco Basin [*Lea et al.*, 2003], Asian monsoon intensity recorded in speleothems from Hulu Cave, eastern China [*Wang et al.*, 2001], and high altitude temperatures recorded in Bolivian ice cores [*Thompson et al.*, 1998].

A freshwater induced reduction in the Atlantic meridional overturning circulation is often invoked as a potential cause or amplifier of the high latitude cooling during the Younger Dryas [*Broecker et al.*, 1989; *Keigwin et al.*, 1991; *Tarasov and Peltier*, 2005]. A decrease in the rate of North Atlantic Deep Water (NADW) formation could cause a reduction in the amount of heat transported by the upper ocean to the North Atlantic, thereby cooling the high northern latitudes [*Broecker et al.*, 1985]. Model simulations predict surface cooling in the high latitudes in response to freshwater forcing, and a warming of the surface and thermocline at lower latitudes [*Manabe and Stouffer*, 1997; *Marchal et al.*, 1999; *Rahmstorf*, 1994; *Rühlemann et al.*, 2004]. Alkenone-derived temperature estimates from the open ocean, western tropical Atlantic suggest that a low latitude surface warming did occur during the Younger Dryas, with sea surface temperatures increasing by 1.2°C [*Rühlemann et al.*, 1999]. However, Mg/Ca-derived sea surface temperatures from the Cariaco Basin off Northern Venezuela suggest a tropical cooling of 3 to 4°C [*Lea et al.*, 2003].

Nutrient evidence from the last glacial suggests that a decrease in NADW formation was associated with a corresponding increase in North Atlantic intermediate water formation (NAIW) [*Boyle and Keigwin*, 1987]. Nutrient evidence [*Marchitto et al.*, 1998; *Zahn and Stüber*, 2002], benthic-planktic radiocarbon pairs [*Keigwin*, 2004], and freshwater forced model simulations [*Rahmstorf*, 1994] suggest a glacial-like subsurface geometry for the Younger Dryas as well. Alternatively, overturning during the early Younger Dryas may have been similar to the modern mode, with significant NADW formation and little NAIW formation [*Sarnthein et al.*, 2001].

A problem with the North Atlantic freshwater forcing hypothesis is that documented North Atlantic freshwater events do not coincide with the onset of the Younger Dryas cooling, leading to investigations of Southern Ocean forcing mechanisms. Recent modeling studies suggest that increased freshwater into the surface of the Southern Ocean intensifies the transformation of dense Circumpolar Deep Water (CDW) into the lighter Antarctic Intermediate Water (AAIW) [*Saenko et al.*, 2003b], which then feeds the return flow of

NADW formation [*Gordon*, 1986], and intensifies the MOC. It has been suggested that meltwater pulse 1a into the Southern Ocean caused this type of MOC intensification, and led to the Bølling-Allerød warming in the North Atlantic [*Weaver et al.*, 2003]. A Southern Ocean forcing mechanism predicts a very different Atlantic subsurface geometry for abrupt climate events like the Younger Dryas: in the "off" mode, NADW is less dense than AAIW, creating a stagnant, poorly ventilated, upper North Atlantic Ocean [*Keeling and Stephens*, 2001; *Saenko et al.*, 2003a]. An intermediate depth paleo-nutrient record from the high latitude north Atlantic may support this interpretation for the Younger Dryas [*Rickaby and Elderfield*, 2005], although previous paleoceanographic studies [*Keigwin*, 2004; *Marchitto et al.*, 1998; *Zahn and Stüber*, 2002] suggest well-ventilated intermediate depths during the YD.

Benthic foraminiferal oxygen isotopes have been used as a tracer of bottom water temperatures (BWT) during the Younger Dryas, and the results compared with BWT estimates from freshwater forcing simulations using zonally averaged models [*Rühlemann et al.*, 2004]. However, one complication with this approach is that both seawater $\delta^{18}O$ ($\delta^{18}O_{sw}$) and calcification temperature influence the $\delta^{18}O$ of foraminifera, making the interpretation of foraminiferal $\delta^{18}O$ as a BWT proxy uncertain. Another complication is that zonally averaged models may not reveal the spatial complexity of the distribution of BWT anomalies within the Atlantic basin, and a particular core location may not be representative of a zonal average.

In this study, we present downcore records of paired benthic Mg/Ca and $\delta^{18}O$ from two cores, from which we determine both temperature and salinity. The two cores lie in key locations for detecting changes in intermediate depth water properties during the Younger Dryas: a core from the Little Bahama Bank monitors variability within the deeper, unventilated portion of the North Atlantic subtropical gyre [*Slowey and Curry*, 1995]; and a core from within the Florida Current monitors variability in the northward return flow of the MOC [*Lynch-Stieglitz et al.*, 1999].

In order to test the sensitivity of the oceanographic changes to a freshening of the surface North Atlantic, the GFDL R30 coupled ocean-atmosphere general circulation model was forced using a North Atlantic freshwater perturbation of 0.1 Sv for a period of 100 years. The purpose of this study is to assess the response of the ocean's subsurface to the type of freshwater perturbation that may have caused the Younger Dryas. The responses are then compared to actual oceanic paleoclimate evidence in an attempt to determine whether a North Atlantic freshwater perturbation is an adequate explanation

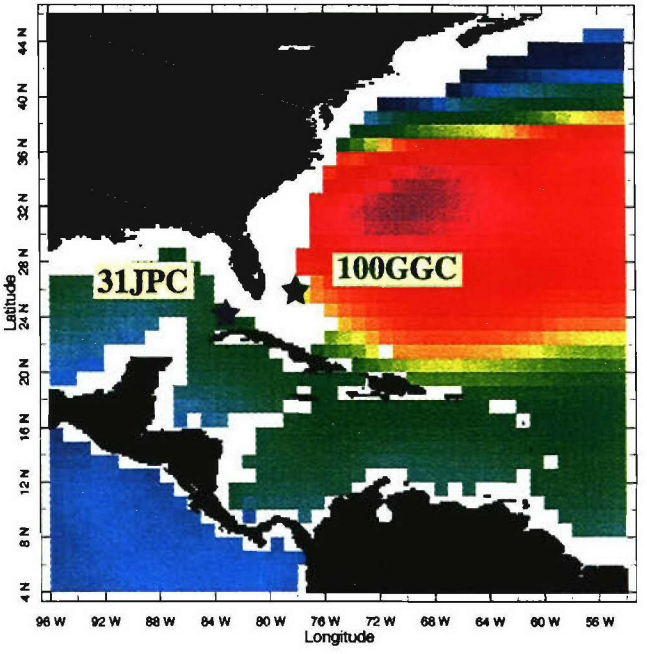

Figure 1. Map of the study area with mean annual temperatures at 1,000 m water depth [*Levitus and Boyer*, 1994] and the locations of OCE205-2-100GGC (26°04'N, 78°02'W, 1,057 m) and KNR166-2-31JPC (24°13'N, 83°18'W, 751 m).

for the observed changes during the Younger Dryas. It should be noted, however, that the GFDL R30 model is designed to simulate modern conditions, not those of the deglacial, so the experiment should be viewed as a sensitivity study.

Study Areas

Sediment core OCE205-2-100GGC (LBB) was taken from the flanks of the Little Bahama Bank, within the Northwest Providence Channel, at 26° 04' North, 78° 02' West, and 1,057 m (Figure 1). Waters of the Northwest Providence Channel flow westward from the Sargasso Sea to the Straits of Florida [*Slowey and Curry*, 1995]. Today, depths above 1,000 m are bathed by waters of the wind-driven North Atlantic subtropical gyre, with the same temperature, salinity, and density structure of the western portion of the gyre [*Slowey and Curry*, 1995]. Waters below 1,000 m are fed by the upper component of North Atlantic Deep Water. These waters are poorly ventilated because they originate in the subpolar gyre, where residence times are long and wind-driven upwelling occurs [*Jenkins*, 1980; *McCartney*, 1982; *Sarmiento et al.*, 1982]. Waters circulate within the

subpolar gyre before entering the subtropical gyre at depth [*Jenkins*, 1980; *Luyten et al.*, 1983; *McCartney*, 1982; *Sarmiento et al.*, 1982].

Sediment core KNR166-2-31JPC (FC) was taken from within the Florida Current, just south of the Florida Keys, at 24° 13' North, 83° 18' West, and 751 m (Figure 1). Today, waters of the Florida Current are a mixture of recirculated North Atlantic subtropical gyre water (17 Sv) and AAIW (13 Sv) [*Schmitz et al.*, 1993; *Schmitz and Richardson*, 1991]. At mid-depths (12-24°C temperature range), ~5% of the Florida Current waters are of South Atlantic origin, but below 400 m, ~80% of the waters are of South Atlantic origin [*Schmitz and Richardson*, 1991]. The intermediate depth southern source waters that feed the Florida Current are observed in the South Atlantic as a northward moving salinity minimum layer that originates near the Antarctic Polar Front [*Lynch-Stieglitz et al.*, 1994]. As the waters move northward through the Florida Strait and toward the polar seas via the North Atlantic Current, the salinity gradually increases [*Tsuchiya*, 1989] due to interaction with Mediterranean Water [*Reid*, 1994] and the temperature gradually decreases.

Today, intermediate depths at these two geographic locations have very different water properties. For example, mean annual temperatures at 1,000 m depth are about 1°C warmer at the Little Bahama Bank than at the Florida Current [*Levitus and Boyer*, 1994]. However, since the Florida Current site is significantly shallower than the Little Bahama Bank site, bottom water temperatures and salinities are very similar: approximately 5.35°C and 35.05 p.s.u. at LBB [*Slowey and Curry*, 1995], and 5.78°C and 34.90 p.s.u. at FC (measured during core collection, KNR166-2).

Methods

Foraminiferal Analyses

For LBB, thirteen accelerator mass spectrometer (AMS) radiocarbon dates were obtained using the planktic foraminifer *G. sacculifer*. For FC, three AMS dates were obtained using *G. sacculifer* and one using the planktic foraminifer *G. ruber* [*Lynch-Stieglitz*, unpublished data]. AMS radiocarbon dates were converted to calendar age using the online calibration program [*Stuiver and Reimer*, 1993], the Marine04 calibration data set [*Hughen et al.*, 2004], and a reservoir correction of 400 years (Table 1). The results indicate that the sedimentation rate for LBB is ~6 cm/kyr, with higher sedimentation rates in the more recent Holocene (~8 cm/kyr) and lower rates near the last glacial (~3 cm/kyr) (Figure 2a). The average sedimentation rate for FC is slightly higher than 8 cm/kyr (Figure 3a).

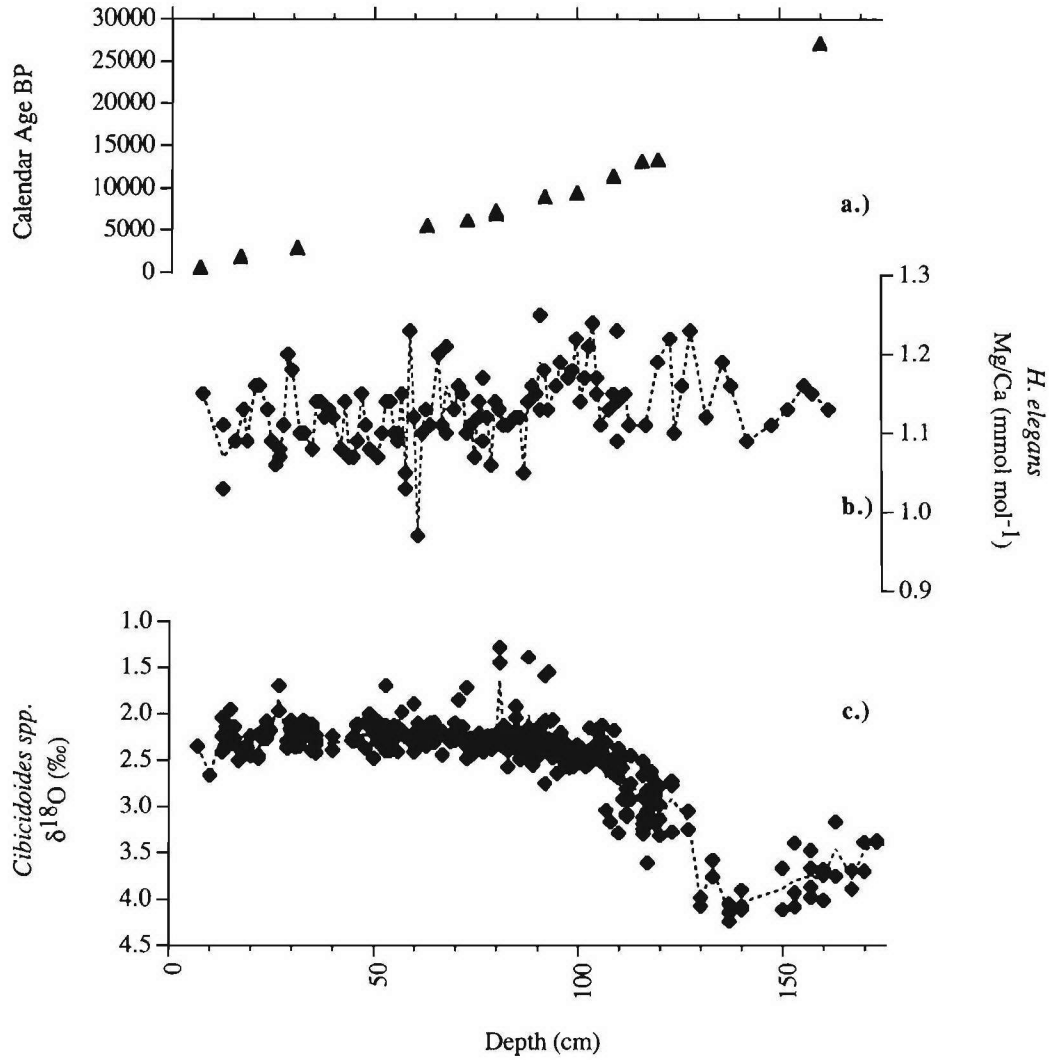

Figure 2. Benthic Mg/Ca and $\delta^{18}O$ data from OCE205-2-100GGC (26°04'N, 78°02'W, 1,057 m) *vs.* depth. **a.)** AMS radiocarbon dates converted to calendar age using Calib 5.01 [*Stuiver and Reimer*, 1993], the calibration data set of Hughen *et al.* [2004], and a reservoir correction of 400 years; **b.)** all *H. elegans* Mg/Ca; **c.)** all previously acquired *Cibicidoides spp.* $\delta^{18}O$ [*Slowey and Curry*, 1995] as well as newly acquired *Cibicidoides spp.* $\delta^{18}O$ [this paper].

Mg/Ca ratios were measured in the tests of the benthic foraminifer *H. elegans*. Each sample consisted of approximately 2-3 individuals, which were crushed and cleaned according to the trace metal protocol [*Boyle and Keigwin*, 1985/6] with a reversal of the oxidative and reductive steps [*Boyle and Rosenthal*, 1996; *Rosenthal*, 1994; *Rosenthal*

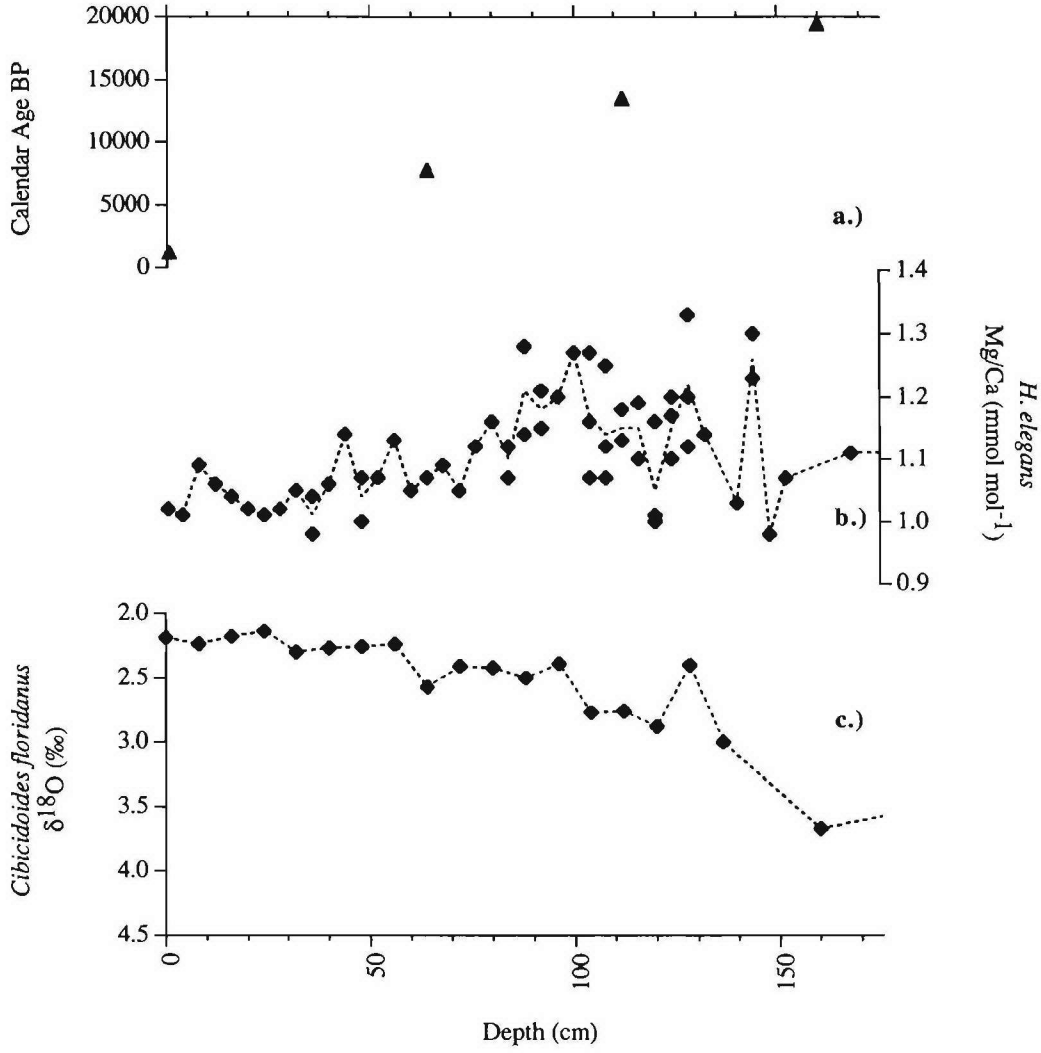

Figure 3. Benthic Mg/Ca and $\delta^{18}O$ data from KNR166-2-31JPC (24°13'N, 83°18'W, 751 m) *vs.* depth. **a.)** AMS radiocarbon dates [*Lynch-Stieglitz*, unpublished data] converted to calendar age using Calib 5.01 [*Stuiver and Reimer*, 1993], the calibration data set of Hughen *et al.* [2004], and a reservoir correction of 400 years; **b.)** all *H. elegans* Mg/Ca; c) all previously acquired *Cibicidoides floridanus* $\delta^{18}O$ [*Lynch-Stieglitz*, unpublished data].

et al., 1995]. Samples were dissolved in trace metal clean HNO_3 to obtain samples of approximately 200 ppm Ca. Mg/Ca ratios were measured using a Thermo-Finnigan Element2 sector field single collector ICP-MS following the method of Rosenthal *et al.* [1999], with the addition of a Ca matrix correction. Mn/Ca and Al/Ca were also measured in order to monitor contamination due to manganese carbonate overgrowths and terrestrial

input. Manganese carbonate overgrowths are a potential source of contamination in many species of benthic foraminifera [*Boyle*, 1983]. However, the species *H. elegans* was chosen for this study because it does not suffer from the contamination caused by such overgrowths [*Boyle et al.*, 1995].

Converting ICP-MS intensity ratios to elemental ratios using an external standard requires similar [Ca] in both the sample and the standard due to a calcium matrix effect. To correct for samples with varying [Ca], we ran a series of standards with identical element to Ca ratios, but with Ca concentrations that varied over the anticipated sample concentration range. The resulting matrix effect was calculated and the sample ratios were corrected. The corrections were less than ±0.03 mmol mol^{-1} Mg/Ca.

In order to assess the precision of measurements on the ICP-MS, three consistency standards were treated as samples in each of the runs in which the data were generated. Mean Mg/Ca values for the three consistency standards were 1.7 mmol mol^{-1}, 3.3 mmol mol^{-1} and 5.0 mmol mol^{-1}. Standard deviations were ±0.02 mmol mol^{-1} (n=9), ±0.03 mmol mol^{-1} (n=9), and ±0.04 mmol mol^{-1} (n=9), respectively. Using the Mg/Ca-temperature equation for *H. elegans* in supersaturated waters [*Rosenthal et al.*, in press], and a new temperature equation determined in this paper, the resulting temperature measurement errors are ±1.2°C and ±0.9°C, respectively.

Oxygen isotopes were analyzed using the tests of the benthic foraminiferal species *Cibicidoides spp.* at LBB [*Slowey and Curry*, 1995] and *C. floridanus* at FC [*Lynch-Stieglitz*, unpublished data]. Mg/Ca-derived temperatures and foraminiferal oxygen isotopic values were used to calculate $\delta^{18}O$ of seawater ($\delta^{18}O_{sw}$) using the conversion equation for *Cibicidoides spp.* [*Lynch-Stieglitz et al.*, 1999]:

$$(1.) \quad \delta^{18}O_{Cib} = [\delta^{18}O_{sw} - 0.27] - 0.21*BWT + 3.38.$$

Seawater $\delta^{18}O$ was not converted to salinity because the evolution of the $\delta^{18}O$-salinity relationship over time is not well constrained. However, using the modern relationship, a $\delta^{18}O_{sw}$ change of 0.1‰ equals a salinity change of about 0.2 p.s.u. [*Lynch-Stieglitz et al.*, 1999].

Model Description

The GFDL R30 coupled climate model consists of an atmospheric general circulation model coupled to an oceanic general circulation model. The R30 model is similar to previous

GFDL models (the GFDL r15, for example), but differs in that it contains higher spatial resolution in both the atmospheric and ocean components. The entire model description is presented in Delworth *et al.* [2002], but a brief summary follows.

The atmospheric component of the model solves the primitive equations on a sphere using a spectral transform method. Fields of horizontal variables are represented by a truncated series of spherical harmonics and grid point values, with zonal truncation at wave number 30. The resolution is approximately 3.75° longitude by 2.25° latitude. In the vertical, a finite difference scheme is used in conjunction with a sigma (σ) coordinate system, where $\sigma = p/p^*$ is the vertical coordinate, and p^* is the surface pressure. There are 14 unevenly spaced levels extending from $\sigma = 0.9965$ near the surface to $\sigma = 0.015$.

The model has a seasonal cycle of insolation, but no diurnal cycle. Insolation is prescribed at the top of the atmosphere, using a solar constant of 1365 W m^{-2}. The calculation of radiation includes the effects of clouds, water vapor, ozone and carbon dioxide. Clouds occur when the relative humidity of an air parcel exceeds a critical value, which varies with height (from 100% at surface, to 90% in the upper atmosphere). Ozone values are based upon observations and vary with latitude, height and season. The mixing ratio of carbon dioxide is assumed to be constant throughout the atmosphere.

Precipitation occurs in the model whenever the simulated moisture content of an air parcel exceeds saturation, with surface air temperature determining whether precipitation is snow or rain. Each land grid box has the capacity to collect 15 cm of rain and snowmelt. When the water content of the grid box exceeds 15 cm in height, the excess is treated as surface runoff. Surface runoff instantly enters the ocean via a routing scheme that is based upon observed drainage patterns. The model parameterizes moist convective processes using a moist convective adjustment scheme [*Manabe et al.*, 1965].

The ocean component of the model uses version 1.1 of the Modular Ocean Model. Resolution in the ocean component is 1.875° longitude by 2.25° latitude, with 18 unevenly spaced levels. The ocean model solves the equations of motion numerically using the Boussinesq, rigid lid, and hydrostatic approximations.

The ocean model requires parameterization of sub grid scale momentum mixing [*Bryan and Lewis*, 1979] and sub grid scale heat and salt mixing along isopycnal surfaces [*Redi*, 1982]. Also, the model uses a horizontal background diffusivity for temperature and salinity of $0.4 * 10^7 cm^2 s^{-1}$ and a horizontal viscosity of $1.2 * 10^9 cm^2 s^{-1}$. Mixing at the grid scale occurs when neighboring grid boxes are statically unstable, at which point the temperature and salinity of the two boxes are completely mixed.

The ocean model includes a sea ice component. If sea ice is less than 4 meters thick, it moves with ocean currents. The thickness of the ice changes by freezing and melting a single ice layer. When sea ice freezes or melts, the model adjusts freshwater fluxes into the ocean. The model also accounts for the latent heat exchanges associated with this freezing and melting. It is assumed that sea ice has no sensible heat content. The albedo of sea ice is dependent upon its surface temperature and thickness.

The two components of the GFDL R30 coupled model interact once per day through fluxes of heat, water and momentum. Heat fluxes include latent heat, sensible heat and radiative heat. Water fluxes include evaporation, precipitation, sublimation and runoff. Runoff from land follows observed drainage patterns and enters the ocean at the grid box closest to the mouth of the river. Runoff usually enters the upper grid box only. However, to reduce numerical instabilities, large river inputs enter the top two grid levels and several adjacent grid boxes. This influx of continental runoff changes ocean salinity and may affect ocean circulation.

Initialization of the model involves an 80-year integration of the atmospheric component using modern boundary conditions, and then a several thousand-year integration of the oceanic component using surface forcings calculated from the atmospheric integration. The oceanic component is integrated until drifts in deep ocean temperature and salinity are acceptably small. Since the atmospheric and oceanic components are not perfectly balanced, flux adjustments are used to prevent long-term drift. The flux adjustment terms are completely fixed prior to coupling of the oceanic and atmospheric components, so they are unlikely to systematically dampen or amplify anomalies.

The Freshwater Experiment

The current freshwater forcing experiment (the same experiment investigated by Dahl *et al.* [2005]) uses the 300th year of the control integration as its initial condition. During years 301-400, a freshwater perturbation of 0.1 Sv was input uniformly over the North Atlantic from 50° north to 70° north. After year 400, the freshwater forcing ceased and recovery began. In this experiment, it was assumed that the temperature of the freshwater perturbation was identical to the local temperature of the mixed-layer. Thus, the freshwater pulse directly affects surface water salinities, but does not directly affect surface water temperatures. The control integration of the GFDL R30 coupled climate model is designed to faithfully simulate modern conditions. A simulation using deglacial conditions could yield very different results.

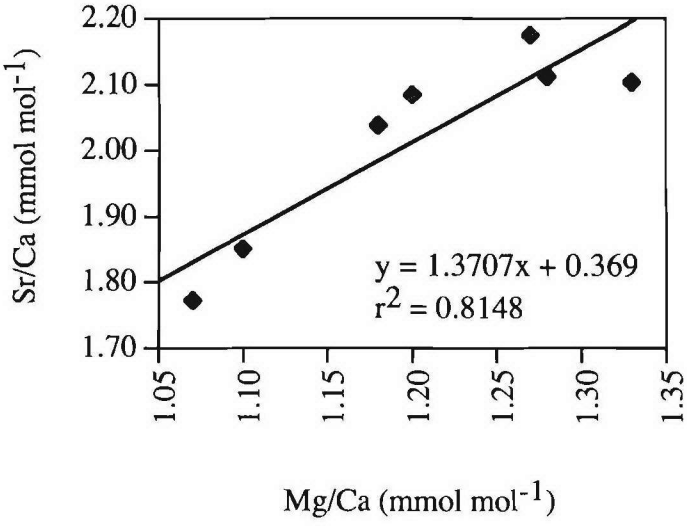

Figure 4. Mg/Ca *vs.* Sr/Ca. Simultaneous analyses of Mg/Ca and Sr/Ca in seven *H. elegans* samples (88cm, 96cm, 104cm, 108cm, 112cm, 124cm, 128cm) from KNR166-2-31JPC (24°13'N, 83°18'W, 751 m). Samples span a temperature range of 4.0°C to 10.8°C.

Benthic Foraminiferal Mg/Ca Results

Average coretop values for depths corresponding to the last 3 kyrs are 1.12 mmol mol^{-1} at LBB and 1.04 mmol mol^{-1} at FC (Figures 2b and 3b). Using the Mg/Ca-temperature relationship of Rosenthal *et al.* [in press], the calculated coretop temperature at LBB (4.8°C) is consistent with the modern bottom water temperature of 5.35°C [*Slowey and Curry*, 1995]. However, the coretop temperature at FC (2.5°C) is significantly lower than the modern bottom water temperature of 5.78°C. This discrepancy at the FC site most likely signifies an inadequacy in the temperature calibration (as discussed below), not a dissolution problem at FC.

Several of the lower-temperature *H. elegans* samples used in the Rosenthal *et al.* [in press] Mg/Ca temperature calibration were obtained from Little Bahama Bank sediments, which may contain a potentially contaminating Mg-rich carbonate phase [*Lear et al.*, 2002]. If the Mg-rich phase caused contamination in the lower-temperature portion of the calibration data set, then the intercept of the Rosenthal *et al.* [in press] Mg/Ca-temperature calibration line would shift to higher values, and the slope would decrease. Application of this contamination-influenced calibration to coretop samples would yield bottom water temperatures similar to the modern at the contaminated site (LBB), and lower than the

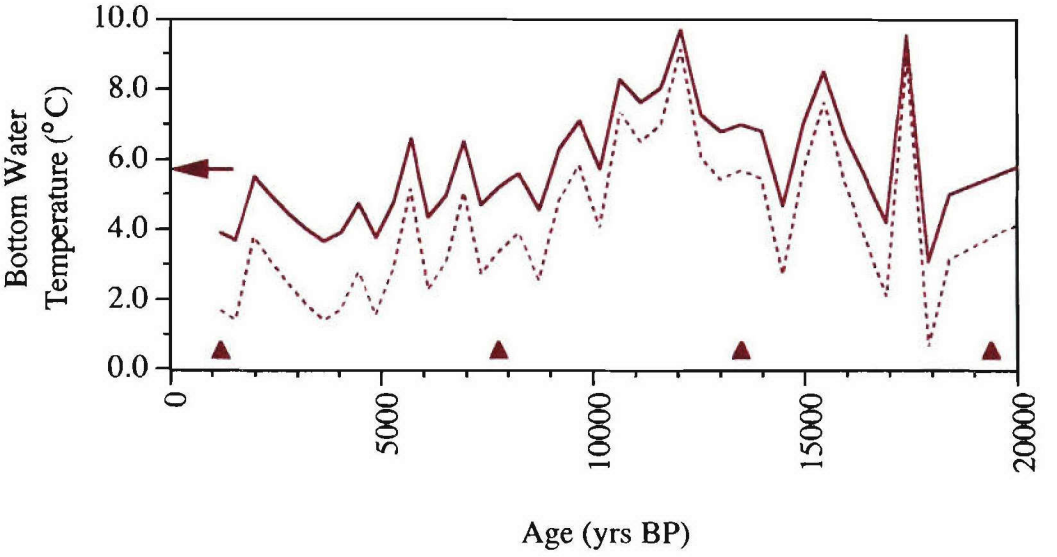

Figure 5. Mg/Ca-derived temperatures from KNR166-2-31JPC (24°13'N, 83°18'W, 751 m) *vs.* calendar age. Dashed line uses the equation $Mg/Ca_{H. elegans} = 0.034*BWT + 0.96$ [*Rosenthal et al.*, in press]; solid line uses the equation $Mg/Ca_{H. elegans} = 0.044*BWT + 0.85$ [this paper]. Arrow marks the modern bottom water temperature of 5.78°C.

modern at a non-contaminated site (FC), consistent with our data.

In order to obtain an appropriate calibration for our non-contaminated site, simultaneous measurements of Mg/Ca and Sr/Ca were obtained for seven *H. elegans* samples from FC core KNR166-2-31JPC. The samples (88cm, 96cm, 104cm, 108cm, 112cm, 124cm, 128cm), span a temperature range from 4.0°C to 10.8°C, and yield a good correlation ($r^2 = 0.81$) between the two temperature proxies (Figure 4). The relationship of Sr/Ca to Mg/Ca obtained from the FC core (eqn. 2), and the Sr/Ca-temperature equation of Rosenthal *et al.* [in press] (eqn. 3), were solved simultaneously to determine a new Mg/Ca-temperature relationship (eqn. 4):

(2.) $Sr/Ca_{H. elegans} = 1.3707*Mg/Ca_{H. elegans} + 0.369$

(3.) $Sr/Ca_{H. elegans} = 0.060*BWT + 1.53$

(4.) $Mg/Ca_{H. elegans} = 0.044*BWT + 0.85.$

Application of the new calibration brings calculated coretop temperatures at FC into agreement with modern bottom water temperatures (Figure 5). Therefore, we use the new

calibration for estimating temperatures at FC. At LBB, however, we use the Rosenthal *et al.* [in press] calibration because it yields temperatures that are more consistent with the modern, although the shallow slope of this calibration line likely amplifies the actual temperature variability at LBB, and the effect of the contaminating phase may not have been constant through time. Further Sr/Ca analyses at both LBB and FC will be required to confirm the temperature signals.

The benthic Mg/Ca data from the LBB site do not reveal a clear glacial-interglacial trend (Figure 2b; Figure 6b). Instead, similar temperatures of 3.8°C and 4.7°C are observed for the glacial (20.1 ka) and interglacial, respectively. However, pronounced sub-orbital variability is present in the record. At ~16 ka, Mg/Ca temperatures decreased by nearly 4°C, perhaps coincident with Heinrich event 1 (although sample resolution and insufficient age control prevent conclusive identification of the event). At ~14.5 ka, coincident with the Bølling-Allerød warming in the high latitude North Atlantic, temperatures increased by ~4°C. At ~13 ka, coincident with the Bølling-Allerød to Younger Dryas cooling, temperatures decreased by ~3.5°C. At 10.4 ka, temperatures returned to pre-Younger Dryas values. By 8 ka, temperatures decreased to near modern values, where they remained for the rest of the Holocene.

Like LBB, the benthic Mg/Ca data from FC do not reveal a clear glacial-interglacial trend (Figure 3b; Figure 6b), but rather, similar temperatures of 5°C and 4.3°C for the glacial (~18 ka) and interglacial, respectively. Pronounced sub-orbital variability is also present in the FC record. At ~16 ka, perhaps coincident with Heinrich event 1, temperatures increased by 4.3°C (but again, sample resolution is a limitation). At ~15 ka, coincident with the Bølling-Allerød warming in the high latitudes, temperatures decreased ~4°C. At ~14 ka, temperatures began to increase in concert with the gradual cooling observed in the GISP2 ice core record. Maximum temperatures were achieved at ~12 ka, suggesting a Bølling-Allerød to Younger Dryas warming of as much as 5°C. By ~9 ka, temperatures returned to Bølling-Allerød-like values, and temperatures remained close to modern values for the remainder of the Holocene.

Comparison of the two intermediate depth records reveals similar temperatures at LBB and FC throughout much of the last 20,000 years. In particular, BWTs were comparable before the Younger Dryas and after 10.5 ka. During the Younger Dryas, however, the temperatures at the two sites diverged significantly. Our data suggest an

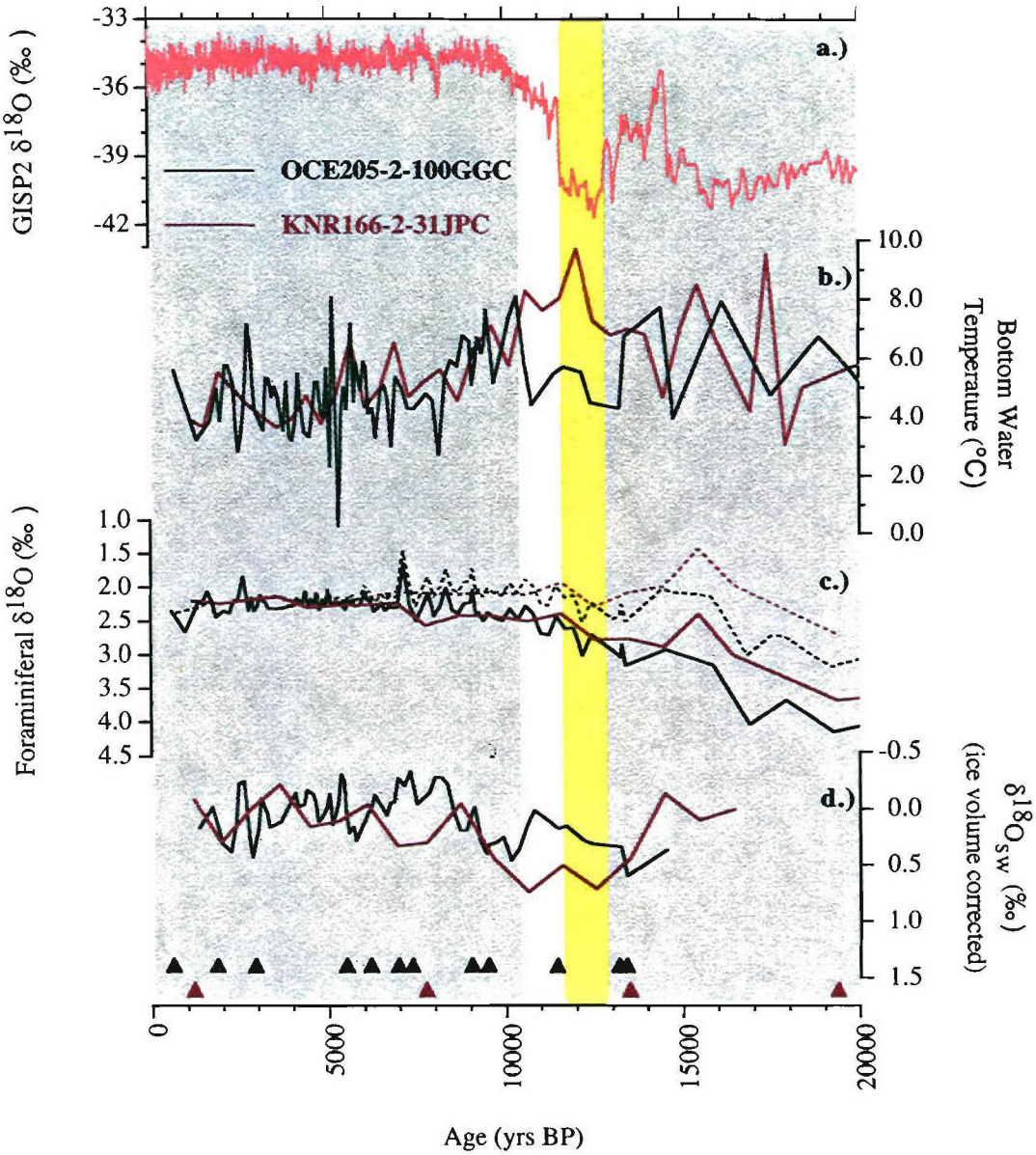

Figure 6. Benthic temperatures and $\delta^{18}O_{sw}$ from OCE205-2-100GGC (26°04'N, 78°02'W, 1,057 m) and KNR166-2-31JPC (24°13'N, 83°18'W, 751 m) *vs.* calendar age. **a.)** GISP2 $\delta^{18}O$ (pink) [*Grootes et al.*, 1993]; **b.)** average Mg/Ca-derived temperatures for 100GGC (green) and 31JPC (purple); **c.)** average benthic foraminiferal $\delta^{18}O$ for 100GGC (green) [*Slowey and Curry*, 1995; this paper] and 31JPC (purple) [*Lynch-Stieglitz*, unpublished data]; dashed lines are $\delta^{18}O$ corrected for ice-volume change using Waelbroeck *et al.* [2002]; **d.)** $\delta^{18}O_{sw}$ calculated using 3-point smoothed Mg/Ca-derived temperatures, 3-point smoothed ice-volume corrected foraminiferal $\delta^{18}O$, and the $\delta^{18}O$-temperature equation for *Cibicidoides spp.*: $\delta^{18}O_{Cib} = [\delta^{18}O_{sw} - 0.27] - 0.21*BWT + 3.38$ [*Lynch-Stieglitz et al.*, 1999]. Triangles are AMS dates converted to calendar age. Yellow shading marks the Younger Dryas interval.

increased temperature gradient between the two sites, with BWTs 4°C warmer at FC than at LBB. While not as well resolved, a similar response was possible during Heinrich event 1. After the Younger Dryas event, the temperature difference between the two sites remained Younger Dryas-like for ~1 kyr after the end of the Younger Dryas event in the North Atlantic. At ~10.5 ka, temperatures at the two sites converged, and a gradient similar to the modern was established. From ~10.5 ka to 9 ka, temperatures at both sites declined synchronously, with modern temperatures achieved at ~8.5 or 9 ka, further supporting a close linkage between intermediate depth variability and North Atlantic climate [*Came et al.*, 2003].

Benthic Foraminiferal $\delta^{18}O$ and $\delta^{18}O_{sw}$ Results

Previously acquired [*Slowey and Curry*, 1995] and newly acquired [this paper] benthic $\delta^{18}O$ results from LBB, and previously acquired benthic $\delta^{18}O$ results from FC [*Lynch-Stieglitz*, unpublished data] are presented in Figures 2c, 3c and 6c. Glacial-interglacial trends are present in the $\delta^{18}O$ records from both cores. At LBB, $\delta^{18}O$ shifts from 4.1‰ during the last glacial to 2.4‰ during the Holocene. At FC, $\delta^{18}O$ shifts from 3.7‰ to 2.2‰. Values at the two sites are offset from each other by about 0.5‰ during the glacial, but converge at ~11 ka, and remain very similar for the remainder of the record. Variability during the Younger Dryas is not prominent in either $\delta^{18}O$ record, but a light excursion of 0.6‰ may be present in the FC record at ~15.5 ka, and a heavy excursion of 0.4‰ may be present in LBB at ~17 ka. However, these older excursions are not well defined.

Seawater $\delta^{18}O$ was calculated using Eqn. (1) and is presented in Figure 6d. Coretop values at both LBB and FC are consistent with modern values. At LBB, a glacial-interglacial trend of decreasing $\delta^{18}O_{sw}$ is present. Using the modern $\delta^{18}O_{sw}$-salinity relationship, the 0.9‰ glacial-interglacial $\delta^{18}O_{sw}$ decrease suggests a freshening of 1.7 p.s.u. Superimposed on the glacial-interglacial trend at LBB are two millennial-scale salinity excursions. During Heinrich event 1, $\delta^{18}O_{sw}$ may have decreased by 0.7‰ (1.3 p.s.u.) and during the Younger Dryas, $\delta^{18}O_{sw}$ decreased by 0.4‰ (0.8 p.s.u.). At FC, there are insufficient data to conclusively determine a glacial-interglacial trend or to identify Heinrich event 1, but during the Younger Dryas, $\delta^{18}O_{sw}$ increased by 0.8‰ (1.5 p.s.u.). Overall, the $\delta^{18}O_{sw}$ data for the two locations suggest similar salinities during most of the record, but an increased salinity gradient during the Younger Dryas, when salinities at FC were significantly higher than at LBB. A similar salinity gradient was also present from ~8.5 to 6.5 ka.

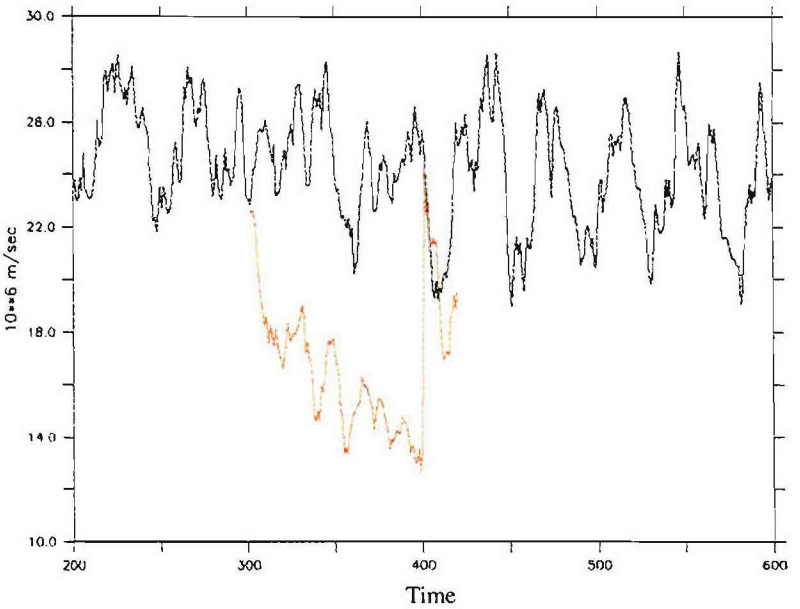

Figure 7. Time-series of the meridional overturning. Black line represents the control integration; red line represents the 100-year freshwater forcing experiment, which started at year 300 of the control.

Model Response

In response to a surface freshwater forcing of 0.1 Sv for a period of 100 years, meridional overturning in the GFDL R30 model is greatly reduced from 25 Sv during the control run to about 13 Sv during the experiment (Figure 7). The addition of freshwater into the North Atlantic causes a large decrease in high latitude surface salinities (Figure 8a) and surface temperatures (Figure 8b). As with previous freshwater forcing experiments [*Manabe and Stouffer*, 1997; *Marchal et al.*, 1999; *Rahmstorf*, 1994], surface temperatures in the lower latitudes increase as a result of the reduction in the northward transport of heat via the upper limb of the Atlantic overturning cell.

The surface stability caused by the freshwater input reduces the strength of deep water formation, but does not cause a cessation of overturning (Figure 9a and b). Instead, convection continues to shallower depths, incorporating the cold, fresh surface waters into the intermediate depth North Atlantic (Figure 10a and b). These cold, fresh waters then deflect southwestward due to Coriolis forces, propagating the cooling and freshening anomalies toward the southwestern side of the North Atlantic basin. The resulting decreases in intermediate depth temperatures and salinities are significantly greater in the western

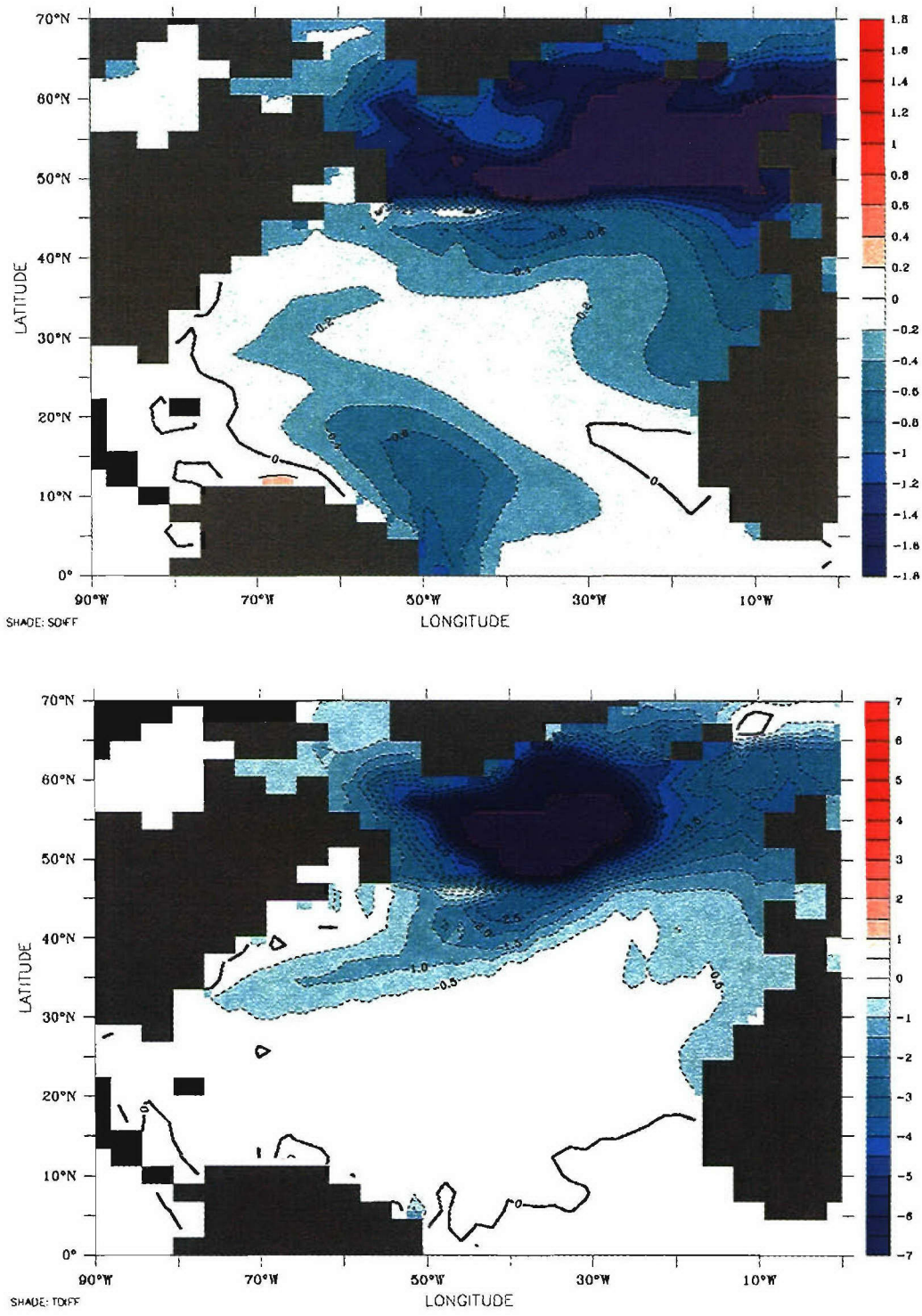

Figure 8. Sea surface anomalies. **a.)** salinity anomalies; **b.)** temperature anomalies. Average of years 380-400 of the experiment minus years 300-400 of the control.

open-ocean North Atlantic than in the eastern Atlantic (Figures 10a and b).

The influence of Mediterranean Outflow Water (MOW) enhances the differences between the anomalies in the eastern and western sides of the basin. MOW is warmer, saltier and denser than other Atlantic waters. When it enters the Atlantic Ocean, it sinks until it reaches the isopycnal surface with the same density (to depths of ~1,000 m in the control run). It then spreads southwestward across the Atlantic along isopycnal surfaces. In the GFDL R30 model, the amount of outflow water entering the Atlantic from the Mediterranean Sea is fixed, but the properties of MOW (such as temperature and salinity) are determined by the gradient between the two water bodies. Therefore, the fresher, colder, intermediate depth Atlantic water creates a stronger gradient between the Atlantic and the Mediterranean, causing a greater influx of salt and heat from the Mediterranean.

Figures 10a and 10b also reveal a striking contrast between the anomalies in the open ocean Atlantic and those at the western boundary. Waters at the western boundary are significantly warmer and saltier due to the reduced northward transport of heat via the North Atlantic Current, and also due to a southward shift in the location of the Intertropical Convergence Zone, which causes increased continental runoff from the Amazon River, increased surface stabilities, and decreased upwelling of colder, deeper water.

The model results also show that the overall shoaling of the North Atlantic overturning cell results in increased ventilation in certain parts of the intermediate depth North Atlantic. The negative age anomaly at 1,142 m water depth shows this increased ventilation (Figure 11). The age of a parcel of water is set at zero when that parcel has contact with the surface, and it begins to "age" after it leaves the surface. During the last 20 years of the 100-year experiment, the negative age anomaly in the intermediate depth open ocean North Atlantic is greater than 40 years, signifying a significant increase in ventilation. In some parts of the eastern Atlantic, there is little change in water mass age, and in others, waters are significantly older. Superimposed on the age anomaly in Figure 11 are the velocity anomalies for this depth, which emphasize the propagation of temperature, salinity and age anomalies to the western side of the Atlantic basin.

Model-Data Comparison

While different in magnitude, the Younger Dryas temperature estimates from the LBB and FC sites are consistent with the results of the freshwater forcing experiment. The model predicts intermediate depth cooling in the open ocean as a result of the incorporation of cool high latitude surface waters into the subsurface, and core LBB, which records

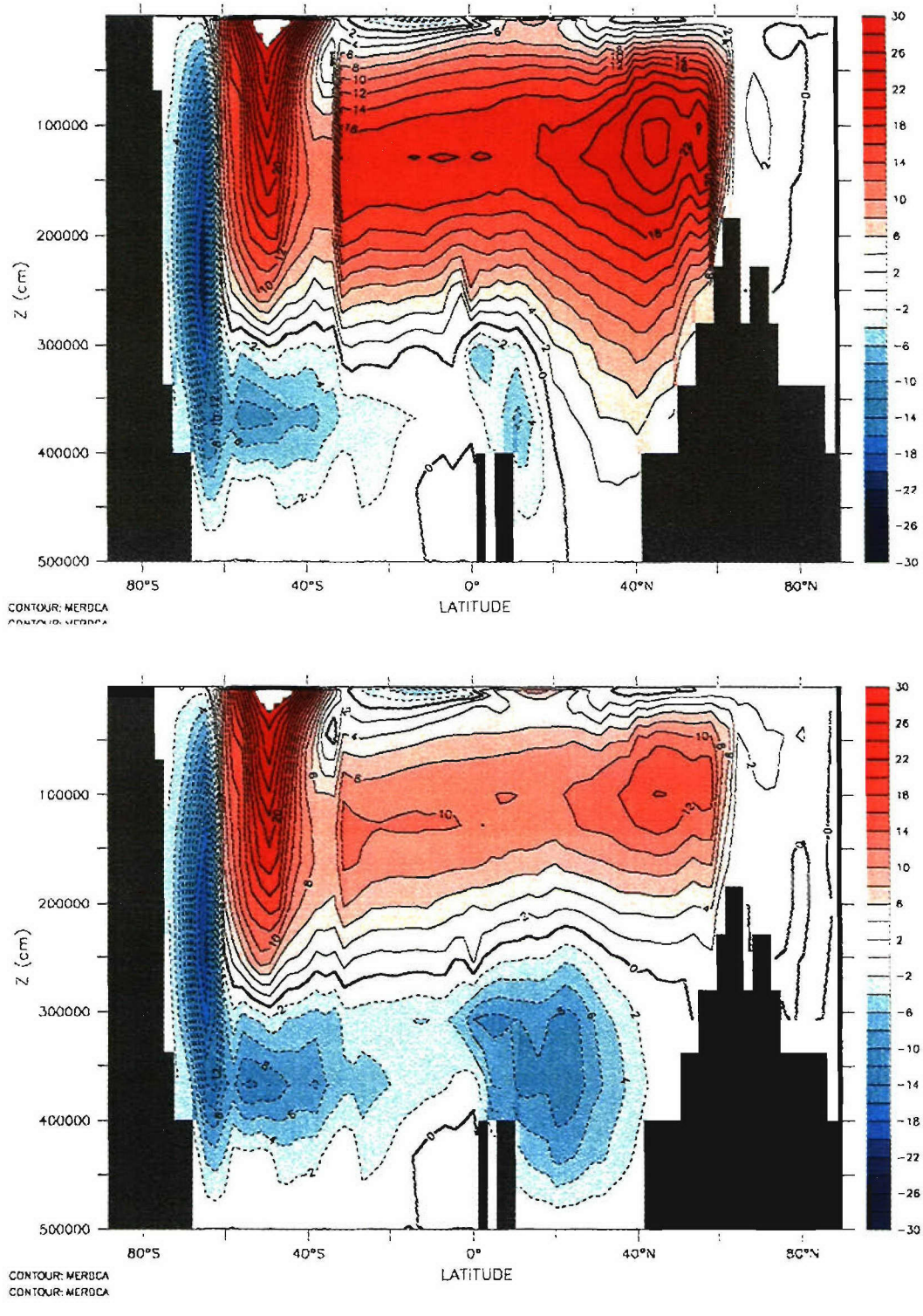

Figure 9. The meridional overturning of the Atlantic Ocean. **a.)** years 300-400 of the control; **b.)** years 380-400 of the experiment.

intermediate depth variability in the Sargasso Sea, suggests a cooling during the Younger Dryas. The model also predicts warming in the Caribbean as a result of reduced upwelling and a reduction in the northward transport of heat, and FC, which lies within the northward moving limb of the MOC return flow, suggests a warming during the Younger Dryas. However, the magnitudes of the temperature anomalies differ significantly: anomalies in the model are on the order of a degree, whereas the data suggest anomalies on the order of several degrees. This may, in part, be due to the duration of the freshwater forcing experiment (100 years, *versus* the ~1,500 year duration of the Younger Dryas). An experiment of longer duration might allow more cold, fresh surface water to propagate into the subsurface. Another possible explanation for the discrepancy is that a freshwater perturbation of the entire North Atlantic region from 50°N to 70°N may not be an appropriate representation of actual forcing, which may have had a point source from the Arctic [*Tarasov and Peltier*, 2005] or from glacial Lake Agassiz [*Teller et al.*, 2002]. A third explanation is that modern boundary conditions may not be an adequate representation of the Bølling-Allerød, which was significantly more glaciated than today. Alternatively, the slope of the Mg/Ca-temperature calibration may be inadequately defined – an increase in the slope would decrease the temperature variability in the sediment records.

The Younger Dryas salinity data from LBB and FC are also consistent with the model, but different in magnitude. The model predicts intermediate depth freshening in the open ocean as a result of the incorporation of fresh, high latitude surface waters into the subsurface, and core LBB suggests decreased salinities during the Younger Dryas. The model also predicts increased salinities in the Caribbean as a result of reduced transport of high salinity waters from the low latitudes to the high latitudes, and FC, which lies within the northward moving limb of the MOC return flow, suggests a increased salinities during the Younger Dryas. However, as with the temperature anomalies, the magnitude of the salinity anomalies in the paleodata is significantly greater than in the model output: anomalies in the model are on the order of 0.05 to 0.10 p.s.u., whereas the paleodata suggest Younger Dryas salinity changes on the order of 1 to 1.5 p.s.u. Again, as with the temperature anomalies, explanations for the discrepancy include the inadequacies associated with the experiment duration, the geographic distribution of the modeled perturbation, and modern rather than Bølling-Allerød boundary conditions.

Intermediate Depth Ventilation Results and Paleoclimate Evidence

The model results predict different intermediate depth ventilation responses

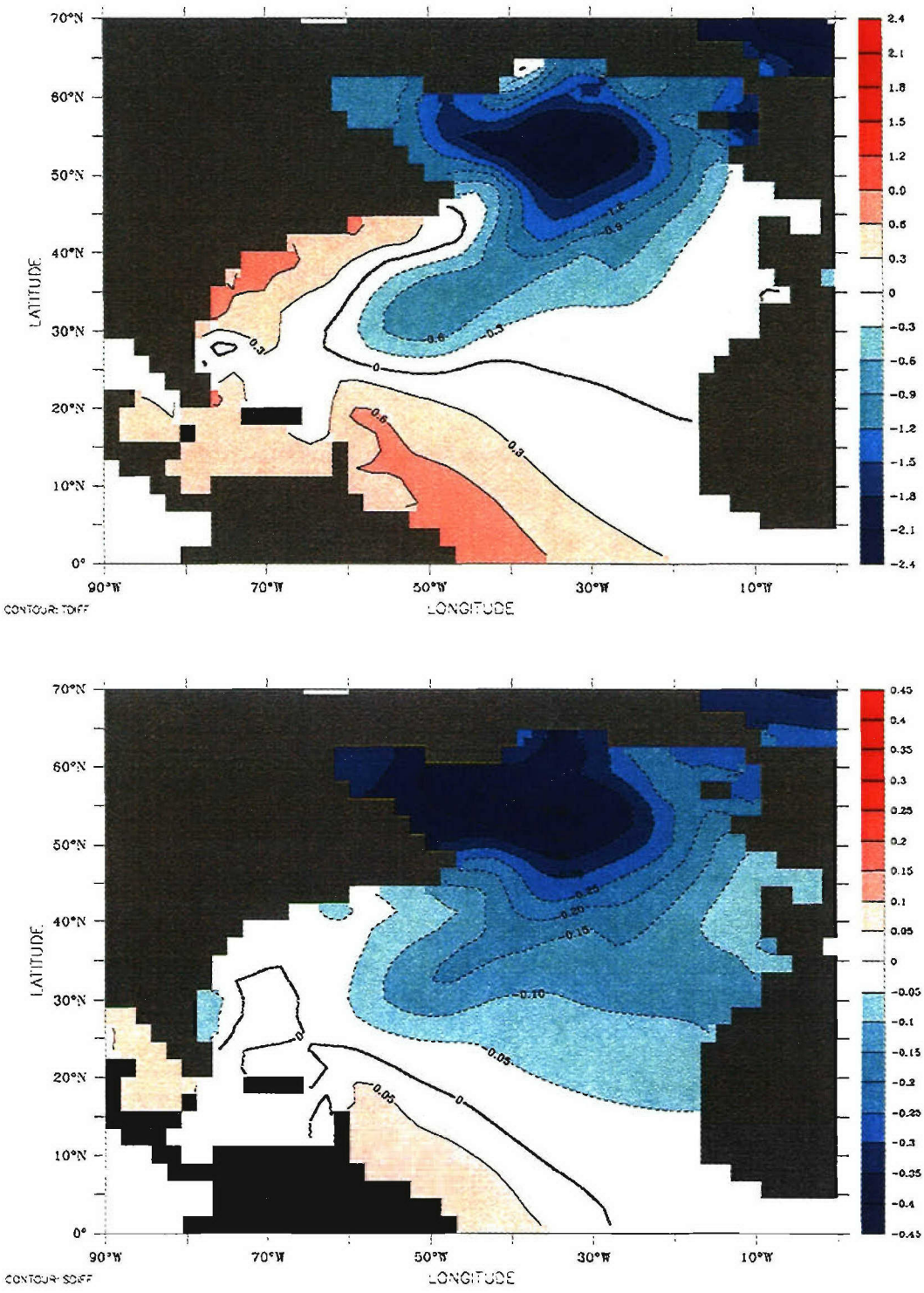

Figure 10. Anomalies at 1,142 m depth. **a)** temperature anomalies; **b)** salinity anomalies. Average of years 380-400 of the experiment minus years 300-400 of the control.

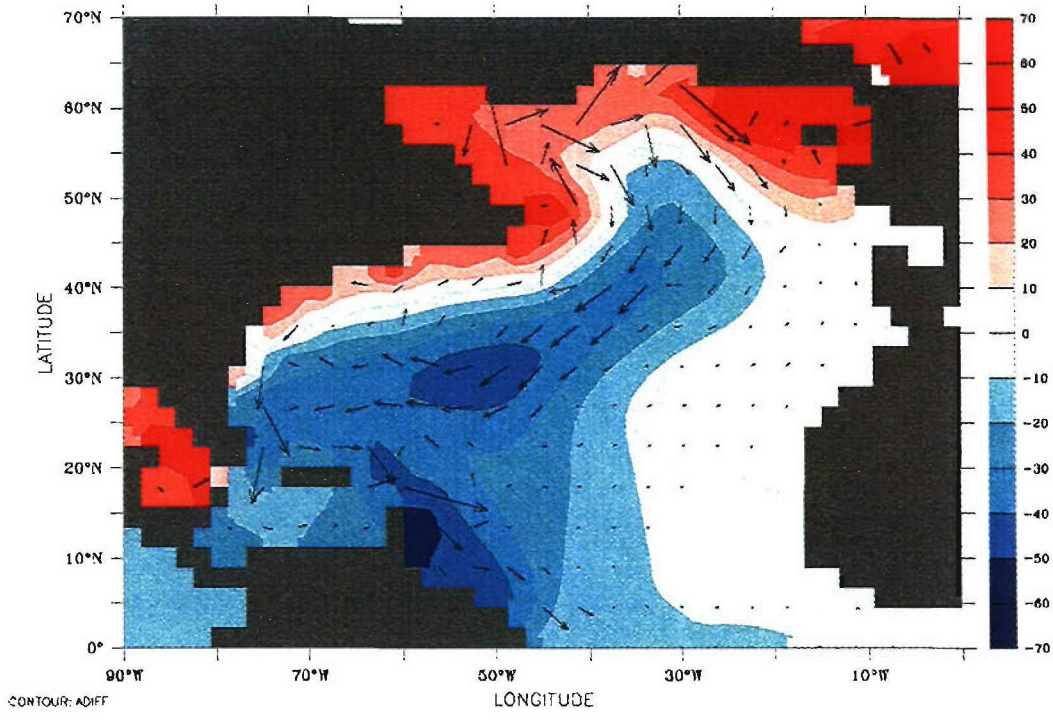

Figure 11. Age tracer anomalies and velocity anomalies at 1,142 m depth. Average of years 380-400 of the experiment minus years 300-400 of the control.

in different regions of the North Atlantic: in the western subtropics the model predicts increased ventilation, but in much of the eastern high latitudes the model predicts decreased ventilation (Figure 11). Nutrient evidence from Little Bahama Bank [*Marchitto et al.*, 1998] and benthic-planktic radiocarbon pairs from the Blake Plateau [*Keigwin*, 2004] both suggest increased intermediate depth ventilation during the Younger Dryas, consistent with the model results for the western subtropical Atlantic. On the eastern side of the Atlantic, nutrient evidence from the Portuguese margin suggests reduced intermediate depth ventilation during Heinrich events [*Zahn et al.*, 1997], but no significant change during the Younger Dryas. For this region of the intermediate depth Atlantic, the model predicts only very slightly reduced ventilation (perhaps an age anomaly of 10 years), consistent with the Younger Dryas data, but not consistent with the Heinrich event data. It is conceivable, however, that a freshwater forcing of a different magnitude could cause an increase in the age anomaly at the Portuguese margin. In the high latitude North Atlantic, nutrient evidence suggests significantly reduced ventilation during both the Younger Dryas and

Heinrich event 1 [*Rickaby and Elderfield*, 2005], also consistent with the increased ages predicted by the model for the high latitudes. Thus, the model results provide one possible explanation for the apparent disagreement between the intermediate depth Younger Dryas evidence from various regions of the North Atlantic.

Conclusions

Several zonally averaged models predict intermediate depth warming in response to North Atlantic freshwater forcing, however, this is the first study to compare the spatial distribution of simulated temperature and salinity anomalies at intermediate depth to paleoclimate data. The model results suggest a more complex pattern of intermediate depth anomalies than can be predicted with a zonally averaged representation. It reveals cooling and freshening of the open ocean North Atlantic and warming and increased salinities at the western boundary, consistent with our two new Younger Dryas temperature and salinity records, and consistent with a previous intermediate depth temperature record from the tropics [*Rühlemann et al.*, 2004]. In addition, the model results are consistent with other paleoclimate data suggesting increased intermediate depth ventilation during the YD [*Keigwin*, 2004; *Marchitto et al.*, 1998] and provide a possible explanation for the apparent discrepancies between data from various regions of the North Atlantic, such as reduced ventilation in the very high latitudes and in the eastern Atlantic during the Younger Dryas and during Heinrich events [*Rickaby and Elderfield*, 2005; *Zahn et al.*, 1997]. The agreement between the model and the data suggests that freshwater forcing is a possible driver or amplifier for Bølling-Allerød to Younger Dryas climate variability. The results are consistent with the hypothesis of freshwater induced climate change, but do not rule out the possibility of an alternative forcing mechanism that could create similar intermediate depth anomalies. An examination of the paleodata in the context of a southern hemisphere freshwater forcing experiment would help to clarify our understanding of the types of forcing mechanisms that could be consistent with the paleoceanographic evidence.

References

Bond, G., W. S. Broecker, S. Johnsen, J. F. McManus, L. Labeyrie, J. Jouzel, and G. Bonani (1993), Correlations between climate records from North Atlantic sediments and Greenland ice, *Nature*, *365*, 143-147.

Boyle, E. A. (1983), Manganese carbonate overgrowths on foraminifera tests, *Geochim. Cosmochim. Acta*, *47*, 1815-1819.

Boyle, E. A., and L. D. Keigwin (1985/6), Comparison of Atlantic and Pacific paleochemical records for the last 215,000 years: changes in deep ocean circulation and chemical inventories, *Earth Planet. Sci. Lett.*, *76*, 135-150.

Boyle, E. A., and L. D. Keigwin (1987), North Atlantic thermohaline circulation during the past 20,000 years linked to high-latitude surface temperature, *Nature*, *330*, 35-40.

Boyle, E. A., L. Labeyrie, and J.-C. Duplessy (1995), Calcitic foraminiferal data confirmed by cadmium in aragonitic Hoeglundina: Application to the Last Glacial Maximum in the northern Indian Ocean, *Paleoceanography*, *10*, 881-900.

Boyle, E. A., and Y. Rosenthal (1996), Chemical hydrography of the South Atlantic during the Last Glacial Maximum: Cd and $\delta^{13}C$, in *The South Atlantic: Present and Past Circulation*, edited by G. Wefer, pp. 423-443, Springer-Verlag, Berlin.

Broecker, W. S., J. P. Kennett, B. P. Flower, J. T. Teller, S. Trumbore, G. Bonani, and W. Wolfli (1989), Routing of meltwater from the Laurentide ice-sheet during the Younger Dryas cold episode, *Nature*, *341*, 318-321.

Broecker, W. S., D. M. Peteet, and D. Rind (1985), Does the ocean-atmosphere system have more than one stable mode of operation? *Nature*, *315*, 21-25.

Bryan, K., and L. J. Lewis (1979), A water mass model of the World Ocean, *J. Geophys. Res.*, *84*, 2503–2517.

Came, R. E., D. W. Oppo, and W. B. Curry (2003), Atlantic Ocean circulation during the Younger Dryas: Insights from a new Cd/Ca record from the western subtropical South Atlantic, *Paleoceanography*, *18*, 1086, doi:1010.1029/2003PA000888.

Dahl, K. A., A. Broccoli, and R. J. Stouffer (2005), Assessing the role of North Atlantic freshwater forcing in millennial scale climate variability: a tropical Atlantic perspective, *Clim. Dyn.*, *24*, 325-346.

Dansgaard, W. (1984), North Atlantic climate oscillations revealed by deep Greenland ice cores, in *Climate Processes and Climate Sensitivity, Geophysical Monograph Series, vol 29*, edited by J. E. Hanson and T. Takahashi, p. 288– 298, American Geophysical Union, Washington, D. C.

Dansgaard, W., et al. (1993), Evidence for general instability of past climate from a 250-Kyr ice-core record, *Nature*, *364*, 218-220.

Delworth, T. L., R. J. Stouffer, K. W. Dixon, M. J. Spelman, T. R. Knutson, A. J. Broccoli, P. J. Kushner, and R. T. Wetherald (2002), Review of simulations of climate variability and change with the GFDL R30 coupled climate model, *Clim. Dyn.*, *19*, 555-574.

Gordon, A. L. (1986), Interocean exchange of thermocline water, *J. Geophys. Res.*, *91*, 5037-5046.

Grootes, P. M., M. Stuiver, J. W. C. White, S. J. Johnsen, and J. Jouzel (1993), Comparison of oxygen-isotope records from the GISP2 and GRIP Greenland ice cores, *Nature*, *366*, 552-554.

Hughen, K. A., et al. (2004), Marine04 marine radiocarbon age calibration, 0–26 cal kyr BP, *Radiocarbon*, *46*, 1059-1086.

Jenkins, W. J. (1980), Tritium and He-3 in the Sargasso Sea, *J. Mar. Res.*, *38*, 533-569.

Keeling, R. F., and B. B. Stephens (2001), Antarctic sea ice and the control of Pleistocene climate instability, *Paleoceanography*, *16*, 112-131.

Keigwin, L. D. (2004), Radiocarbon and stable isotope constraints on Last Glacial Maximum and Younger Dryas ventilation in the western North Atlantic, *Paleoceanography*, *19*, PA4012, doi:4010.1029/2004PA001029.

Keigwin, L. D., G. A. Jones, S. J. Lehman, and E. A. Boyle (1991), Deglacial meltwater discharge, North-Atlantic deep circulation, and abrupt climate change, *J. Geophys. Res.*, *96*, 16811-16826.

Lea, D. W., D. K. Pak, L. C. Peterson, and K. A. Hughen (2003), Synchroneity of tropical and high-latitude Atlantic temperatures over the last glacial termination, *Science*, *301*, 1361-1364.

Lear, C. H., Y. Rosenthal, and N. C. Slowey (2002), Benthic foraminiferal Mg/Ca-paleothermometry: A revised core-top calibration, *Geochim. Cosmochim. Acta*, *66*, 3375-3387.

Lehman, S. J., and L. D. Keigwin (1992), Sudden changes in North-Atlantic circulation during the last deglaciation, *Nature*, *356*, 757-762.

Levitus, S., and T. Boyer (1994), *World Ocean Atlas 1994 Volume 4: Temperature. NOAA Atlas NESDIS 4*, U.S. Department of Commerce, Washington, D.C.

Luyten, J. R., J. Pedlosky, and H. Stommel (1983), The ventilated thermocline, *J. Phys. Oceanogr.*, *13*, 192-309.

Lynch-Stieglitz, J., unpublished data.

Lynch-Stieglitz, J., W. B. Curry, and N. C. Slowey (1999), A geostrophic transport estimate for the Florida Current from the oxygen isotope composition of benthic foraminifera, *Paleoceanography*, *14*, 360-373.

Lynch-Stieglitz, J., R. G. Fairbanks, and C. D. Charles (1994), Glacial-interglacial history of Antarctic Intermediate Water: Relative strengths of Antarctic versus Indian Ocean sources, *Paleoceanography*, *9*, 7-29.

Manabe, S., J. Smagorinsky, and R. F. Strickler (1965), Simulated climatology of a general circulation model with a hydrologic cycle, *Mon. Weather Rev.*, *93*, 769–798.

Manabe, S., and R. J. Stouffer (1997), Coupled ocean-atmosphere model response to freshwater input: Comparison to Younger Dryas event, *Paleoceanography*, *12*, 321-336.

Marchal, O., T. F. Stocker, and F. Joos (1999), Physical and biogeochemical responses to freshwater induced thermohaline variability in a zonally averaged ocean model, in *Mechanisms of Global Climate Change at Millennial Time Scales, Geophysical Monograph Series, vol. 112*, edited by P. U. Clark, et al., pp. 263-284, American

Geophysical Union, Washington, D.C.

Marchitto, T. M., W. B. Curry, and D. W. Oppo (1998), Millennial-scale changes in North Atlantic circulation since the last glaciation, *Nature*, *393*, 557-561.

McCartney, M. S. (1982), The subtropical recirculation of mode waters, *J. Mar. Res.*, *40, suppl.*, 427-464.

Rahmstorf, S. (1994), Rapid climate transitions in a coupled ocean-atmosphere model, *Nature*, *372*, 82-85.

Redi, M. H. (1982), Oceanic isopycnal mixing by coordinate rotation, *J. Phys. Oceanogr.*, *12*, 1154–1158.

Reid, J. L. (1994), On the total geostrophic circulation of the North-Atlantic Ocean - flow patterns, tracers, and transports, *Prog. Oceanogr.*, *33*, 1-92.

Rickaby, R. E. M., and H. Elderfield (2005), Evidence from the high-latitude North Atlantic for variations in Antarctic Intermediate water flow during the last deglaciation, *Geochem. Geophys. Geosys.*, *6*, Q05001, doi:05010.01029/02004GC000858.

Rosenthal, Y. (1994), Late quaternary paleochemistry of the Southern Ocean: evidence from cadmium variablity in sediments and foraminifera, Ph.D. thesis, 186 pp, Massachusetts Institute of Technology and Woods Hole Oceanographic Institution.

Rosenthal, Y., M. P. Field, and R. M. Sherrell (1999), Precise determination of element/ calcium ratios in calcareous samples using sector field inductively coupled plasma mass spectrometry, *Anal. Chem.*, *71*, 3248-3253.

Rosenthal, Y., P. Lam, E. A. Boyle, and J. Thomson (1995), Authigenic cadmium enrichments in suboxic sediments: Precipitation and postdepositional mobility, *Earth Planet. Sci. Lett.*, *132*, 99-111.

Rosenthal, Y., C. H. Lear, D. W. Oppo, and B. Linsley (in press), Temperature and carbonate ion effects on Mg/Ca and Sr/Ca ratios in benthic foraminifera: The aragonitic species *Hoeglundina elegans*, *Paleoceanography*.

Ruddiman, W. F., and A. McIntyre (1981), The North Atlantic Ocean during the last deglaciation, *Palaeogeogr. Paleoclimatol. Paleoecol.*, *35*, 145-214.

Rühlemann, C., S. Mulitza, G. Lohmann, A. Paul, M. Prange, and G. Wefer (2004), Intermediate depth warming in the tropical Atlantic related to weakened thermohaline circulation: Combining paleoclimate data and modeling results for the last deglaciation, *Paleoceanography*, *19*, PA1025, doi:1010.1029/2003PA000948.

Rühlemann, C., S. Mulitza, P. J. Muller, G. Wefer, and R. Zahn (1999), Warming of the tropical Atlantic Ocean and slowdown of thermohaline circulation during the last deglaciation, *Nature*, *402*, 511-514.

Saenko, O. A., A. J. Weaver, and J. M. Gregory (2003a), On the link between the two modes of the ocean thermohaline circulation and the formation of global-scale water masses, *J. Clim.*, *16*, 2797-2801.

Saenko, O. A., A. J. Weaver, and A. Schmittner (2003b), Atlantic deep circulation controlled by freshening in the Southern Ocean, *Geophys. Res. Lett.*, *30*, 1754, doi:1710.1029/ 2003GL017681.

Sarmiento, J. L., C. G. Rooth, and W. Roether (1982), The North Atlantic tritium distribution in 1972, *J. Geophys. Res.*, *87*, 8047-8056.

Sarnthein, M., et al. (2001), Fundamental modes and abrupt changes in North Atlantic circulation and climate over the last 60 kyr—Concepts, reconstruction and numerical modeling, in *The Northern North Atlantic: A Changing Environment*, edited by P. Schafer, et al., pp. 365-410, Springer-Verlag, New York.

Schmitz, W. J., J. R. Luyten, and R. W. Schmitt (1993), On the Florida Current T/S envelope, *Bull. Mar. Sci.*, *53*, 1048-1065.

Schmitz, W. J., and P. L. Richardson (1991), On the sources of the Florida Current, *Deep-Sea Res.*, *38*, S379-S409.

Slowey, N. C., and W. B. Curry (1995), Glacial-interglacial differences in circulation and carbon cycling within the upper western North-Atlantic, *Paleoceanography*, *10*, 715-732.

Stuiver, M., and P. J. Reimer (1993), Extended ^{14}C database and revised CALIB radiocarbon calibration program, *Radiocarbon*, *35*, 215-230.

Tarasov, L., and W. R. Peltier (2005), Arctic freshwater forcing of the Younger Dryas cold reversal, *Nature*, *435*, 662-665.

Teller, J. T., D. W. Leverington, and J. D. Mann (2002), Freshwater outbursts to the oceans from glacial Lake Agassiz and their role in climate change during the last deglaciation, *Quat. Sci. Rev.*, *21*, 879-887.

Thompson, L. G., et al. (1998), A 25,000-year tropical climate history from Bolivian ice cores, *Science*, *282*, 1858-1864.

Tsuchiya, M. (1989), Circulation of the Antarctic Intermediate Water in the North-Atlantic Ocean, *J. Mar. Res.*, *47*, 747-755.

Waelbroeck, C., L. Labeyrie, E. Michel, J.-C. Duplessy, J. F. McManus, K. Lambeckd, E. Balbona, and M. Labracherie (2002), Sea-level and deep water temperature changes derived from benthic foraminifera isotopic records, *Quat. Sci. Rev.*, *21*, 295-305.

Wang, Y. J., H. Cheng, R. L. Edwards, Z. S. An, J. Y. Wu, C. C. Shen, and J. A. Dorale (2001), A high-resolution absolute-dated Late Pleistocene monsoon record from Hulu Cave, China, *Science*, *294*, 2345-2348.

Weaver, A. J., O. A. Saenko, P. U. Clark, and J. Mitrovica (2003), Meltwater pulse 1A from Antarctica as a trigger of the Bølling-Allerød warm interval, *Science*, *299*, 1709-1713.

Zahn, R., J. Schonfeld, H. R. Kudrass, M. H. Park, H. Erlenkeuser, and P. Grootes (1997), Thermohaline instability in the North Atlantic during meltwater events: Stable isotope and ice-rafted detritus records from core SO75-26KL, Portuguese margin, *Paleoceanography*, *12*, 696-710.

Zahn, R., and A. Stüber (2002), Suborbital intermediate water variability inferred from paired benthic foraminiferal Cd/Ca and $\delta^{13}C$ in the tropical West Atlantic and linking with North Atlantic climates, *Earth Planet. Sci. Lett.*, *200*, 191-205.

Tables

Table 1. AMS dates and calendar ages*.

Depth (cm)	Species	NOSAMS ID	AMS Date	AMS Error	1 or 2 σ	Age Lower (yrs BP)	Age Upper (yrs BP)	Prob	Age (yrs BP)	Source
OCE205-2-100GGC										
7	*G. sacculifer*	OS-181	1,040	30	1	567	581	0.15	613	this study
					1	594	648	0.85		
					2	544	663	1		
17	*G. sacculifer*	OS-27756	2,250	40	1	1,807	1,911	1	1,856	this study
					2	1,737	1,964	1		
31	*G. sacculifer*	OS-27757	3,150	40	1	2,864	2,993	1	2,936	this study
					2	2,810	3,070	1		
63	*G. sacculifer*	OS-27758	5,150	45	1	5,472	5,566	1	5,515	this study
					2	5,402	5,611	1		
73	*G. sacculifer*	OS-27759	5,770	40	1	6,165	6,257	1	6,200	this study
					2	6,085	6,285	1		
80	*G. sacculifer*	OS-27834	6,850	45	1	7,323	7,413	1	7,368	this study
					2	7,268	7,450	1		
80	*G. sacculifer*	OS-180	6,470	55	1	6,884	7,049	1	6,970	this study
					2	6,824	7,140	1		
92	*G. sacculifer*	OS-27835	8,440	85	1	8,959	9,197	1	9,059	this study
					2	8,775	9,294	1		
100	*G. sacculifer*	OS-178	8,870	55	1	9,464	9,574	1	9,525	this study
					2	9,427	9,668	1		
109	*G. sacculifer*	OS-27836	10,400	55	1	11,294	11,433	0.51	11,468	this study
					1	11478	11624	0.49		
					2	11,243	11,707	1		
116	*G. sacculifer*	OS-27837	11,750	110	1	13,118	13,303	1	13,218	this study
					2	13,020	13,415	1		
120	*G. sacculifer*	OS-176	12,000	45	1	13,347	13,483	1	13,427	this study
					2	13,310	13,586	1		
160	*G. sacculifer*	OS-174	23,800	110					27,800	this study
KNR166-2-31JPC										
0.5	*G. sacculifer*	OS-39424	1,640	40	1	1,166	1,254	1	1,204	*Lynch-Stieglitz* [unpubl.]
					2	1,100	1,283	1	1,204	*Lynch-Stieglitz* [unpubl.]
64	*G. sacculifer*	OS-42460	7,310	50	1	7,708	7,831	1	7,773	*Lynch-Stieglitz* [unpubl.]
					2	7,663	7,899	1	7,773	*Lynch-Stieglitz* [unpubl.]
112	*G. sacculifer*	OS-42461	12,050	75	1	13,401	13,598	1	13,500	*Lynch-Stieglitz* [unpubl.]
					2	13,322	13,684	1	13,500	*Lynch-Stieglitz* [unpubl.]
160	*G. ruber*	OS-42462	16,650	160	1	19,198	19,537	1	19,397	*Lynch-Stieglitz* [unpubl.]
					2	19,048	19,612	0.9	19,397	*Lynch-Stieglitz* [unpubl.]
					2	19656	19806	0.1		

* AMS radiocarbon dates were converted to calendar age using CALIB 5.01 [*Stuiver and Reimer,* 1993], the Marine04 dataset [*Hughen et al.,* 2004], and a reservoir correction of 400 years.

Table 2. OCE205-2-100GGC *H. elegans* Mg/Ca data.

Depth (cm)	Age (yrs BP)	[Ca] (ppm)	Al/Ca (μmol mol^{-1})	Mg/Ca (mmol mol^{-1})	Mean Mg/Ca (mmol mol^{-1})	BWT* (°C; RLOL**)
OCE205-2-100GGC						
8	737	211	-0.17	1.15	1.15	5.6
13	1,359	191	6.12	1.11	1.07	3.2
13	1,359	216	0.68	1.03		
16	1,732	259	0.61	1.09	1.09	3.9
18	1,933	277	0.72	1.13	1.13	5.0
19	2,010	296	0.98	1.09	1.09	3.9
21	2,165	200	3.89	1.16	1.16	5.8
22	2,242	229	0.83	1.16	1.16	5.8
24	2,396	188	3.26	1.13	1.13	5.1
25	2,473	284	0.70	1.09	1.09	3.8
26	2,550	258	0.57	1.06	1.06	2.8
27	2,627	259	0.55	1.08	1.07	3.3
27	2,627	246		1.07		
28	2,705	228	1.03	1.11	1.11	4.5
29	2,782	281	0.87	1.20	1.20	7.1
29	2,782	206		1.20		
30	2,859	241	0.52	1.18	1.18	6.6
32	3,017	299		1.10	1.10	4.2
33	3,097	265	3.23	1.10	1.10	4.0
35	3,258	246	-0.06	1.08	1.08	3.6
36	3,339	303	1.20	1.14	1.14	5.4
37	3,420	224	0.92	1.14	1.14	5.3
38	3,500	335	3.16	1.12	1.12	4.7
39	3,581	251	1.77	1.13	1.13	5.1
40	3,661	272	0.68	1.12	1.12	4.6
42	3,823	296		1.08	1.08	3.6
43	3,903	274	1.95	1.14	1.14	5.2
44	3,984	276	3.35	1.07	1.07	3.3
45	4,064	255	1.29	1.07	1.07	3.2
46	4,145	280	0.96	1.09	1.09	3.9
47	4,226	367	2.20	1.15	1.15	5.5
48	4,306	288	4.32	1.11	1.11	4.4
49	4,387	264	1.27	1.08	1.08	3.5
51	4,548	237	0.70	1.07	1.07	3.3
52	4,629	251	0.67	1.10	1.10	4.3
53	4,709	321		1.14	1.14	5.2
54	4,790	143	2.61	1.14	1.14	5.2
55	4,870	260		1.10	1.10	4.1
56	4,951	265	4.37	1.10	1.09	4.0
56	4,951	233	9.64	1.09		
57	5,031	283		1.15	1.15	5.7
58	5,112	292	1.30	1.05	1.04	2.3
58	5,112	203	1.21	1.03		
59	5,193	275	0.98	1.23	1.23	8.0
60	5,273	238	1.01	1.12	1.12	4.6
61	5,354	239		0.97	0.97	0.3

Table 2 (cont.).

Depth (cm)	Age (yrs BP)	[Ca] (ppm)	Al/Ca (μmol mol^{-1})	Mg/Ca (mmol mol^{-1})	Mean Mg/Ca (mmol mol^{-1})	BWT* (°C; RLOL**)
OCE205-2-100GGC						
62	5,434	305	0.98	1.10	1.10	4.2
63	5,515	263		1.13	1.13	5.0
64	5,584	269		1.11	1.11	4.3
66	5,721	277	1.79	1.20	1.20	7.2
67	5,789	255	17.98	1.11	1.11	4.5
68	5,858	284		1.21	1.16	5.8
68	5,858	253	2.45	1.10		
70	5,995	320	-0.02	1.13	1.13	4.9
71	6,063	314	0.36	1.16	1.16	5.9
72	6,132	224	0.64	1.15	1.15	5.7
73	6,200	258	0.63	1.10	1.10	4.1
74	6,310	272	1.85	1.11	1.11	4.3
75	6,420	280		1.07	1.07	3.3
76	6,530	311	5.65	1.12	1.13	4.9
76	6,530	254	0.06	1.14		
77	6,640	206	0.85	1.17	1.13	5.1
77	6,640	293	0.24	1.09		
78	6,750	269	3.56	1.12	1.12	4.7
79	6,860	241	0.77	1.06	1.06	3.0
80	6,970	280	0.65	1.14	1.14	5.4
81	7,144	232	0.38	1.13	1.13	5.0
82	7,318	294	2.00	1.11	1.11	4.3
83	7,492	246		1.11	1.11	4.3
85	7,840	266	0.54	1.12	1.12	4.8
86	8,015	211	0.80	1.12	1.12	4.6
87	8,189	188	1.23	1.05	1.05	2.7
88	8,363	288	1.38	1.14	1.14	5.4
89	8,537	249	0.43	1.16	1.16	5.9
90	8,711	253		1.15	1.15	5.7
91	8,885	279	0.25	1.25	1.19	6.8
91	8,885	289	0.11	1.13		
92	9,059	237	1.22	1.18	1.18	6.6
93	9,117	290	0.78	1.13	1.13	5.1
95	9,234	298	0.45	1.16	1.16	5.9
96	9,292	107	1.51	1.19	1.19	6.7
98	9,409	128	1.19	1.17	1.17	6.1
99	9,467	278	0.75	1.18	1.18	6.5
100	9,525	278	0.49	1.22	1.22	7.6
101	9,741	302	0.28	1.14	1.14	5.2
102	9,957	183	0.82	1.17	1.17	6.2
103	10,173	188	0.36	1.21	1.21	7.4
104	10,389	216	0.52	1.24	1.24	8.1
105	10,604	389	0.38	1.15	1.16	5.8
105	10,604	311		1.17		
106	10,820	84	0.77	1.11	1.11	4.4
108	11,252	112	0.67	1.13	1.13	5.1

Table 2 (cont.).

Depth (cm)	Age (yrs BP)	[Ca] (ppm)	Al/Ca (μmol mol^{-1})	Mg/Ca (mmol mol^{-1})	Mean Mg/Ca (mmol mol^{-1})	BWT* (°C; RLOL**)
OCE205-2-100GGC						
109	11,468	305	0.95	1.15	1.15	5.5
110	11,718	84	1.01	1.09	1.15	5.7
110	11,718	185	0.56	1.23		
110	11,718	231	1.83	1.14		
112	12,218	200	1.69	1.15	1.15	5.5
113	12,468	283	0.59	1.11	1.11	4.5
117	13,270	70	2.43	1.11	1.11	4.3
120	13,427	248	0.58	1.19	1.19	6.8
123	14,452	228	0.56	1.22	1.22	7.7
124	14,794	238	1.07	1.10	1.10	4.0
126	15,478	242	0.36	1.16	1.16	5.9
128	16,162	236	0.50	1.23	1.23	7.9
132	17,529	231	0.26	1.12	1.12	4.8
136	18,896	178	0.56	1.19	1.19	6.8
138	19,580	255	1.34	1.16	1.16	5.9
142	20,947	180	0.31	1.09	1.09	3.9
148	22,998	269		1.11	1.11	4.4
152	24,365	218	0.76	1.13	1.13	5.1
156	25,733	227	1.25	1.16	1.16	5.8
158	26,416	221	2.63	1.15	1.15	5.7
162	27,784	221	0.90	1.13	1.13	4.9

* BWT is bottom water temperature.

** Temperatures were calculated using the equation of Rosenthal *et al.* [in press].

Table 3. KNR166-2-31JPC *H. elegans* Mg/Ca and Sr/Ca data.

Depth (cm)	Age (yrs BP)	[Ca] (ppm)	Al/Ca (μmol mol^{-1})	Sr/Ca (mmol mol^{-1})	Mg/Ca (mmol mol^{-1})	Mean Mg/Ca (mmol mol^{-1})	BWT* RLOL** (°C)	BWT* this study (°C)
KNR166-2-31JPC								
0.5	1,204	61	2.91		1.02	1.02	1.7	3.9
4	1,566	192	0.54		1.01	1.01	1.4	3.7
8	1,980	268	0.55		1.09	1.09	3.8	5.5
12	2,394	51	3.41		1.06	1.06	3.1	5.0
16	2,808	284	0.63		1.04	1.04	2.4	4.5
20	3,221	271	1.05		1.02	1.02	1.8	4.0
24	3,635	188			1.01	1.01	1.4	3.7
28	4,049	262	2.53		1.02	1.02	1.7	3.9
32	4,463	210			1.05	1.05	2.8	4.7
36	4,876	85	3.14		1.04	1.01	1.5	3.8
36	4,876	257	0.53		0.98			
40	5,290	268			1.06	1.06	2.8	4.8
44	5,704	243	3.12		1.14	1.14	5.2	6.6
48	6,118	49	2.25		1.00	1.04	2.3	4.4
48	6,118	298	0.75		1.07			
52	6,532	109	0.77		1.07	1.07	3.1	5.0
56	6,945	319	0.37		1.13	1.13	5.1	6.5
60	7,359	182	0.95		1.05	1.05	2.7	4.7
64	7,773	272			1.07	1.07	3.4	5.2
68	8,250	150			1.09	1.09	3.9	5.6
72	8,728	130			1.05	1.05	2.6	4.6
76	9,205	71	5.60		1.12	1.12	4.8	6.3
80	9,682	238	0.60		1.16	1.16	5.8	7.1
84	10,159	168			1.07	1.10	4.1	5.7
84	10,159	214			1.12			
88	10,636	52	0.31		1.14	1.21	7.3	8.3
88	10,636	147	1.24	2.11	1.28			
92	11,114	217	0.17		1.21	1.18	6.5	7.6
92	11,114	81	1.98		1.15			
96	11,591	204			1.20	1.20	7.0	8.0
96	11,591	151	1.00	2.09	1.20			
100	12,068	135	0.58		1.27	1.27	9.2	9.7
104	12,546	217	0.36		1.07	1.17	6.0	7.3
104	12,546	189	3.67		1.16			
104	12,546	130	1.66	2.18	1.27			
108	13,023	141	1.15		1.25	1.14	5.4	6.8
108	13,023	266	0.38		1.12			
108	13,023	162	2.54	1.77	1.07			
112	13,500	153	0.37		1.13	1.15	5.7	7.0
112	13,500	138	4.79	2.04	1.18			
116	13,991	181			1.10	1.15	5.5	6.8
116	13,991	187			1.19			
120	14,483	44	8.49		1.00	1.05	2.7	4.7
120	14,483	314	0.15		1.16			
120	14,483	200			1.01			
124	14,974	158	6.05		1.17	1.15	5.7	7.0
124	14,974	217			1.20			
124	14,974	224	5.07	1.85	1.10			
128	15,465	309	0.76		1.12	1.22	7.7	8.5
128	15,465	252	0.74		1.20			

Table 3 (cont.).

Depth (cm)	Age (yrs BP)	[Ca] (ppm)	Al/Ca (μmol mol^{-1})	Sr/Ca (mmol mol^{-1})	Mg/Ca (mmol mol^{-1})	Mean Mg/Ca (mmol mol^{-1})	BWT* RLOL** (°C)	BWT* this study (°C)
KNR166-2-31JPC								
128	15,465	196	1.83	2.10	1.33			
132	15,957	177			1.14	1.14	5.3	6.7
140	16,940	255			1.03	1.03	2.1	4.2
144	17,431	260	1.15		1.23	1.26	9.0	9.5
144	17,431	171			1.30			
148	17,923	272	0.30		0.98	0.98	0.7	3.1
152	18,414	265		2.43	1.07	1.07	3.1	5.0
168	20,382	273			1.11	1.11	4.4	6.0
220	26,778	650			1.11	1.11	4.3	5.9
228	27,762	276			1.08	1.08	3.7	5.4
244	29,730	284			1.13	1.13	5.1	6.5
260	31,698	227	0.37		1.14	1.14	5.2	6.6
264	32,190	209			1.15	1.15	5.6	7.0
268	32,682	268			1.21	1.21	7.4	8.3

* BWT is bottom water temperature.

** Temperatures were calculated using the equation of Rosenthal *et al.* [in press].

Table 4. OCE205-2-100GGC *Cibicidoides spp.* $\delta^{18}O$ data*.

Depth (cm)	Age (yrs BP)	$\delta^{18}O$ (‰)	Mean $\delta^{18}O$ (‰)
OCE205-2-100GGC			
7	613	2.35	2.35
10	986	2.66	2.66
13	1,359	2.04	2.23
13	1,359	2.24	
13	1,359	2.41	
14	1,483	2.14	2.23
14	1,483	2.20	
14	1,483	2.22	
14	1,483	2.36	
15	1,607	2.16	2.06
15	1,607	1.95	
16	1,732	2.14	2.20
16	1,732	2.26	
17	1,856	2.50	2.44
17	1,856	2.37	
19	2,010	2.34	2.37
19	2,010	2.40	
20	2,087	2.45	2.35
20	2,087	2.24	
22	2,242	2.22	2.38
22	2,242	2.45	
22	2,242	2.48	
23	2,319	2.25	2.24
23	2,319	2.27	
23	2,319	2.19	
24	2,396	2.27	2.19
24	2,396	2.08	
24	2,396	2.25	
24	2,396	2.17	
25	2,473	2.18	2.18
27	2,627	1.70	1.84
27	2,627	1.97	
29	2,782	2.29	2.34
29	2,782	2.37	
29	2,782	2.36	
30	2,859	2.26	2.16
30	2,859	2.16	
30	2,859	2.19	
30	2,859	2.12	
30	2,859	2.07	
31	2,936	2.36	2.35
31	2,936	2.34	
32	3,017	2.27	2.28
32	3,017	2.29	
32	3,017	2.35	
33	3,097	2.07	2.12

Table 4 (cont.)

Depth (cm)	Age (yrs BP)	$\delta^{18}O$ (‰)	Mean $\delta^{18}O$ (‰)
OCE205-2-100GGC			
33	3,097	2.17	
34	3,178	2.16	2.20
34	3,178	2.23	
35	3,258	2.11	2.22
35	3,258	2.15	
35	3,258	2.40	
36	3,339	2.23	2.32
36	3,339	2.29	
36	3,339	2.33	
36	3,339	2.42	
40	3,661	2.39	2.32
40	3,661	2.24	
45	4,064	2.25	2.27
45	4,064	2.26	
45	4,064	2.30	
46	4,145	2.28	2.17
46	4,145	2.13	
46	4,145	2.11	
48	4,306	2.37	2.24
48	4,306	2.10	
49	4,387	2.00	2.07
49	4,387	2.14	
50	4,467	2.11	2.27
50	4,467	2.48	
50	4,467	2.21	
51	4,548	2.08	2.19
51	4,548	2.30	
52	4,629	2.17	2.25
52	4,629	2.34	
52	4,629	2.23	
53	4,709	1.70	2.10
53	4,709	2.40	
53	4,709	2.12	
53	4,709	2.19	
54	4,790	2.28	2.33
54	4,790	2.35	
54	4,790	2.40	
54	4,790	2.30	
55	4,870	2.26	2.21
55	4,870	2.13	
55	4,870	2.25	
56	4,951	2.24	2.26
56	4,951	2.14	
56	4,951	2.41	
57	5,031	2.18	2.08
57	5,031	1.98	

Table 4 (cont.).

Depth (cm)	Age (yrs BP)	$\delta^{18}O$ (‰)	Mean $\delta^{18}O$ (‰)
OCE205-2-100GGC			
58	5,112	2.25	2.24
58	5,112	2.22	
60	5,273	1.89	2.24
60	5,273	2.30	
60	5,273	2.29	
60	5,273	2.23	
60	5,273	2.21	
60	5,273	2.33	
60	5,273	2.41	
61	5,354	2.10	2.22
61	5,354	2.34	
61	5,354	2.20	
61	5,354	2.24	
62	5,434	2.23	2.26
62	5,434	2.25	
62	5,434	2.26	
62	5,434	2.29	
63	5,515	2.35	2.33
63	5,515	2.31	
64	5,584	2.26	2.20
64	5,584	2.27	
64	5,584	2.15	
64	5,584	2.10	
65	5,652	2.09	2.23
65	5,652	2.31	
65	5,652	2.29	
66	5,721	2.22	2.20
66	5,721	2.18	
67	5,789	2.44	2.28
67	5,789	2.21	
67	5,789	2.19	
69	5,926	2.23	2.27
69	5,926	2.30	
70	5,995	2.19	2.19
70	5,995	2.10	
70	5,995	2.29	
71	6,063	2.16	2.07
71	6,063	1.85	
71	6,063	2.20	
72	6,132	2.14	2.20
72	6,132	2.25	
73	6,200	2.35	2.18
73	6,200	1.72	
73	6,200	2.48	
74	6,310	2.45	2.36
74	6,310	2.26	

Table 4 (cont.).

Depth (cm)	Age (yrs BP)	$\delta^{18}O$ (‰)	Mean $\delta^{18}O$ (‰)
OCE205-2-100GGC			
75	6,420	2.28	2.32
75	6,420	2.35	
76	6,530	2.30	2.24
76	6,530	2.22	
76	6,530	2.21	
77	6,640	2.41	2.35
77	6,640	2.28	
77	6,640	2.29	
77	6,640	2.40	
78	6,750	2.24	2.29
78	6,750	2.35	
78	6,750	2.28	
79	6,860	2.24	2.31
79	6,860	2.31	
79	6,860	2.38	
80	6,970	2.27	2.30
80	6,970	2.33	
81	7,144	1.45	1.64
81	7,144	2.18	
81	7,144	1.28	
82	7,318	2.28	2.26
82	7,318	2.25	
82	7,318	2.13	
82	7,318	2.36	
83	7,492	2.39	2.51
83	7,492	2.57	
83	7,492	2.57	
84	7,666	2.36	2.30
84	7,666	2.24	
85	7,840	1.92	2.09
85	7,840	2.18	
85	7,840	2.23	
85	7,840	2.04	
86	8,015	2.41	2.42
86	8,015	2.48	
86	8,015	2.49	
86	8,015	2.29	
87	8,189	2.32	2.28
87	8,189	2.23	
87	8,189	2.29	
87	8,189	2.29	
88	8,363	2.15	2.01
88	8,363	2.50	
88	8,363	1.39	
89	8,537	2.29	2.34
89	8,537	2.21	

Table 4 (cont.).

Depth (cm)	Age (yrs BP)	$\delta^{18}O$ (‰)	Mean $\delta^{18}O$ (‰)
OCE205-2-100GGC			
89	8,537	2.25	
89	8,537	2.39	
89	8,537	2.55	
90	8,711	2.39	2.38
90	8,711	2.47	
90	8,711	2.28	
91	8,885	2.22	2.24
91	8,885	2.39	
91	8,885	2.12	
92	9,059	2.07	2.22
92	9,059	2.08	
92	9,059	2.75	
92	9,059	2.37	
92	9,059	2.27	
92	9,059	2.40	
92	9,059	1.59	
93	9,117	2.27	2.05
93	9,117	2.32	
93	9,117	1.55	
94	9,176	2.40	2.31
94	9,176	2.47	
94	9,176	2.29	
94	9,176	2.06	
95	9,234	2.25	2.41
95	9,234	2.42	
95	9,234	2.32	
95	9,234	2.64	
96	9,292	2.20	2.37
96	9,292	2.47	
96	9,292	2.36	
96	9,292	2.43	
97	9,350	2.34	2.44
97	9,350	2.31	
97	9,350	2.57	
97	9,350	2.52	
98	9,409	2.43	2.49
98	9,409	2.44	
98	9,409	2.51	
98	9,409	2.58	
99	9,467	2.37	2.46
99	9,467	2.43	
99	9,467	2.57	
99	9,467	2.46	
100	9,525	2.33	2.37
100	9,525	2.40	
100	9,525	2.40	

Table 4 (cont.).

Depth (cm)	Age (yrs BP)	$\delta^{18}O$ (‰)	Mean $\delta^{18}O$ (‰)
OCE205-2-100GGC			
100	9,525	2.39	
100	9,525	2.35	
100	9,525	2.34	
101	9,741	2.39	2.45
101	9,741	2.53	
101	9,741	2.42	
101	9,741	2.45	
102	9,957	2.57	2.49
102	9,957	2.41	
103	10,173	2.42	2.32
103	10,173	2.15	
103	10,173	2.39	
104	10,389	2.49	2.48
104	10,389	2.47	
105	10,604	2.33	2.28
105	10,604	2.31	
105	10,604	2.20	
106	10,820	2.12	2.39
106	10,820	2.51	
106	10,820	2.52	
106	10,820	2.41	
107	11,036	2.31	2.68
107	11,036	3.04	
108	11,252	2.56	2.71
108	11,252	2.50	
108	11,252	2.61	
108	11,252	3.17	
109	11,468	2.18	2.43
109	11,468	2.48	
109	11,468	2.64	
110	11,718	2.48	2.61
110	11,718	2.47	
110	11,718	2.59	
110	11,718	2.37	
110	11,718	2.46	
110	11,718	2.54	
110	11,718	3.29	
110	11,718	2.69	
111	11,968	2.44	2.60
111	11,968	2.47	
111	11,968	2.58	
111	11,968	2.92	
112	12,218	2.81	3.00
112	12,218	3.11	
112	12,218	3.08	
113	12,468	2.45	2.71

Table 4 (cont.).

Depth (cm)	Age (yrs BP)	$\delta^{18}O$ (‰)	Mean $\delta^{18}O$ (‰)
OCE205-2-100GGC			
113	12,468	2.75	
113	12,468	2.92	
116	13,218	2.51	2.99
116	13,218	3.25	
116	13,218	2.66	
116	13,218	3.30	
116	13,218	3.12	
116	13,218	2.90	
116	13,218	3.19	
117	13,270	2.61	3.03
117	13,270	2.94	
117	13,270	3.08	
117	13,270	2.83	
117	13,270	3.08	
117	13,270	3.05	
117	13,270	3.61	
118	13,322	2.62	2.85
118	13,322	2.68	
118	13,322	2.93	
118	13,322	3.16	
119	13,375	2.88	3.04
119	13,375	3.19	
120	13,427	3.32	3.15
120	13,427	2.98	
120	13,427	3.14	
120	13,427	2.78	
123	14,548	2.72	2.92
123	14,548	3.28	
123	14,548	2.77	
127	15,905	3.05	3.15
127	15,905	3.25	
130	16,923	3.98	4.03
130	16,923	4.07	
133	17,940	3.58	3.67
133	17,940	3.76	
137	19,297	4.14	4.14
137	19,297	4.05	
137	19,297	4.24	
140	20,315	3.90	4.03
140	20,315	4.07	
140	20,315	4.11	
150	23,708	4.11	3.89
150	23,708	3.67	
153	24,725	3.40	3.80
153	24,725	3.93	
153	24,725	4.08	

Table 4 (cont.).

Depth (cm)	Age (yrs BP)	$\delta^{18}O$ (‰)	Mean $\delta^{18}O$ (‰)
OCE205-2-100GGC			
157	26,082	3.48	3.75
157	26,082	3.87	
157	26,082	3.67	
157	26,082	3.98	
160	27,100	3.71	3.79
160	27,100	4.01	
160	27,100	3.74	
160	27,100	3.68	

* Both previously published data [*Slowey and Curry,* 1995] and newly acquired data [this study].

Table 5. OCE205-2-100GGC residual seawater $\delta^{18}O$.

Depth (cm)	Age (yrs BP)	Smoothed Temp (°C)	Smoothed $\delta^{18}O_c$ Uncorrected (‰)	Ice Volume Correction* (‰)	Smoothed $\delta^{18}O_c$ Corrected (‰)	$\delta^{18}O_{sw}$** Corrected (‰)
OCE205-2-100GGC						
7	613					
8	737					
10	986		2.41	-0.02	2.43	
13	1,359	4.2	2.37	-0.02	2.39	0.17
14	1,483		2.17	-0.02	2.19	
15	1,607		2.16	-0.02	2.18	
16	1,732	4.0	2.23	-0.01	2.24	-0.02
17	1,856		2.34	-0.01	2.35	
18	1,933	4.2				
19	2,010	4.9	2.38	-0.01	2.39	0.31
20	2,087		2.37	-0.01	2.37	
21	2,165	5.1				
22	2,242	5.6	2.32	-0.01	2.33	0.38
23	2,319		2.27	0.00	2.27	
24	2,396	4.9	2.20	0.00	2.21	0.12
25	2,473	3.9	2.07	0.00	2.07	-0.22
26	2,550	3.3				
27	2,627	3.6	2.12	0.00	2.12	-0.24
28	2,705	5.0				
29	2,782	6.1	2.11	0.01	2.11	0.28
30	2,859	6.0	2.28	0.01	2.28	0.43
31	2,936		2.26	0.01	2.25	
32	3,017	5.0	2.25	0.01	2.24	0.17
33	3,097	3.9	2.20	0.01	2.19	-0.09
34	3,178		2.18	0.01	2.17	
35	3,258	4.3	2.24	0.01	2.23	0.03
36	3,339	4.7	2.28	0.01	2.27	0.16
37	3,420	5.1				
38	3,500	5.0				
39	3,581	4.8				
40	3,661	4.4	2.30	0.01	2.29	0.11
42	3,823	4.5				
43	3,903	4.0				
44	3,984	3.9				
45	4,064	3.5	2.25	0.01	2.24	-0.14
46	4,145	4.2	2.23	0.02	2.21	-0.02
47	4,226	4.6				
48	4,306	4.4	2.16	0.02	2.14	-0.04
49	4,387	3.7	2.19	0.03	2.16	-0.16
50	4,467		2.18	0.03	2.15	
51	4,548	3.7	2.23	0.03	2.20	-0.13
52	4,629	4.3	2.18	0.03	2.15	-0.07
53	4,709	4.9	2.23	0.04	2.19	0.11
54	4,790	4.8	2.22	0.04	2.17	0.08
55	4,870	4.4	2.27	0.05	2.22	0.04

Table 5 (cont.).

Depth (cm)	Age (yrs BP)	Smoothed Temp (°C)	Smoothed $\delta^{18}O_c$ Uncorrected (‰)	Ice Volume Correction* (‰)	Smoothed $\delta^{18}O_c$ Corrected (‰)	$\delta^{18}O_{sw}$** Corrected (‰)
OCE205-2-100GGC						
56	4,951	4.6	2.19	0.05	2.14	-0.01
57	5,031	4.0	2.19	0.05	2.14	-0.13
58	5,112	5.3	2.18	0.06	2.13	0.14
59	5,193	5.0				
60	5,273	4.3	2.23	0.07	2.17	-0.04
61	5,354	3.0	2.24	0.07	2.17	-0.30
62	5,434	3.2	2.27	0.07	2.20	-0.24
63	5,515	4.5	2.26	0.08	2.19	0.02
64	5,584	5.5	2.25	0.08	2.17	0.21
65	5,652		2.21	0.08	2.13	
66	5,721	5.3	2.24	0.09	2.15	0.16
67	5,789	5.8	2.25	0.09	2.16	0.28
68	5,858	5.1				
69	5,926		2.25	0.10	2.15	
70	5,995	5.5	2.18	0.10	2.08	0.13
71	6,063	5.5	2.15	0.10	2.05	0.09
72	6,132	5.2	2.15	0.11	2.04	0.03
73	6,200	4.7	2.24	0.11	2.13	0.01
74	6,310	3.9	2.28	0.12	2.16	-0.12
75	6,420	4.2	2.30	0.13	2.18	-0.06
76	6,530	4.4	2.30	0.14	2.17	-0.01
77	6,640	4.9	2.29	0.15	2.15	0.06
78	6,750	4.3	2.32	0.15	2.16	-0.05
79	6,860	4.3	2.30	0.16	2.14	-0.06
80	6,970	4.5	2.08	0.17	1.91	-0.26
81	7,144	4.9	2.06	0.19	1.88	-0.20
82	7,318	4.5	2.13	0.30	1.83	-0.32
83	7,492	4.5	2.36	0.22	2.14	-0.04
84	7,666		2.30	0.24	2.06	
85	7,840	4.6	2.27	0.26	2.02	-0.14
86	8,015	4.0	2.26	0.27	1.99	-0.27
87	8,189	4.2	2.24	0.28	1.96	-0.27
88	8,363	4.7	2.21	0.29	1.92	-0.21
89	8,537	5.7	2.24	0.30	1.95	0.03
90	8,711	6.1	2.32	0.31	2.02	0.19
91	8,885	6.4	2.28	0.32	1.97	0.19
92	9,059	6.2	2.17	0.32	1.85	0.03
93	9,117	5.9	2.19	0.33	1.87	-0.01
94	9,176		2.25	0.33	1.92	
95	9,234	5.9	2.36	0.33	2.03	0.16
96	9,292	6.3	2.40	0.34	2.07	0.27
97	9,350		2.43	0.34	2.09	
98	9,409	6.4	2.46	0.34	2.12	0.36
99	9,467	6.8	2.44	0.35	2.09	0.40
100	9,525	6.4	2.42	0.35	2.08	0.32

Table 5 (cont.).

Depth (cm)	Age (yrs BP)	Smoothed Temp (°C)	Smoothed $\delta^{18}O_c$ Uncorrected (‰)	Ice Volume Correction* (‰)	Smoothed $\delta^{18}O_c$ Corrected (‰)	$\delta^{18}O_{sw}$** Corrected (‰)
OCE205-2-100GGC						
101	9,741	6.3	2.44	0.36	2.08	0.30
102	9,957	6.2	2.42	0.37	2.05	0.25
103	10,173	7.2	2.43	0.38	2.05	0.46
104	10,389	7.1	2.36	0.39	1.97	0.35
105	10,604	6.1	2.38	0.40	1.98	0.16
106	10,820	5.1	2.45	0.41	2.04	0.01
107	11,036		2.59	0.42	2.17	
108	11,252	5.0	2.61	0.44	2.17	0.11
109	11,468	5.4	2.58	0.45	2.13	0.17
110	11,718	5.6	2.55	0.46	2.09	0.15
111	11,968		2.74	0.48	2.26	
112	12,218	5.2	2.77	0.48	2.29	0.28
113	12,468	4.8	2.90	0.48	2.42	0.31
116	13,218		2.91	0.52	2.39	
117	13,270	5.2	2.96	0.60	2.36	0.33
118	13,322		2.97	0.60	2.37	
119	13,375		3.01	0.64	2.37	
120	13,427	6.3	3.04	0.64	2.40	0.60
123	14,548	6.2	3.07	0.89	2.18	0.36
124	14,794	5.9				
126	15,478	5.9				
127	15,905		3.37	1.02	2.34	
128	16,162	6.2				
130	16,923		3.62	1.02	2.60	
132	17,529	6.5				
133	17,940		3.95	0.95	3.00	
136	18,896	5.8				
137	19,297		3.95	0.96	2.98	
138	19,580	5.5				
140	20,315		4.02	1.01	3.01	
142	20,947	4.7				
148	22,998	4.5				
150	23,708		3.91	0.73	3.18	
152	24,365	5.1				
153	24,725		3.81			
156	25,733	5.5				
157	26,082		3.78			
158	26,416	5.5				

* Ice volume correction is from Waelbroeck *et al.* [2002].

** Seawater $\delta^{18}O$ was calculated using the equation of Lynch-Stieglitz [1999].

Table 6. KNR166-2-31JPC residual seawater $\delta^{18}O$.

Composite Depth (cm)	Age (yrs BP)	Temp (°C)	$\delta^{18}O_c$* Uncorrected (‰)	Ice Volume Correction** (‰)	$\delta^{18}O_c$ Corrected (‰)	$\delta^{18}O_{sw}$*** Corrected (‰)
0	1,204	3.9	2.19	-0.02	2.20	-0.09
8	1,980	5.5	2.24	-0.01	2.25	0.29
16	2,808	4.5	2.18	0.01	2.17	0.00
24	3,635	3.7	2.14	0.01	2.13	-0.21
32	4,463	4.7	2.30	0.03	2.27	0.15
40	5,290	4.8	2.27	0.07	2.21	0.10
48	6,118	4.4	2.26	0.11	2.16	-0.04
56	6,945	6.5	2.24	0.17	2.07	0.33
64	7,773	5.2	2.57	0.25	2.32	0.30
72	8,728	4.6	2.41	0.31	2.10	-0.05
80	9,682	7.1	2.42	0.36	2.07	0.45
88	10,636	8.3	2.50	0.40	2.11	0.74
96	11,591	8.0	2.39	0.46	1.93	0.51
104	12,546	7.3	2.77	0.48	2.29	0.71
112	13,500	7.0	2.76	0.68	2.08	0.44
120	14,483	4.7	2.88	0.90	1.99	-0.13
128	15,466	8.5	2.40	0.98	1.42	0.10
136	16,448	5.5	3.00	1.04	1.96	0.00
160	19,397		3.67	0.97	2.70	

* Oxygen isotopic data for KNR166-2-31JPC are from Lynch-Stieglitz [unpublished data].
** Ice volume correction is from Waelbroeck *et al.* [2002].
*** Seawater $\delta^{18}O$ was calculated using the equation of Lynch-Stieglitz [1999].

Chapter 5. Variability in the Influence of Southern Source Waters within the Florida Current Over the Last 20,000 Years

Abstract

Benthic foraminiferal Cd/Ca from a Florida Current core documents the history of the northward penetration of southern source waters within the return flow of the Atlantic meridional overturning circulation (MOC). Cd seawater estimates (Cd_w) for the last glacial are consistent with the reduced influence of southern source waters at this location relative to the present. At ~18.5 ka, the southern source contribution to the Florida Current began to increase significantly, marking the onset of a transition from a glacial circulation pattern to a deglacial pattern, which lasted from ~17 ka to ~14 ka. At ~12.5 ka, following the onset of the Younger Dryas cooling in the North Atlantic [*Grootes et al.*, 1993] and the reduction in North Atlantic Deep Water (NADW) production [*Boyle and Keigwin*, 1987], the influence of southern source waters within the Florida Current decreased abruptly. A renewed influence of southern source waters occurred at ~9 ka, concurrent with the establishment of Holocene warmth in the North Atlantic region.

Introduction

Variability in the strength of the Atlantic Ocean's meridional overturning circulation (MOC) is often invoked as a cause or amplifier of millennial scale climate events such as the Younger Dryas. A decrease in the strength of the MOC would cause a reduction in the amount of heat transported by the upper ocean to the North Atlantic, thereby cooling the high northern latitudes [*Broecker et al.*, 1985a]. Models predict that a large decrease in the strength of MOC not only cools the surface North Atlantic but also warms the thermocline of the low latitudes as a result of the reduced northward heat transport [*Manabe and Stouffer*, 1997; *Marchal et al.*, 1999; *Rahmstorf*, 1994; *Rühlemann et al.*, 2004]. In the previous Chapter, paleoceanographic evidence was presented, confirming a Younger Dryas warming within the Florida Current, which feeds the northward return flow of the MOC. Model results were also presented, confirming the possibility that the warming at the Florida Current site could have been caused by a reduction in the strength of the Atlantic overturning. However, to my knowledge, no paleoceanographic evidence suggesting an actual reduction in the northward return flow of the MOC during the Younger Dryas has ever been documented.

Nutrient proxies are often used to trace changes in ocean water mass geometry. In the modern ocean, North Atlantic Deep Water (NADW) originates from nutrient depleted

surface waters, while Circumpolar Deep Water (CDW) forms in the Southern Ocean from relatively nutrient enriched waters that upwell from great depth [*Broecker et al.*, 1985b]. The result is a pattern of nutrient distributions in the Atlantic Ocean that reflects water circulation patterns: northern source waters form a southward penetrating tongue of nutrient depleted NADW, and southern source waters form the northward moving, nutrient rich Antarctic Bottom Water (AABW) and Antarctic Intermediate Water (AAIW).

Cd and $\delta^{13}C$ are two nutrient proxies used to trace subsurface circulation patterns [*Boyle*, 1988; *Boyle and Keigwin*, 1982; *Curry et al.*, 1988; *Curry and Lohmann*, 1982; *Duplessy et al.*, 1988]. In the modern ocean, a positive correlation exists between sea water Cd concentrations (Cd_w) and PO_4 concentrations. Since foraminifera incorporate Cd into their $CaCO_3$ tests in direct proportion to the Cd concentration in the water in which they calcify, the Cd/Ca ratio of the tests can be used as an indicator of Cd_w (and thus PO_4) at the time the foraminiferal test formed [*Hester and Boyle*, 1982]. The $\delta^{13}C$ distribution is the result of the isotopic fractionation of carbon associated with photosynthesis, which favors ^{12}C over ^{13}C. The oxidation and remineralization at depth of low $\delta^{13}C$ organic material produces a negative correlation between oceanic $\delta^{13}C_{DIC}$ and PO_4 [*Kroopnick*, 1985]. Like Cd_w, the oceanic $\delta^{13}C_{DIC}$ signal is recorded in the tests of benthic foraminifera, making them useful tools in the study of paleocean circulation. The $\delta^{13}C$ distribution, however, is complicated by the influence of the $\delta^{13}C$ air-sea exchange signature ($\delta^{13}C_{AS}$). When ocean water has contact with the atmosphere, a temperature dependent fractionation of the carbon isotopes in CO_2 occurs [*Mook et al.*, 1974]. For a given atmospheric $\delta^{13}C$, colder temperatures result in higher $\delta^{13}C_{DIC}$. However, since different parcels of water spend varying amounts of time in contact with the atmosphere, the degree to which a parcel equilibrates with the atmosphere also varies. High wind speeds increase exchange rates, bringing the $\delta^{13}C_{DIC}$ closer to equilibrium with the atmosphere [*Broecker and Maier-Reimer*, 1992; *Liss and Merlivat*, 1986].

During the last glacial, deep waters of the North Atlantic were nutrient enriched relative to the present and intermediate waters were nutrient depleted, suggesting a reduction in NADW formation and an increase in Glacial North Atlantic Intermediate Water (GNAIW) formation [*Boyle and Keigwin*, 1987]. Many studies have confirmed this glacial subsurface geometry of GNAIW overlying waters of southern origin [*Duplessy et al.*, 1988; *Marchitto et al.*, 2002; *Oppo and Lehman*, 1993]. There are conflicting interpretations for the subsurface geometry during the Younger Dryas, however. It has been suggested that deep water formation decreased [*Boyle and Keigwin*, 1987] and intermediate water

formation increased, signifying a glacial-like stratification for the Younger Dryas [*Marchitto et al.*, 1998; *Zahn and Stüber*, 2002]. Sarnthein *et al.* [2001] also suggest that deep water formation decreased during the Younger Dryas, however, they suggest that the reduction occurred late, near the end of the Younger Dryas. My previous work [*Came et al.*, 2003] suggests a reduction in the export of North Atlantic Intermediate Water during the Younger Dryas, possibly indicating a reduction in intermediate water formation concurrent with the reduction in deep water formation. Alternatively, Rickaby and Elderfield [2005] suggest a radically different subsurface geometry, with an increase in the northward penetration of AAIW at depths just above AABW. Because the production of NADW at high latitudes results in greater heat loss to the atmosphere than the production of intermediate water at lower latitudes, the above interpretations predict very different roles of the MOC in cooling the North Atlantic during the Younger Dryas. Thus, it is clear that a better understanding of the variability in the MOC on millennial timescales is required.

In this study, two new records of intermediate depth variability are presented using Cd/Ca data from the low latitude North Atlantic. The sediment cores used in this study lie in key locations for studying variability in the Atlantic MOC: the Florida Margin site is bathed by the northward moving waters of the MOC return flow; the Little Bahama Bank site is bathed by waters of the North Atlantic subtropical gyre. When taken together with previously published records [*Boyle and Keigwin*, 1987; *Came et al.*, 2003; *Marchitto et al.*, 1998; *Rickaby and Elderfield*, 2005] the new Florida Current paleo-nutrient record provides insights into the relative influences of northern *versus* southern source waters during the last 20,000 years.

Study Areas

The descriptions of the Little Bahama Bank and Florida Current study areas were presented in Chapter 4, and are repeated below.

Sediment core OCE205-2-100GGC (LBB) was taken from the flanks of the Little Bahama Bank, within the Northwest Providence Channel, at 26°04' North, 78°02' West, and 1,057 m (Figure 1). Waters of the Northwest Providence Channel flow westward from the Sargasso Sea to the Straits of Florida [*Slowey and Curry*, 1995]. Today, depths above 1,000 m are bathed by waters of the wind driven North Atlantic subtropical gyre, with the same temperature, salinity, and density structure of the western portion of the gyre [*Slowey and Curry*, 1995]. Waters below 1,000 m are fed by the upper component of North Atlantic Deep Water. These waters are poorly ventilated because they originate

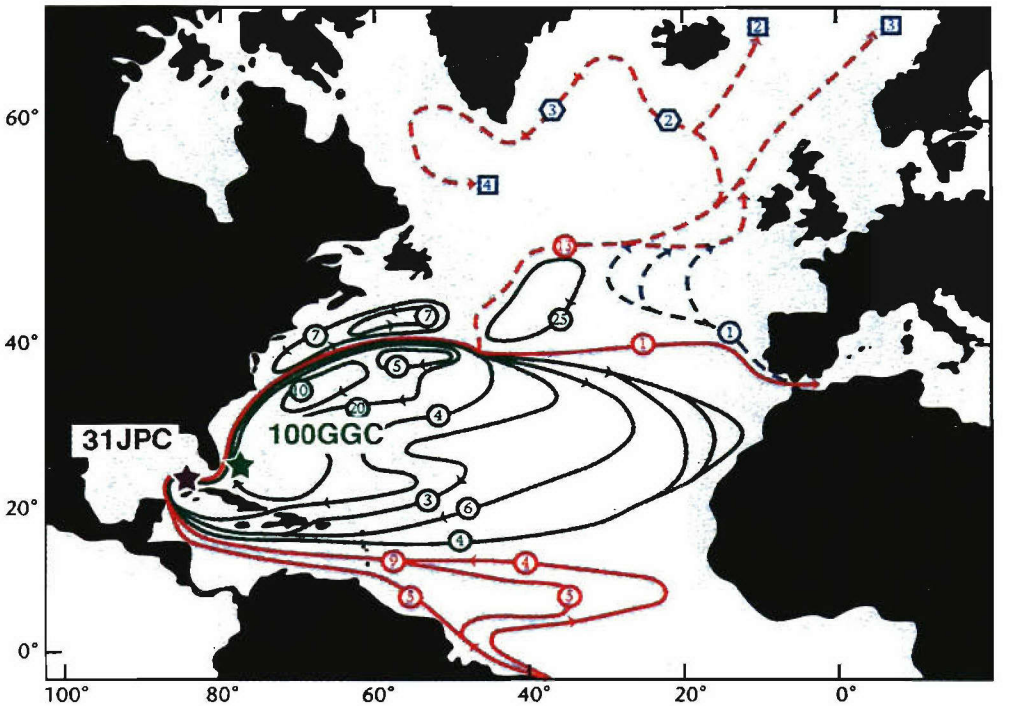

Figure 1. Map of the North Atlantic showing the locations of OCE205-2-100GGC (26°04'N, 78°02'W, 1,057 m) and KNR166-2-31JPC (24°13'N, 83°18'W, 751 m), and the transport estimates for waters entering the Florida Current (adapted from Schmitz and McCartney [1993]).

in the subpolar gyre, where residence times are long and wind driven upwelling occurs [*Jenkins*, 1980; *McCartney*, 1982; *Sarmiento et al.*, 1982]. Waters circulate within the subpolar gyre before entering the subtropical gyre at depth [*Jenkins*, 1980; *Luyten et al.*, 1983; *McCartney*, 1982; *Sarmiento et al.*, 1982].

Sediment core KNR166-2-31JPC (FC) was taken from within the Florida Current, just south of the Florida Keys, at 24° 13' North, 83° 18' West, and 751 m (Figure 1). Today, waters of the Florida Current are a mixture of recirculated North Atlantic subtropical gyre water (17 Sv) and Antarctic Intermediate Water AAIW (13 Sv) [*Schmitz et al.*, 1993; *Schmitz and Richardson*, 1991]. At mid-depths (12-24°C temperature range), ~5% of the Florida Current waters are of South Atlantic origin, but below 400 m, ~80% of the waters are of South Atlantic origin [*Schmitz and Richardson*, 1991]. The intermediate depth southern source waters that feed the Florida Current are observed in the South Atlantic as a northward moving salinity minimum layer that originates near the Antarctic Polar

Front [*Lynch-Stieglitz et al.*, 1994]. As the waters move northward through the Florida Strait and toward the polar seas via the North Atlantic Current, the salinity gradually increases [*Tsuchiya*, 1989] due to interaction with Mediterranean Water [*Reid*, 1994] and the temperature gradually decreases. Gordon [1986] notes that AAIW contributes to both the warm and cold water return routes of NADW formation.

Today, intermediate depths at these two geographic locations have very different water properties. For example, mean annual temperatures at 1,000 m depth are about 1°C warmer at the Little Bahama Bank than at the Florida Current [*Levitus and Boyer*, 1994]. However, since the Florida Current site is significantly shallower than the Little Bahama Bank site, bottom water temperatures and salinities are very similar: approximately 5.35°C and 35.05 p.s.u. at LBB [*Slowey and Curry*, 1995], and 5.78°C and 34.90 p.s.u. at FC (measured during core collection, KNR166-2). Nutrient concentrations are also very different at the two intermediate depth locations: all gyre, intermediate, and deep waters of the North Atlantic have low initial phosphate concentrations of <0.8 μmol kg^{-1}, while Florida Current waters have phosphate concentrations intermediate between North Atlantic waters (<0.8 μmol kg^{-1}) and AAIW (>1.4 μmol kg^{-1}) [*Slowey and Curry*, 1995].

Methods

Accelerator mass spectrometer (AMS) radiocarbon dates for the LBB and FC cores are presented in Chapter 4, Table 1. The results indicate that the sedimentation rate for LBB is ~6 cm/kyr, with higher sedimentation rates in the more recent Holocene (~8 cm/kyr) and lower rates near the last glacial (~3 cm/kyr) (Figure 2a). The average sedimentation rate for FC is slightly higher than 8 cm/kyr (Figure 3a). All further discussion of the FC record is based on the assumption that the four AMS dates provide an adequate age model for 31JPC. However, I await three new AMS dates in order to confirm the tentative age model.

The AMS dates presented in Came *et al.*, [2003] for KNR159-5-36GGC and EN120GGC-1 were revised after publication using the updated calibration program, CALIB v. 5.0.1 [*Stuiver and Reimer*, 1993], the updated Marine04 calibration data set [*Hughen et al.*, 2004], and a reservoir correction of 400 years. The new results are presented in Table 1.

Cd/Ca ratios were measured in the tests of the benthic foraminifer *Hoeglundina elegans*. This aragonitic species faithfully records bottom water Cd concentrations with a partition coefficient $D_p = [(Cd/Ca)_{foram}/(Cd/Ca)_{water}] \approx 1.0$ [*Boyle et al.*, 1995]. The

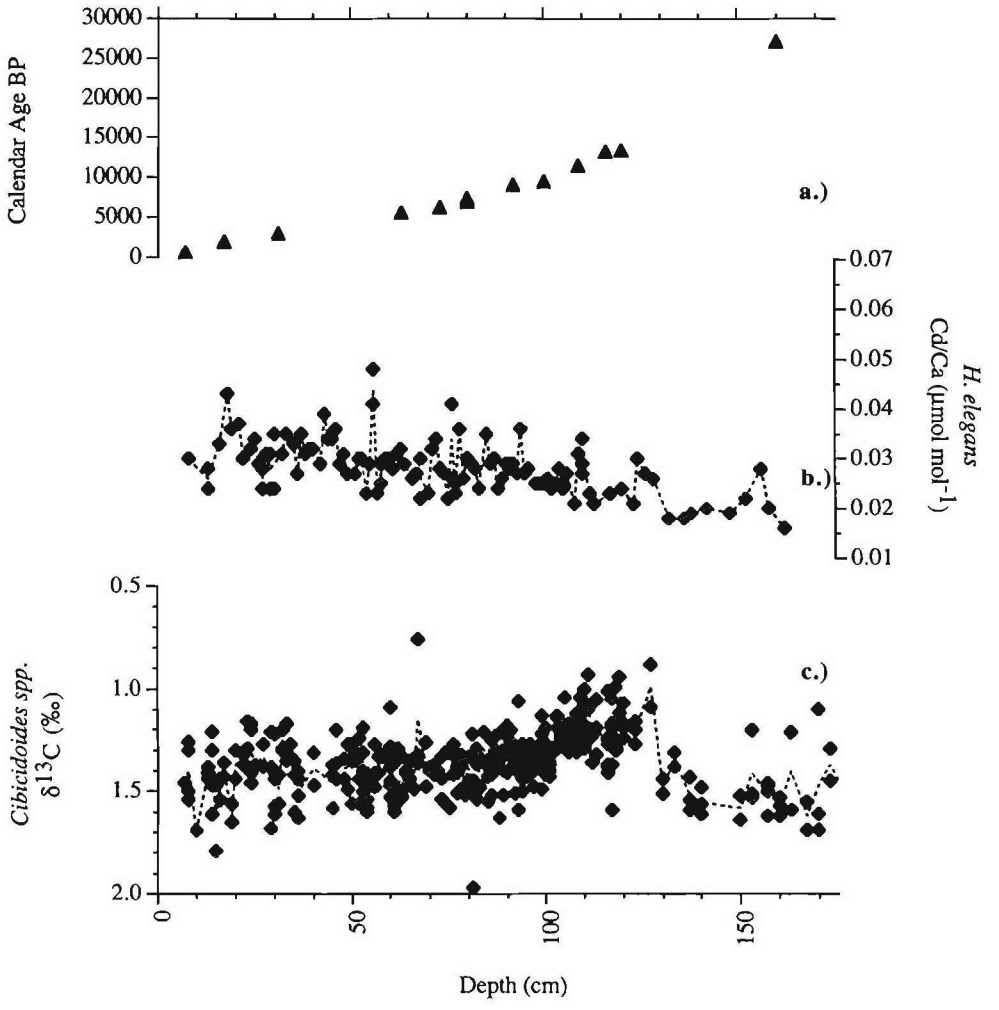

Figure 2. Benthic Cd/Ca and $\delta^{13}C$ data from OCE205-2-100GGC (26°04'N, 78°02'W, 1,057 m) *vs.* depth. **a.)** AMS radiocarbon dates converted to calendar age using Calib 5.01 [*Stuiver and Reimer*, 1993], the calibration data set of Hughen *et al.* [2004], and a reservoir correction of 400 years; **b.)** all *H. elegans* Cd/Ca; **c)** all previously acquired *Cibicidoides spp.* $\delta^{13}C$ [*Slowey and Curry*, 1995] and newly acquired *Cibicidoides spp.* $\delta^{13}C$ [this study].

partition coefficient for the aragonitic *H. elegans* is constant with depth, unlike the partition coefficients of calcitic foraminifera, which are depth dependent [*Boyle*, 1992]. A constant seawater Ca concentration of 0.01 mol kg^{-1} was assumed to estimate Cd water concentrations (Cd_w). Zn/Ca ratios were simultaneously analyzed along with Cd/Ca, and those results are presented in Appendix 1.

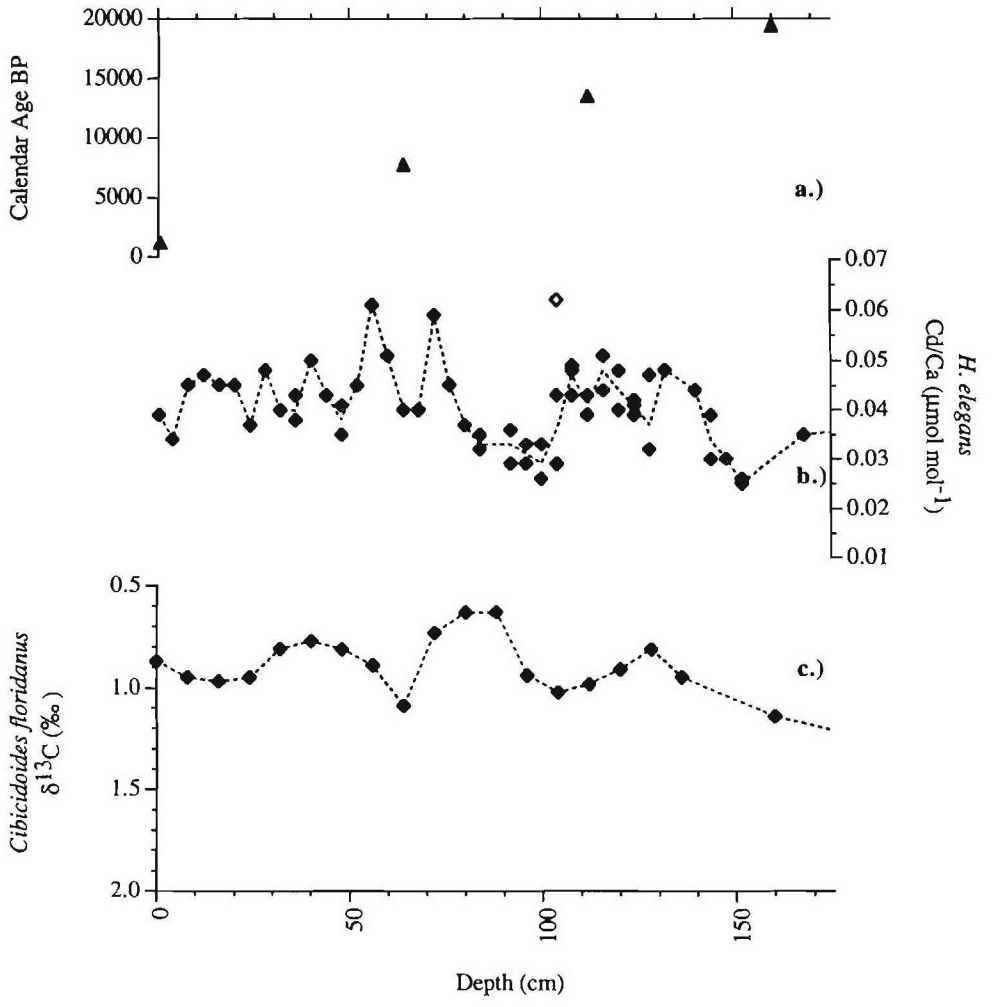

Figure 3. Benthic Cd/Ca and $\delta^{13}C$ data from KNR166-2-31JPC (24°13'N, 83°18'W, 751 m) *vs.* depth. **a.)** AMS radiocarbon dates [*Lynch-Stieglitz*, unpublished data] converted to calendar age using Calib 5.01 [*Stuiver and Reimer*, 1993], the calibration data set of Hughen *et al.* [2004], and a reservoir correction of 400 years; **b.)** all *H. elegans* Cd/Ca; **c)** all previously acquired *Cibicidoides floridanus* $\delta^{13}C$ [*Lynch-Stieglitz*, unpublished data]. Open symbols are excluded data.

Each foraminiferal sample consisted of approximately 2-3 individuals, which were crushed and cleaned according to the full trace metal protocol [*Boyle and Keigwin*, 1985/6] with a reversal of the oxidative and reductive steps [*Boyle and Rosenthal*, 1996; *Rosenthal*, 1994; *Rosenthal et al.*, 1995]. Samples were dissolved in trace metal clean HNO_3 to obtain samples of approximately 200 ppm Ca. Ratios were measured using a Thermo-Finnigan

Element2 sector field single collector ICP-MS following the method of Rosenthal *et al.* [1999], with the addition of a Ca matrix correction. Mn/Ca and Al/Ca were also measured in order to monitor contamination due to manganese carbonate overgrowths and terrestrial input. Manganese carbonate overgrowths are a potential source of contamination in many species of benthic foraminifera [*Boyle*, 1983]. However, the species *H. elegans* was chosen for this study because it does not suffer from the contamination caused by such overgrowths [*Boyle et al.*, 1995].

Converting ICP-MS intensity ratios to elemental ratios using an external standard requires similar [Ca] in both the sample and the standard due to a calcium matrix effect. To correct for samples with varying [Ca], we ran a series of standards with identical element to Ca ratios, but with Ca concentrations that varied over the anticipated sample concentration range. The resulting matrix effect was calculated and the sample ratios were corrected. The corrections were less than ±0.012 μmol mol^{-1} Cd/Ca.

In order to assess the precision of measurements on the ICP-MS, three consistency standards were treated as samples in each of the runs in which the data were generated. Mean Cd/Ca values for the three consistency standards were 0.127 μmol mol^{-1}, 0.044 μmol mol^{-1}, and 0.083 μmol mol^{-1}. Relative standard deviations were ±0.6% (n=5), ±3.7% (n=3), and ±1.3% (n=4), respectively. For *H. elegans*, which has a partition coefficient of 1, the resulting Cd_w error is ±0.016 nmol kg^{-1}.

Results and Discussion

The Cd_w results from Little Bahama Bank core OCE205-2-100GGC reveal an overall glacial-interglacial trend of increasing Cd_w (Figures 2b and 4b), similar to the trend observed by Marchitto *et al.* [1998] in nearby core OCE205-2-103GGC (26°04'N, 78°03'W; 965 m). For a more complete discussion of the paleoceanographic implications of the LBB Cd_w results, refer to Marchitto *et al.* [1998]. For a comparison of the two similar data sets (103GGC obtained by atomic absorption spectrophotometry; 100GGC obtained by ICP-MS), refer to Appendix 2.

The Cd_w results from Florida Current core KNR166-2-31JPC also reveal an overall glacial-interglacial trend of increasing Cd_w beginning at ~18.5 ka (Figures 3b, 4b and 5b). The increase in Cd_w values at this site within the northward return flow of the MOC is indicative of increased nutrient concentrations, and thus an overall increase in the relative influence of southern source waters since the last glacial. These results are consistent with many previous studies that suggest an increase in the strength of the MOC since the last

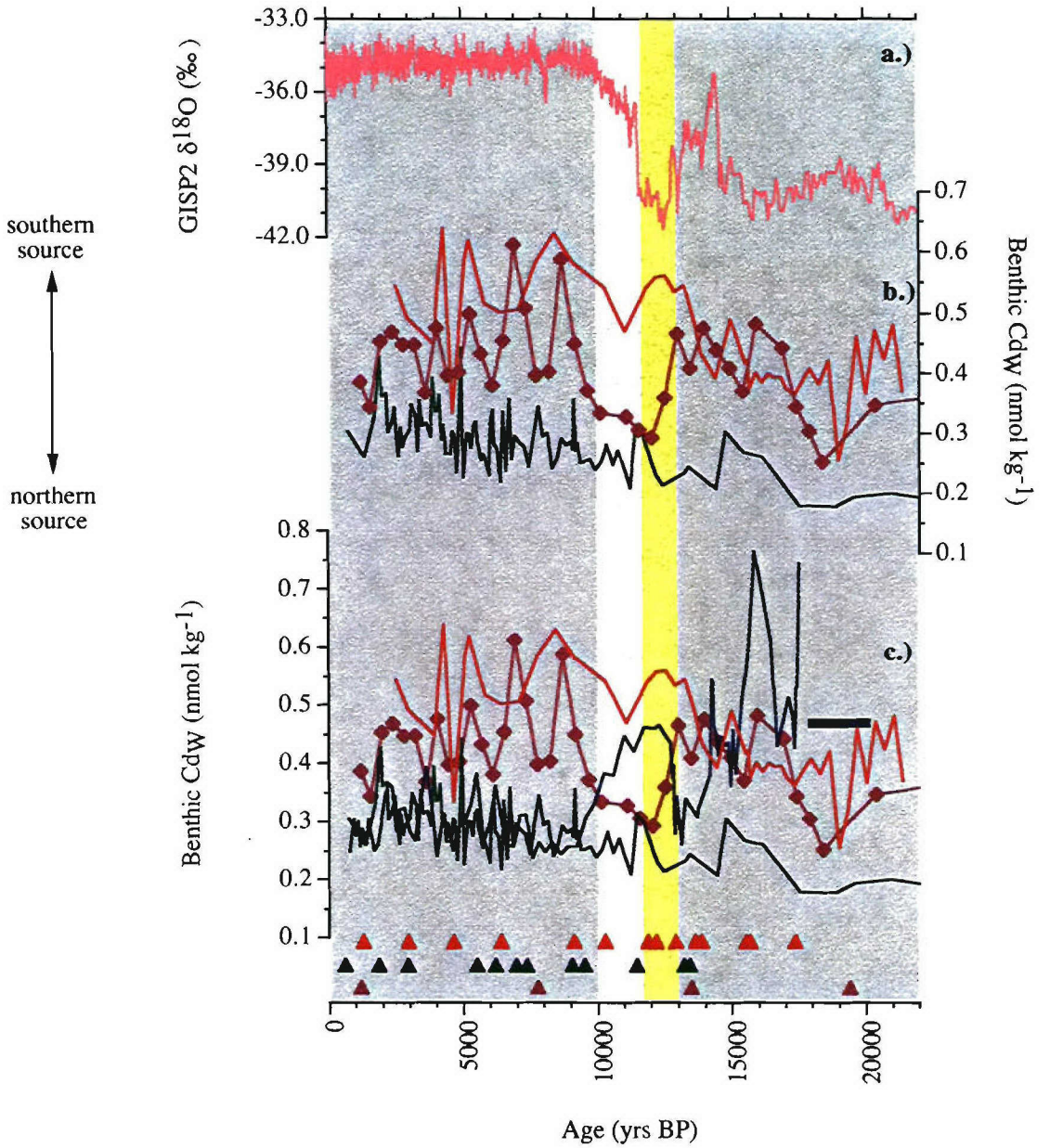

Figure 4. Benthic Cd_w data *vs.* calendar age. **a.)** GISP2 $\delta^{18}O$ (pink) [*Grootes et al.*, 1993]; **b.)** average Cd_w from KNR166-2-31JPC (24°13'N, 83°18'W, 751 m; purple), OCE205-2-100GGC (26°04'N, 78°02'W, 1,057 m; green), and KNR159-5-36GGC (27°31'S, 46°28'W, 1,268 m; red); **c.)** average Cd_w from KNR166-2-31JPC (purple), OCE205-2-100GGC (green), KNR159-5-36GGC (red) and EN120-GGC1 (33°40'N, 57°37'W, 4,450 m; blue) [*Boyle and Keigwin*, 1987]. The glacial Cd_w estimate for the deep North Atlantic (blue bar) is based on data from IOS82 PC SO1 (42°23'N, 23°31'W, 3,540 m) [*Boyle*, 1992]. Triangles are AMS dates converted to calendar age. Yellow shading marks the Younger Dryas interval.

glacial.

Millennial scale variability is superimposed on the glacial-interglacial trend. At ~12.8 ka, a sharp depletion in the $\delta^{18}O$ of Greenland ice marks the rapid northern hemisphere cooling of the Younger Dryas. Shortly after, at ~12.5 ka, a rapid decrease occurred in the Cd_w at the FC site, culminating in Cd_w values of 0.29 nmol kg^{-1} during the late Younger Dryas, almost as low as glacial values. The low Cd_w suggests a decrease in nutrient concentrations at the Florida Current site during the late Younger Dryas, consistent with a decrease in the influence of southern source waters, and an increase in the influence of northern source waters. At ~11.5 ka, the GISP2 $\delta^{18}O$ record suggests a rapid warming in the high northern latitudes, marking the end of the Younger Dryas cold period. At the FC site, however, Cd_w remained low until ~9 ka, nearly 2,000 years after the rapid warming in the high latitude North Atlantic. After ~9 ka, Cd_w increased, indicating a Holocene-like water mass with the renewed contribution of nutrient rich southern source waters.

Comparison of the Cd_w results with simultaneously measured Mg/Ca-derived temperatures and calculated $\delta^{18}O_{sw}$ data (presented in Chapter 4) provides further evidence supporting the reduced influence of southern source waters at the FC site during the Younger Dryas (Figure 5). From ~12.5 ka to ~9 ka, the decreased nutrients at the FC site were accompanied by increased temperatures and increased salinities, consistent with the decreased influence of cold, fresh southern source waters.

Comparison of the FC results with other intermediate depth results from the Brazil Margin in the western South Atlantic [*Came et al.*, 2003] and from LBB provides insights into the evolution of the water mass within the Florida Current (Figure 4b). As stated above, waters at the FC site are influenced by both southern source waters and recirculated North Atlantic subtropical gyre waters, making it an ideal location to monitor the relative influences of the two end member sources. During the last glacial, FC Cd_w values were intermediate between the intermediate depth North Atlantic and South Atlantic, consistent with the combined influence of northern and southern source waters. At ~18.5 ka, coincident with the onset of deglaciation, Cd_w values began to increase toward South Atlantic values, consistent with an increasing influence of southern source waters. At ~12.5 ka, FC Cd_w values abruptly became more like those in the North Atlantic subtropical gyre. The nearly identical values of 0.29 nmol kg^{-1} at FC and LBB at ~12 ka suggest that waters of the Florida Current may have had little or no southern source component during the later part of the Younger Dryas. At ~9 ka, Cd_w at the FC site became more like the South Atlantic again, and varied considerably between the two end member concentrations for the remainder of

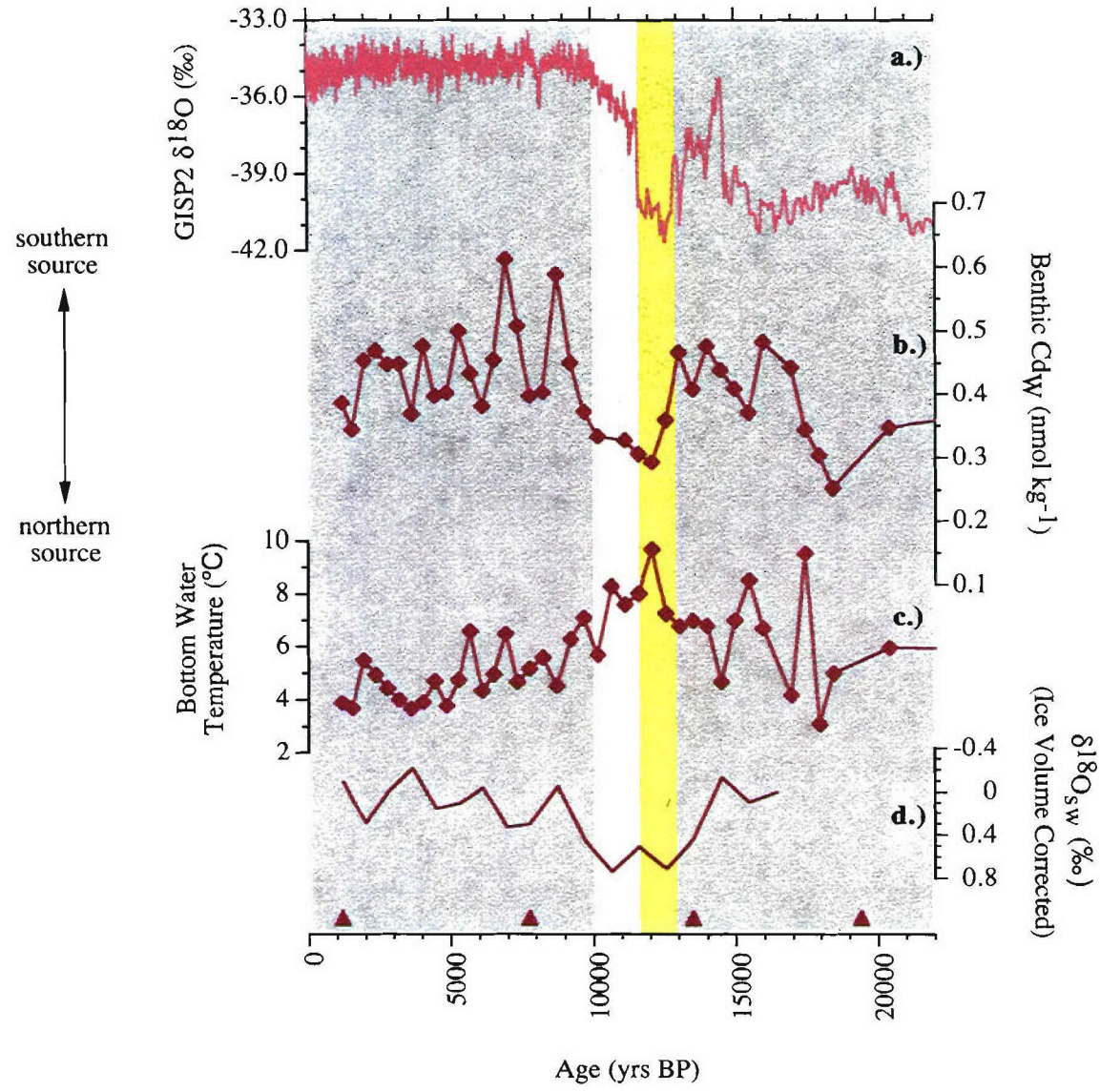

Figure 5. Benthic Cd_w and temperature data from KNR166-2-31JPC *vs.* calendar age. **a.)** GISP2 $\delta^{18}O$ (pink) [*Grootes et al.*, 1993]; **b.)** average Cd_w from 31JPC (24°13'N, 83°18'W, 751 m); **c.)** average Mg/Ca-derived temperatures from 31JPC [presented in Chapter 4]; **d.)** $\delta^{18}O_{sw}$ from 31JPC [presented in Chapter 4]. Triangles are AMS dates converted to calendar age. Yellow shading marks the Younger Dryas interval.

the record, suggesting considerable variability in the influence of northern *versus* southern source waters throughout the Holocene. Additional Cd/Ca data and AMS radiocarbon dates will be required in order to fully assess the significance of the Holocene variability.

Comparison of the intermediate depth Cd_w results with results from the deep North Atlantic provides further insights into the evolution of the water mass within the Florida Current (Figure 4c). Prior to ~17.5 ka, all three intermediate water sites were lower in Cd_w (and hence nutrients) than the deep North Atlantic, consistent with the interpretation of decreased NADW formation and increased GNAIW formation (affecting all three intermediate depth locations) during the last glacial [*Boyle and Keigwin*, 1987]. At ~14 ka, the deep North Atlantic became more nutrient depleted than both the intermediate depth South Atlantic and the waters of the Florida Current, marking a transition between glacial and interglacial subsurface geometry [*Came et al.*, 2003]. The interglacial subsurface geometry persisted for the remainder of the record, with the exception of the interval from ~12.5 to 10 ka, when the deep North Atlantic was more nutrient enriched than the waters of the Florida Current. At ~9 ka the modern geometry was firmly established: the North Atlantic deep and intermediate sites were all nutrient depleted, the intermediate depth South Atlantic was nutrient rich, and the Florida Current waters were intermediate between the South Atlantic and the North Atlantic intermediate depth sites.

The reduction in the influence of southern source waters within the Florida Current during the later part of the Younger Dryas and until 10.5 ka suggests an overturning circulation that was radically different from the modern, and also different from the last glacial. Today, southern source waters are a significant component of the northward return flow of NADW formation. A reduction in their influence at the FC site suggests a significant reduction in the deep overturning circulation, consistent with previous studies [*Boyle and Keigwin*, 1987]. However, the new results do not rule out significant overturning at intermediate depth [*Marchitto et al.*, 1998], since the formation of North Atlantic Intermediate Water (NAIW) would not require a northward return flow that originates from waters upwelled from great depths.

The $\delta^{13}C$ results from FC [*Lynch-Stieglitz*, unpublished data], LBB [*Slowey and Curry*, 1995], the Brazil Margin [*Oppo and Horowitz*, 2000], and the deep North Atlantic [*Boyle and Keigwin*, 1987] suggest glacial-interglacial circulation changes that are similar to those suggested by the Cd_w results (Figure 6). During the last glacial, the $\delta^{13}C$ results suggest that nutrient concentrations at the FC site were intermediate between the North Atlantic and South Atlantic intermediate depth sites, and more nutrient depleted relative

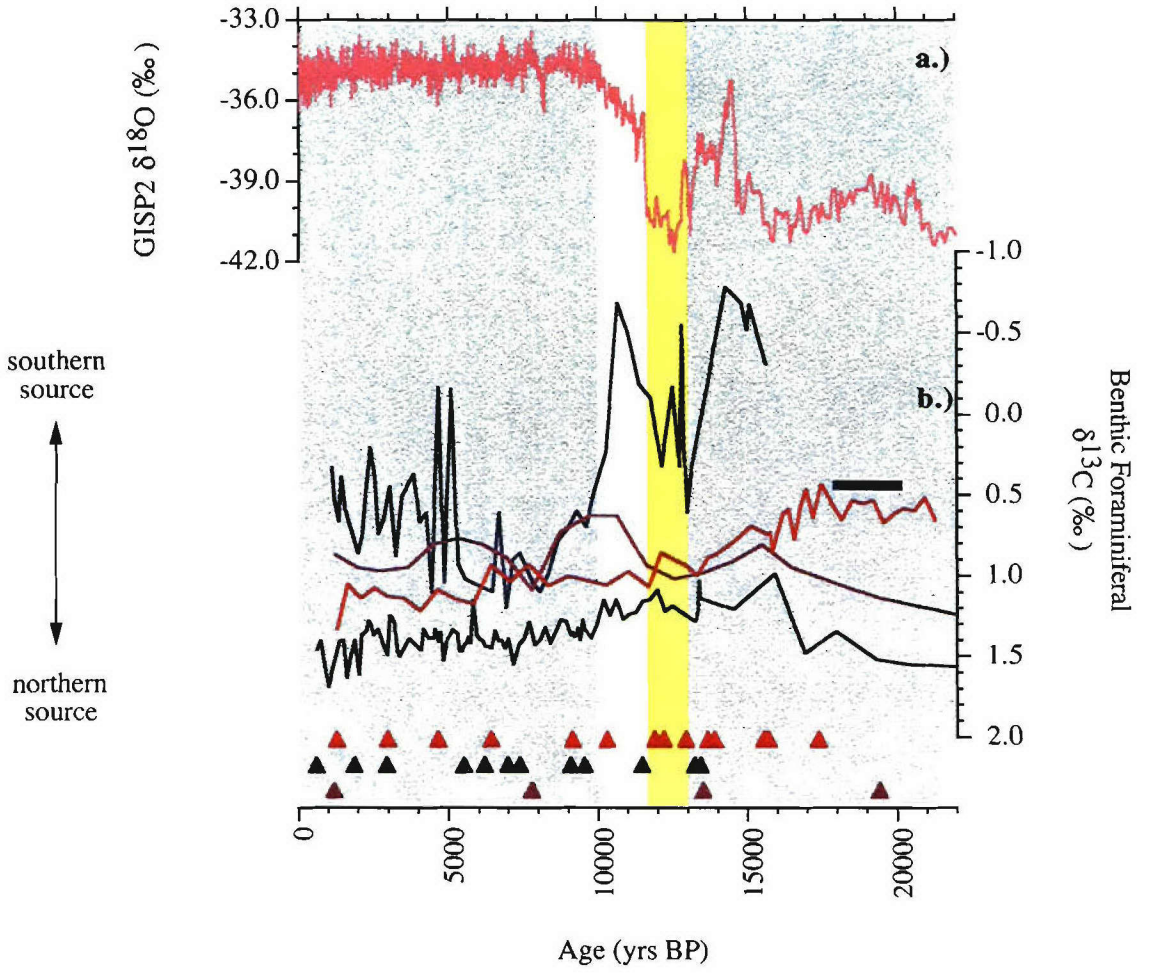

Figure 6. Benthic $\delta^{13}C$ data *vs.* calendar age. **a.)** GISP2 $\delta^{18}O$ (pink) [*Grootes et al.*, 1993]; **b.)** average $\delta^{13}C$ from KNR166-2-31JPC (24°13'N, 83°18'W, 751 m; purple) [*Lynch-Stieglitz*, unpublished data], OCE205-2-100GGC (26°04'N, 78°02'W, 1,057 m; green) [*Slowey and Curry*, 1995; this study], KNR159-5-36GGC (27°31'S, 46°28'W, 1,268 m; red) [*Oppo and Horowitz*, 2000], and EN120-GGC1 (33°40'N, 57°37'W, 4,450 m; blue) [*Boyle and Keigwin*, 1987]. The glacial $\delta^{13}C$ estimate for the deep North Atlantic (blue bar) is based on data from IOS82 PC SO1 (42°23'N, 23°31'W, 3,540 m) [*Boyle*, 1992]. Triangles are AMS dates converted to calendar age. Yellow shading marks the Younger Dryas interval.

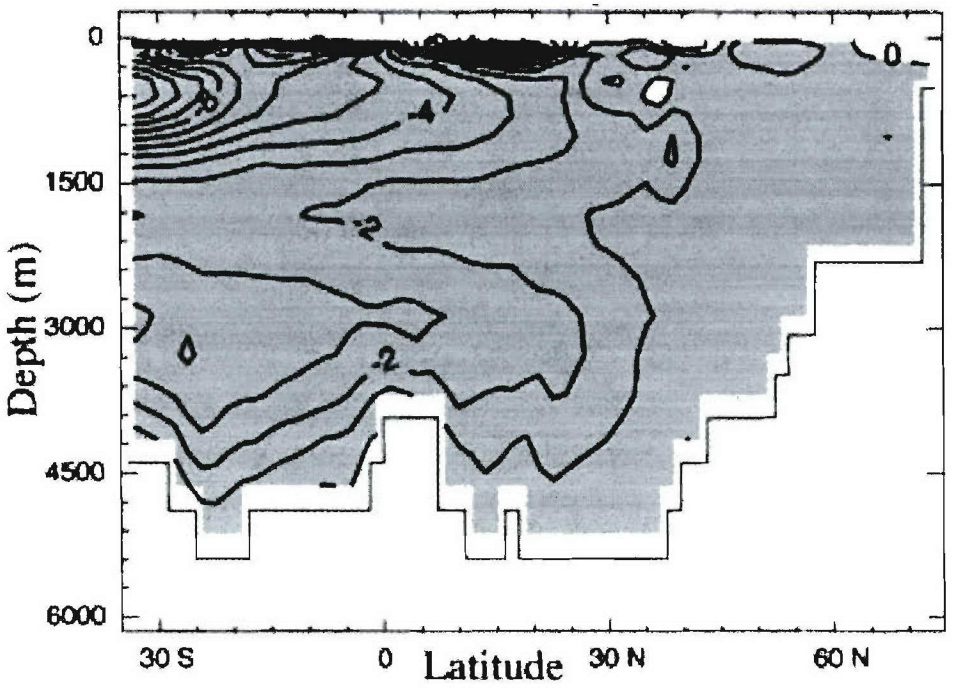

Figure 7. Atlantic meridional overturning circulation in the "off" mode. From Weaver *et al.*, [2003].

to the deep North Atlantic, consistent with the Cd_w results. Overall, the $\delta^{13}C$ results from FC suggest a glacial-interglacial trend of increasing nutrients, again, consistent with the Cd_w results. However, during the Holocene, the Brazil Margin $\delta^{13}C$ values were higher than those at the FC site. As discussed in Came *et al.* [2003], this is due to the increasing influence of a high $\delta^{13}C_{AS}$ water mass at the Brazil Margin site.

An Alternative Younger Dryas Subsurface Geometry

Alternatively, the northward penetration of AAIW during the Younger Dryas may have been similar, or even enhanced, relative to today [*Rickaby and Elderfield*, 2005]. Keeling and Stephens [2001] hypothesized that the ocean may have an "off" mode in which the density of AAIW is greater than the density of NADW:

$$\rho_{AAIW} > \rho_{NADW}.$$

Theoretically, a large freshwater flux to the surface of the Atlantic could cause this density

configuration to occur. The result would be a complete cessation of NADW formation, an intensification of the northward penetration of "AAIW" at depths just above AABW, and a compensating southward outflow of saline thermocline water (Figure 7) [*Weaver et al.*, 2003]. If this hypothesized density configuration existed during the late Younger Dryas, then the deeper "AAIW" would have bypassed the Florida Strait entirely en route to the North Atlantic, causing an increase in the influence of low Cd North Atlantic source waters at the FC site.

Rickaby and Elderfield [2005] suggest that nutrient results from sediment core NEAP 4K (61°30'N, 24°10'W, 1,627 m) in the high latitude North Atlantic support this alternative interpretation for both the Younger Dryas and Heinrich event 1 (H1). A central component of the Rickaby and Elderfield argument is that a similar water mass existed at both the intermediate depth Brazil Margin and NEAP 4K during the Younger Dryas and H1, suggesting the northward penetration of AAIW into the high latitude North Atlantic during these events. Comparison of the results from both sites does reveal similar Cd_w values at NEAP 4K and the Brazil Margin during the two cooling events (Figure 8c). However, comparison of the benthic foraminiferal $\delta^{18}O$ from the two sites suggests that these water masses were in fact very different during these events (Figure 8b): during H1, benthic $\delta^{18}O$ at the NEAP 4K site was ~1.0‰ lower relative to the Brazil Margin site; during the Younger Dryas, benthic $\delta^{18}O$ at NEAP 4K was ~0.8‰ higher relative to the Brazil Margin. Since $\delta^{18}O$ is conservative within a water mass, such large differences in $\delta^{18}O$ cannot come from the same water mass.

A simpler explanation for the high Cd_w values at the NEAP 4K site during the Younger Dryas and during Heinrich event 1 is reduced ventilation and organic matter remineralization. NEAP 4K is located on the Björn drift in the high latitude North Atlantic, and is bathed by Iceland-Faeroe Ridge overflow waters, which sink to great depths in the formation of NADW. If changes in high latitude convective activity occurred as a result of surface freshening events, waters at the NEAP 4K site could become less ventilated and more nutrient enriched.

Comparison of the NEAP 4K benthic $\delta^{18}O$ data with planktic $\delta^{18}O$ data from nearby core VM29-204 (61°11'N, 23°01'W, 1,849 m) provides further evidence suggesting a northern source for intermediate waters at the Björn drift during the Younger Dryas and H1 (Figure 8b). From 20 ka to ~13 ka, the nearly identical benthic and planktic $\delta^{18}O$ values suggest that surface and subsurface waters were very similar at this location. At ~16 ka, coincident with H1, there was a sharp decrease in both the planktic and benthic $\delta^{18}O$. Taken

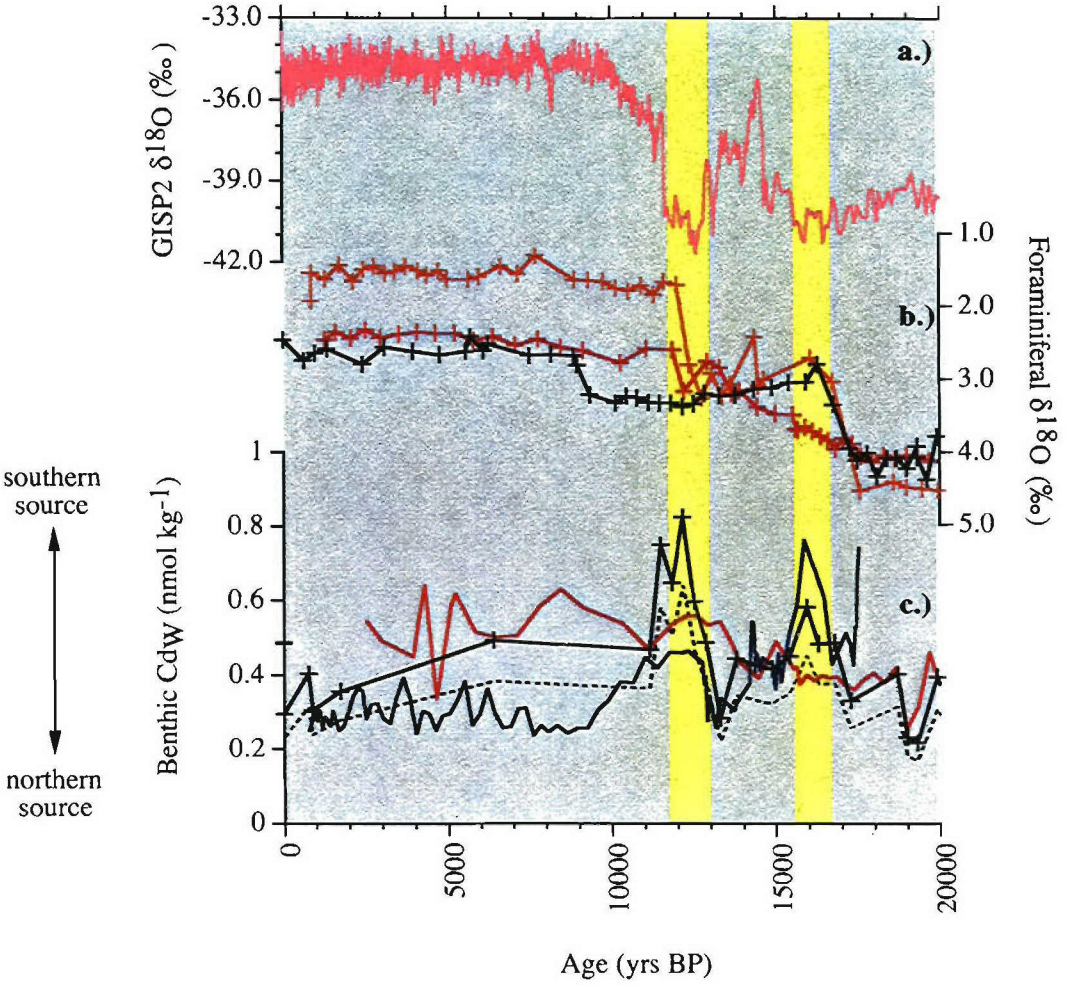

Figure 8. Comparison with NEAP 4K. **a.)** GISP2 $\delta^{18}O$ (pink) [*Grootes et al.*, 1993]; **b.)** planktic foraminiferal $\delta^{18}O$ from VM29-204 (61°11'N, 23°01'W, 1,849 m; orange), and benthic foraminiferal $\delta^{18}O$ from KNR159-5-36GGC (27°31'S, 46°28'W, 1,268 m; red) [*Oppo and Horowitz*, 2000] and NEAP 4K (61°30'N, 24°10'W, 1,627 m; black) [*Rickaby and Elderfield*, 2005]; **c.)** Cd_w from EN120-GGC1 (33°40'N, 57°37'W, 4,450 m; blue) [*Boyle and Keigwin*, 1987], KNR159-5-36GGC (red) [*Came et al.*, 2003], and NEAP 4K (black) [*Rickaby and Elderfield*, 2005]. Dashed line is Cd_w values calculated using the D_p of Bertram *et al.* [1995]; solid line is Cd_w values calculated using the D_p of Boyle [1992].

together with the concurrent increase in Cd_w, the $\delta^{18}O$ data suggest a freshening event at the sea surface, which caused a reduction in ventilation at NEAP 4K, although not a complete cessation, since the benthic $\delta^{18}O$ suggests that the surface signal continued to propagate into the subsurface during the freshening event. At ~12.5 ka, another sharp decrease in the planktic $\delta^{18}O$ occurred, however, there was no associated decrease in benthic $\delta^{18}O$. The divergence in the surface and subsurface signals suggests that a freshening event occurred in the surface at the onset of the Younger Dryas, but did not propagate into the subsurface. This could have occurred due to enhanced surface stability in response to the freshening, which caused a reduction in ventilation at the NEAP 4K site. The concurrent increase in Cd_w at NEAP 4K supports this interpretation of reduced ventilation and increased organic matter remineralization. Interestingly, however, increased nutrients are also observed in the deep North Atlantic, but Cd_w values are not as high as at the NEAP 4K site. This implies that deep water formation continued during the Younger Dryas, despite its reduced influence at the NEAP 4K site. However, it is also possible that the high Cd_w values at NEAP 4K are the result of Cd contamination.

To summarize, it is possible to account for the nutrient enrichment in the high latitude North Atlantic without invoking the "off" circulation mode, which requires a complete cessation of NADW production and a southward surface return flow. A simpler scenario, involving reduced ventilation and organic matter remineralization at the NEAP 4K site during the Younger Dryas, is consistent with the paleo-nutrient distributions. In addition, a scenario in which the northward penetration of AAIW increases, but the deep AAIW "off" mode is not invoked, is not consistent with the new FC Cd_w results, since a scenario in which

$$\rho_{AAIW} < \rho_{NADW}$$

would require the buoyant, nutrient rich AAIW to pass through the Florida Strait en route to the North Atlantic.

Conclusion

The new Cd_w results from core KNR166-2-31JPC suggest a significant reduction in the presence of southern source water within the Florida Current during the later part of the Younger Dryas, suggesting an overturning circulation during this event that was radically different from the modern, and also different from the last glacial. A northward return flow

with little or no nutrient rich southern ocean component suggests an overturning circulation that may not require significant compensation for southward penetrating deep waters. This suggests a strongly decreased MOC, and a possible reduction in northward heat transport. However, an overturning of North Atlantic waters at intermediate depth, as suggested by Marchitto *et al.* [1998], is consistent with the new results.

In addition, the new results suggest that the abrupt change in source waters at the FC site occurred well after the onset of the Younger Dryas cooling in the North Atlantic and after the reduction in North Atlantic Deep Water (NADW) production. Also, the duration of the event was significantly longer at the FC site than in the high latitude North Atlantic. This suggests that variability in the return flow of the MOC lagged climate change in the North Atlantic, lending support to North Atlantic forcing hypotheses.

References

Bertram, C. J., H. Elderfield, N. J. Shackleton, and J. A. MacDonald (1995), Cadmium/ calcium and carbon isotope reconstructions of the glacial northeast Atlantic Ocean, *Paleoceanography*, *10*, 563-578.

Boyle, E. A. (1983), Manganese carbonate overgrowths on foraminifera tests, *Geochim. Cosmochim. Acta*, *47*, 1815-1819.

Boyle, E. A. (1988), Cadmium: chemical tracer of deep water paleoceanography, *Paleoceanography*, *3*, 471-489.

Boyle, E. A. (1992), Cadmium and $\delta^{13}C$ paleochemical ocean distributions during the stage 2 glacial maximum, *Annu. Rev. Earth Planet. Sci.*, *20*, 245-287.

Boyle, E. A., and L. D. Keigwin (1982), Deep circulation of the North Atlantic over the last 200,000 years: geochemical evidence, *Science*, *218*, 784-787.

Boyle, E. A., and L. D. Keigwin (1985/6), Comparison of Atlantic and Pacific paleochemical records for the last 215,000 years: changes in deep ocean circulation and chemical inventories, *Earth Planet. Sci. Lett.*, *76*, 135-150.

Boyle, E. A., and L. D. Keigwin (1987), North Atlantic thermohaline circulation during the past 20,000 years linked to high-latitude surface temperature, *Nature*, *330*, 35-40.

Boyle, E. A., L. Labeyrie, and J.-C. Duplessy (1995), Calcitic foraminiferal data confirmed by cadmium in aragonitic Hoeglundina: Application to the Last Glacial Maximum in the northern Indian Ocean, *Paleoceanography*, *10*, 881-900.

Boyle, E. A., and Y. Rosenthal (1996), Chemical hydrography of the South Atlantic during the Last Glacial Maximum: Cd and $\delta^{13}C$, in *The South Atlantic: Present and Past Circulation*, edited by G. Wefer, pp. 423-443, Springer-Verlag, Berlin.

Broecker, W. S., and E. Maier-Reimer (1992), The influence of air-sea exchange on the carbon isotope distribution in the sea, *Global Biogeochem. Cycles*, 315-320.

Broecker, W. S., D. M. Peteet, and D. Rind (1985a), Does the ocean-atmosphere system have more than one stable mode of operation? *Nature*, *315*, 21-25.

Broecker, W. S., T. Takahashi, and T. Takahashi (1985b), Sources and flow patterns of deep ocean waters as deduced from potential temperature, salinity, and initial phosphate concentration, *J. Geophys. Res.*, *90*, 6925-6939.

Came, R. E., D. W. Oppo, and W. B. Curry (2003), Atlantic Ocean circulation during the Younger Dryas: Insights from a new Cd/Ca record from the western subtropical South Atlantic, *Paleoceanography*, *18*, 1086, doi:1010.1029/2003PA000888.

Curry, W. B., J.-C. Duplessy, L. D. Labeyrie, and N. J. Shackleton (1988), Changes in the distribution of $\delta^{13}C$ of deep water $\sum CO_2$ between the last glaciation and the Holocene, *Paleoceanography*, *3*, 317-341.

Curry, W. B., and G. P. Lohmann (1982), Carbon isotopic changes in benthic foraminifera from the western South Atlantic: reconstruction of glacial abyssal circulation patterns, *Quat. Res.*, *18*, 218-235.

Duplessy, J.-C., N. J. Shackleton, R. G. Fairbanks, L. D. Labeyrie, D. W. Oppo, and N. Kallel (1988), Deep water source variations during the last climatic cycle and their

impact on the global deep water circulation, *3*, 343-360.
Gordon, A. L. (1986), Interocean exchange of thermocline water, *J. Geophys. Res.*, *91*, 5037-5046.
Grootes, P. M., M. Stuiver, J. W. C. White, S. J. Johnsen, and J. Jouzel (1993), Comparison of oxygen-isotope records from the GISP2 and GRIP Greenland ice cores, *Nature*, *366*, 552-554.
Hester, K., and E. A. Boyle (1982), Water chemistry control of cadmium content in Recent benthic foraminifera, *Nature*, *298*, 260-262.
Hughen, K. A., et al. (2004), Marine04 marine radiocarbon age calibration, 0–26 cal kyr BP, *Radiocarbon*, *46*, 1059-1086.
Jenkins, W. J. (1980), Tritium and He-3 in the Sargasso Sea, *J. Mar. Res.*, *38*, 533-569.
Keeling, R. F., and B. B. Stephens (2001), Antarctic sea ice and the control of Pleistocene climate instability, *Paleoceanography*, *16*, 112-131.
Kroopnick, P. M. (1985), The distribution of $\delta^{13}C$ of $\sum CO2$ in the world oceans, *Deep-Sea Res.*, 57-84.
Levitus, S., and T. Boyer (1994), *World Ocean Atlas 1994 Volume 4: Temperature. NOAA Atlas NESDIS 4*, U.S. Department of Commerce, Washington, D.C.
Liss, P. S., and L. Merlivat (1986), Air-sea gas exchange rates: Introduction and synthesis, in *The Role of Air-Sea Exchange in Geochemical Cycling*, edited by P. Buat-Menard, pp. 113-127, D. Reidel, Norwell, Mass.
Luyten, J. R., J. Pedlosky, and H. Stommel (1983), The ventilated thermocline, *J. Phys. Oceanogr.*, *13*, 192-309.
Lynch-Stieglitz, J., unpublished data.
Lynch-Stieglitz, J., R. G. Fairbanks, and C. D. Charles (1994), Glacial-interglacial history of Antarctic Intermediate Water: Relative strengths of Antarctic versus Indian Ocean sources, *Paleoceanography*, *9*, 7-29.
Manabe, S., and R. J. Stouffer (1997), Coupled ocean-atmosphere model response to freshwater input: Comparison to Younger Dryas event, *Paleoceanography*, *12*, 321-336.
Marchal, O., T. F. Stocker, and F. Joos (1999), Physical and biogeochemical responses to freshwater induced thermohaline variability in a zonally averaged ocean model, in *Mechanisms of Global Climate Change at Millennial Time Scales, Geophysical Monograph Series, vol. 112*, edited by P. U. Clark, et al., pp. 263-284, American Geophysical Union, Washington, D.C.
Marchitto, T. M., W. B. Curry, and D. W. Oppo (1998), Millennial-scale changes in North Atlantic circulation since the last glaciation, *Nature*, *393*, 557-561.
Marchitto, T. M., D. W. Oppo, and W. B. Curry (2002), Paired benthic foraminiferal Cd/Ca and Zn/Ca evidence for a greatly increased presence of Southern Ocean Water in the glacial North Atlantic, *Paleoceanography*, *17*, 1038, doi:1010.1029/2000PA000598.
McCartney, M. S. (1982), The subtropical recirculation of mode waters, *J. Mar. Res.*, *40, suppl.*, 427-464.

Mook, W. G., J. C. Bommerson, and W. H. Staverman (1974), Carbon isotope fractionation between dissolved bicarbonate and gaseous carbon dioxide, *Earth Planet. Sci. Lett.*, *22*, 169-176.

Oppo, D. W., and M. Horowitz (2000), Glacial deep water geometry: South Atlantic benthic foraminiferal Cd/Ca and $\delta^{13}C$ evidence, *Paleoceanography*, *15*, 147-160.

Oppo, D. W., and S. J. Lehman (1993), Mid-Depth circulation of the subpolar North Atlantic during the Last Glacial Maximum, *Science*, 1148-1152.

Rahmstorf, S. (1994), Rapid climate transitions in a coupled ocean-atmosphere model, *Nature*, *372*, 82-85.

Reid, J. L. (1994), On the total geostrophic circulation of the North-Atlantic Ocean - flow patterns, tracers, and transports, *Prog. Oceanogr.*, *33*, 1-92.

Rickaby, R. E. M., and H. Elderfield (2005), Evidence from the high-latitude North Atlantic for variations in Antarctic Intermediate water flow during the last deglaciation, *Geochem. Geophys. Geosys.*, *6*, Q05001, doi:05010.01029/02004GC000858.

Rosenthal, Y. (1994), Late quaternary paleochemistry of the Southern Ocean: evidence from cadmium variablity in sediments and foraminifera, Ph.D. thesis, 186 pp, Massachusetts Institute of Technology and Woods Hole Oceanographic Institution.

Rosenthal, Y., M. P. Field, and R. M. Sherrell (1999), Precise determination of element/ calcium ratios in calcareous samples using sector field inductively coupled plasma mass spectrometry, *Anal. Chem.*, *71*, 3248-3253.

Rosenthal, Y., P. Lam, E. A. Boyle, and J. Thomson (1995), Authigenic cadmium enrichments in suboxic sediments: Precipitation and postdepositional mobility, *Earth Planet. Sci. Lett.*, *132*, 99-111.

Rühlemann, C., S. Mulitza, G. Lohmann, A. Paul, M. Prange, and G. Wefer (2004), Intermediate depth warming in the tropical Atlantic related to weakened thermohaline circulation: Combining paleoclimate data and modeling results for the last deglaciation, *Paleoceanography*, *19*, PA1025, doi:1010.1029/2003PA000948.

Sarmiento, J. L., C. G. Rooth, and W. Roether (1982), The North Atlantic tritium distribution in 1972, *J. Geophys. Res.*, *87*, 8047-8056.

Sarnthein, M., et al. (2001), Fundamental modes and abrupt changes in North Atlantic circulation and climate over the last 60 kyr—Concepts, reconstruction and numerical modeling, in *The Northern North Atlantic: A Changing Environment*, edited by P. Schafer, et al., pp. 365-410, Springer-Verlag, New York.

Schmitz, W. J., J. R. Luyten, and R. W. Schmitt (1993), On the Florida Current T/S envelope, *Bull. Mar. Sci.*, *53*, 1048-1065.

Schmitz, W. J., and M. S. McCartney (1993), On the North Atlantic circulation, *Rev. Geophys.*, *31*, 29-49.

Schmitz, W. J., and P. L. Richardson (1991), On the sources of the Florida Current, *Deep-Sea Res.*, *38*, S379-S409.

Slowey, N. C., and W. B. Curry (1995), Glacial-interglacial differences in circulation and carbon cycling within the upper western North-Atlantic, *Paleoceanography*, *10*,

715-732.

Stuiver, M., and P. J. Reimer (1993), Extended ^{14}C database and revised CALIB radiocarbon calibration program, *Radiocarbon*, *35*, 215-230.

Tsuchiya, M. (1989), Circulation of the Antarctic Intermediate Water in the North-Atlantic Ocean, *J. Mar. Res.*, *47*, 747-755.

Weaver, A. J., O. A. Saenko, P. U. Clark, and J. Mitrovica (2003), Meltwater pulse 1A from Antarctica as a trigger of the Bølling-Allerød warm interval, *Science*, *299*, 1709-1713.

Zahn, R., and A. Stüber (2002), Suborbital intermediate water variability inferred from paired benthic foraminiferal Cd/Ca and $\delta^{13}C$ in the tropical West Atlantic and linking with North Atlantic climates, *Earth Planet. Sci. Lett.*, *200*, 191-205.

Tables

Table 1. Previously published AMS dates* and revised calendar ages**.

Depth (cm)	Species	NOSAMS ID	AMS Date	AMS Error	Age (yrs BP)
KNR159-5-36GGC					
1	*G. ruber*	OS-22674	1,740	30	1,290
16	*G. ruber*	OS-25478	3,170	60	2,968
28	*G. ruber*	OS-22675	4,450	40	4,653
28	*G. ruber*	OS-22681	4,480	55	4,672
40	*G. ruber*	OS-23216	6,000	35	6,412
56	*G. ruber*	OS-22676	8,510	50	9,141
60	*G. ruber*	OS-27350	9,450	50	10,301
64	*G. ruber*	OS-25479	10,750	90	12,182
68	*G. ruber*	OS-23210	10,600	45	11,884
80	*G. ruber*	OS-23211	11,400	50	12,924
88	*G. ruber*	OS-23212	12,200	50	13,665
92	*G. ruber*	OS-22677	12,450	60	13,900
104	*G. ruber*	OS-23318	13,550	60	15,553
112	*G. ruber*	OS-23317	13,650	60	15,695
141	*G. ruber*	OS-23213	14,850	120	17,371
148	*G. ruber*	OS-22678	12,350	65	13,808
148	*C. pachyderma*	OS-23214	16,050	65	18,896
200	*G. ruber*	OS-22679	19,300	95	22,416
EN120-GGC1					
93	*G. ruber*	OS-33623	9,040	50	9,739
107	*G. ruber*	OS-33624	10,850	60	12,381
115	*G. ruber*	OS-33625	11,250	60	12,849
115	*G. ruber*	OS-33626	11,200	65	12,826

* Came *et al* ., [2003].

** AMS radiocarbon dates were converted to calendar age using CALIB 5.01 [*Stuiver and Reimer,* 1993], the Marine04 dataset [*Hughen et al.,* 2004],

Table 2. OCE205-2-100GGC *H. elegans* Cd/Ca data.

Depth (cm)	Age (yrs BP)	[Ca] (ppm)	Mn/Ca (μmol mol^{-1})	Cd/Ca (μmol mol^{-1})	Mean Cd/Ca (μmol mol^{-1})	Cd_w* (nmol kg^{-1})	Mean Cd_w* (nmol kg^{-1})
OCE205-2-100GGC							
8	737	211	0.14	0.030	0.030	0.30	0.30
13	1,359	191	0.95	0.028	0.026	0.28	0.26
13	1,359	216	0.44	0.024		0.24	
16	1,732	259	0.06	0.033	0.033	0.33	0.33
18	1,933	277	0.33	0.043	0.043	0.43	0.43
19	2,010	296	0.35	0.036	0.036	0.36	0.36
21	2,165	200	0.39	0.037	0.037	0.37	0.37
22	2,242	229	0.18	0.030	0.030	0.30	0.30
24	2,396	188	0.43	0.032	0.032	0.32	0.32
25	2,473	284	0.29	0.034	0.034	0.34	0.34
26	2,550	258	0.30	0.029	0.029	0.29	0.29
27	2,627	259	0.44	0.028	0.026	0.28	0.26
27	2,627	246	0.41	0.024		0.24	
28	2,705	228	0.46	0.031	0.031	0.31	0.31
29	2,782	281	0.42	0.031	0.028	0.31	0.28
29	2,782	206	0.41	0.024		0.24	
30	2,859	301	0.42	0.035	0.029	0.35	0.29
30	2,859	241	0.60	0.024		0.24	
32	3,017	299	0.41	0.031	0.031	0.31	0.31
33	3,097	265	0.59	0.035	0.035	0.35	0.35
35	3,258	246	0.44	0.033	0.033	0.33	0.33
36	3,339	303	0.35	0.027	0.027	0.27	0.27
37	3,420	224	0.48	0.035	0.035	0.35	0.35
38	3,500	335	0.58	0.031	0.031	0.31	0.31
39	3,581	251	0.59	0.032	0.032	0.32	0.32
40	3,661	272	0.41	0.032	0.032	0.32	0.32
42	3,823	296	0.79	0.029	0.029	0.29	0.29
43	3,903	274	0.44	0.039	0.039	0.39	0.39
44	3,984	276	0.38	0.034	0.034	0.34	0.34
45	4,064	255	0.33	0.034	0.034	0.34	0.34
46	4,145	280	0.46	0.036	0.036	0.36	0.36
47	4,226	367	0.60	0.029	0.029	0.29	0.29
48	4,306	288	0.76	0.031	0.031	0.31	0.31
49	4,387	264	0.65	0.027	0.027	0.27	0.27
51	4,548	237	0.40	0.027	0.027	0.27	0.27
52	4,629	251	0.37	0.030	0.030	0.30	0.30
53	4,709	321	0.46	0.030	0.030	0.30	0.30
54	4,790	143	0.52	0.023	0.023	0.23	0.23
55	4,870	260	0.48	0.029	0.029	0.29	0.29
56	4,951	265	1.14	0.048	0.044	0.48	0.44
56	4,951	233	2.18	0.041		0.41	
57	5,031	283	0.45	0.023	0.023	0.23	0.23
58	5,112	292	0.36	0.029	0.027	0.29	0.27
58	5,112	203	0.41	0.025		0.25	
59	5,193	275	0.46	0.030	0.030	0.30	0.30
60	5,273	238	0.46	0.030	0.030	0.30	0.30

Table 2 (cont.).

Depth (cm)	Age (yrs BP)	[Ca] (ppm)	Mn/Ca (μmol mol^{-1})	Cd/Ca (μmol mol^{-1})	Mean Cd/Ca (μmol mol^{-1})	Cd_w* (nmol kg^{-1})	Mean Cd_w* (nmol kg^{-1})
OCE205-2-100GGC							
61	5,354	239	0.26	0.028	0.028	0.28	0.28
62	5,434	305	0.51	0.031	0.031	0.31	0.31
63	5,515	263	0.91	0.032	0.032	0.32	0.32
64	5,584	269	0.58	0.029	0.029	0.29	0.29
66	5,721	277	0.64	0.026	0.026	0.26	0.26
67	5,789	255	0.53	0.027	0.027	0.27	0.27
68	5,858	284	2.41	0.030	0.026	0.30	0.26
68	5,858	253	0.38	0.022		0.22	
70	5,995	320	0.44	0.023	0.023	0.23	0.23
71	6,063	314	0.72	0.032	0.032	0.32	0.32
72	6,132	224	0.50	0.034	0.034	0.34	0.34
73	6,200	258	0.37	0.028	0.028	0.28	0.28
74	6,310	272	0.49	0.027	0.027	0.27	0.27
75	6,420	280	0.34	0.022	0.022	0.22	0.22
76	6,530	311	0.73	0.041	0.034	0.41	0.34
76	6,530	254	0.54	0.026		0.26	
77	6,640	206	0.45	0.025	0.024	0.25	0.24
77	6,640	293	0.42	0.023		0.23	
78	6,750	269	0.54	0.036	0.036	0.36	0.36
79	6,860	241	0.44	0.026	0.026	0.26	0.26
80	6,970	280	0.66	0.030	0.030	0.30	0.30
81	7,144	232	0.50	0.029	0.029	0.29	0.29
82	7,318	294	0.45	0.028	0.028	0.28	0.28
83	7,492	246	0.54	0.024	0.024	0.24	0.24
85	7,840	266	0.53	0.035	0.035	0.35	0.35
86	8,015	211	0.42	0.029	0.029	0.29	0.29
87	8,189	188	0.39	0.030	0.030	0.30	0.30
88	8,363	288	0.46	0.024	0.024	0.24	0.24
89	8,537	249	0.68	0.026	0.026	0.26	0.26
90	8,711	253	0.88	0.029	0.029	0.29	0.29
91	8,885	279	0.60	0.028	0.028	0.28	0.28
91	8,885	289	0.44	0.029		0.29	
92	9,059	237	0.48	0.029	0.029	0.29	0.29
93	9,117	290	0.48	0.027	0.027	0.27	0.27
94	9,176	229	10.45	0.036	0.036	0.36	0.36
95	9,234	298	0.53	0.027	0.027	0.27	0.27
96	9,292	107	0.54	0.028	0.028	0.28	0.28
98	9,409	128	0.62	0.025	0.025	0.25	0.25
99	9,467	278	0.52	0.025	0.025	0.25	0.25
100	9,525	278	0.60	0.025	0.025	0.25	0.25
101	9,741	302	0.43	0.026	0.026	0.26	0.26
102	9,957	183	0.46	0.024	0.024	0.24	0.24
103	10,173	188	0.51	0.025	0.025	0.25	0.25
104	10,389	216	0.51	0.028	0.028	0.28	0.28
105	10,604	389	0.38	0.024	0.025	0.24	0.25
105	10,604	311	0.52	0.025		0.25	

Table 2 (cont.).

Depth (cm)	Age (yrs BP)	[Ca] (ppm)	Mn/Ca (μmol mol^{-1})	Cd/Ca (μmol mol^{-1})	Mean Cd/Ca (μmol mol^{-1})	Cd_w* (nmol kg^{-1})	Mean Cd_w* (nmol kg^{-1})
OCE205-2-100GGC							
106	10,820	84	0.57	0.027	0.027	0.27	0.27
108	11,252	112	0.51	0.021	0.021	0.21	0.21
109	11,468	305	0.50	0.031	0.031	0.31	0.31
110	11,718	84	1.06	0.029	0.030	0.29	0.30
110	11,718	185	0.47	0.034		0.34	
110	11,718	231	0.68	0.027		0.27	
112	12,218	200	0.48	0.023	0.023	0.23	0.23
113	12,468	283	0.49	0.021	0.021	0.21	0.21
117	13,270	70	0.87	0.023	0.023	0.23	0.23
120	13,427	248	0.61	0.024	0.024	0.24	0.24
123	14,452	228	0.78	0.021	0.021	0.21	0.21
124	14,794	238	0.57	0.030	0.030	0.30	0.30
126	15,478	242	0.70	0.027	0.027	0.27	0.27
128	16,162	236	0.88	0.026	0.026	0.26	0.26
132	17,529	231	1.05	0.018	0.018	0.18	0.18
136	18,896	178	0.94	0.018	0.018	0.18	0.18
138	19,580	255	1.14	0.019	0.019	0.19	0.19
142	20,947	180	0.71	0.020	0.020	0.20	0.20
148	22,998	269	0.33	0.019	0.019	0.19	0.19
152	24,365	218	0.70	0.022	0.022	0.22	0.22
156	25,733	227	0.69	0.028	0.028	0.28	0.28
158	26,416	221	0.94	0.020	0.020	0.20	0.20
162	27,784	221	1.12	0.016	0.016	0.16	0.16

* D_P = 1 [*Boyle et al.*, 1995].

Table 3. KNR166-2-31JPC *H. elegans* Cd/Ca data.

Depth (cm)	Age (yrs BP)	[Ca] (ppm)	Mn/Ca (μmol mol^{-1})	Cd/Ca (μmol mol^{-1})	Mean Cd/Ca (μmol mol^{-1})	Cd_w* (nmol kg^{-1})	Mean Cd_w* (nmol kg^{-1})
KNR166-2-31JPC							
0.5	1,204	61	0.41	0.039	0.039	0.39	0.39
4	1,566	192	0.21	0.034	0.034	0.34	0.34
8	1,980	268	0.95	0.045	0.045	0.45	0.45
12	2,394	51	0.92	0.047	0.047	0.47	0.47
16	2,808	284	0.25	0.045	0.045	0.45	0.45
20	3,221	271	0.39	0.045	0.045	0.45	0.45
24	3,635	188	0.37	0.037	0.037	0.37	0.37
28	4,049	262	0.43	0.048	0.048	0.48	0.48
32	4,463	210	0.40	0.040	0.040	0.40	0.40
36	4,876	85	0.61	0.043	0.040	0.43	0.40
36	4,876	257	0.46	0.038		0.38	
40	5,290	268	0.60	0.050	0.050	0.50	0.50
44	5,704	243	0.55	0.043	0.043	0.43	0.43
48	6,118	49	0.49	0.041	0.038	0.41	0.38
48	6,118	298	0.35	0.035		0.35	
52	6,532	109	0.37	0.045	0.045	0.45	0.45
56	6,945	319	0.41	0.061	0.061	0.61	0.61
60	7,359	182	0.38	0.051	0.051	0.51	0.51
64	7,773	272	0.44	0.040	0.040	0.40	0.40
68	8,250	150	0.40	0.040	0.040	0.40	0.40
72	8,728	130	0.35	0.059	0.059	0.59	0.59
76	9,205	71	0.36	0.045	0.045	0.45	0.45
80	9,682	238	0.36	0.037	0.037	0.37	0.37
84	10,159	168	0.31	0.035	0.033	0.35	0.33
84	10,159	214	0.41	0.032		0.32	
92	11,114	217	0.27	0.029	0.033	0.29	0.33
92	11,114	81	0.36	0.036		0.36	
96	11,591	204	0.30	0.029	0.031	0.29	0.31
96	11,591	151	0.37	0.033		0.33	
100	12,068	135	0.32	0.026	0.029	0.26	0.29
100	12,068	237	0.28	0.033		0.33	
104	12,546	217	0.28	(0.062)	0.036	(0.62)	0.361
104	12,546	189	0.71	0.043		0.43	
104	12,546	130	0.43	0.029		0.29	
108	13,023	141	0.46	0.043	0.047	0.43	0.47
108	13,023	266	0.51	0.048		0.48	
108	13,023	162	0.42	0.049		0.49	
112	13,500	153	0.46	0.043	0.041	0.43	0.41
112	13,500	138	2.76	0.039		0.39	
116	13,991	181	0.61	0.051	0.048	0.51	0.48
116	13,991	187	0.40	0.044		0.44	
120	14,483	314	0.37	0.040	0.044	0.40	0.44
120	14,483	200	0.69	0.048		0.48	
124	14,974	158	0.29	0.041	0.041	0.41	0.41
124	14,974	217	0.57	0.042		0.42	
124	14,974	224	0.58	0.039		0.39	

Table 3 (cont.).

Depth (cm)	Age (yrs BP)	[Ca] (ppm)	Mn/Ca (μmol mol^{-1})	Cd/Ca (μmol mol^{-1})	Mean Cd/Ca (μmol mol^{-1})	Cd_w* (nmol kg^{-1})	Mean Cd_w* (nmol kg^{-1})
KNR166-2-31JPC							
128	15,465	309	0.23	0.047	0.037	0.47	0.37
128	15,465	252	0.25	0.032		0.32	
128	15,465	196	0.30	0.032		0.32	
132	15,957	177	0.55	0.048	0.048	0.48	0.48
140	16,940	255	0.26	0.044	0.044	0.44	0.44
144	17,431	260	0.33	0.030	0.034	0.30	0.34
144	17,431	171	0.49	0.039		0.39	
148	17,923	272	0.30	0.030	0.030	0.30	0.30
152	18,414	265	0.46	0.026	0.025	0.26	0.25
152	18,414	242	0.44	0.025		0.25	
168	20,382	273	0.38	0.035	0.035	0.35	0.35
220	26,778	650	0.39	0.039	0.039	0.39	0.39
228	27,762	276	0.78	0.025	0.025	0.25	0.25
244	29,730	284	0.35	0.038	0.038	0.38	0.38
260	31,698	227	0.36	0.031	0.031	0.31	0.31
264	32,190	209	0.34	0.029	0.029	0.29	0.29
268	32,682	268	0.52	0.022	0.022	0.22	0.22

Values in parentheses were omitted.
* D_P = 1 [*Boyle et al.,* 1995].

Table 4. OCE205-2-100GGC *Cibicidoides spp.* $\delta^{13}C$ data*.

Depth (cm)	Age (yrs BP)	$\delta^{13}C$ (‰)	Mean $\delta^{13}C$ (‰)
OCE205-2-100GGC			
7	613	1.46	1.46
8	737	1.26	1.40
8	737	1.30	
8	737	1.50	
8	737	1.54	
10	986	1.69	1.69
13	1,359	1.38	1.41
13	1,359	1.41	
13	1,359	1.44	
14	1,483	1.21	1.40
14	1,483	1.30	
14	1,483	1.47	
14	1,483	1.61	
15	1,607	1.47	1.63
15	1,607	1.79	
16	1,732	1.44	1.49
16	1,732	1.54	
17	1,856	1.36	1.40
17	1,856	1.43	
19	2,010	1.56	1.61
19	2,010	1.65	
20	2,087	1.30	1.37
20	2,087	1.44	
22	2,242	1.32	1.34
22	2,242	1.32	
22	2,242	1.37	
23	2,319	1.16	1.28
23	2,319	1.29	
23	2,319	1.38	
24	2,396	1.17	1.31
24	2,396	1.20	
24	2,396	1.41	
24	2,396	1.46	
25	2,473	1.37	1.37
27	2,627	1.27	1.33
27	2,627	1.38	
29	2,782	1.21	1.42
29	2,782	1.38	
29	2,782	1.68	
30	2,859	1.22	1.45
30	2,859	1.41	
30	2,859	1.44	
30	2,859	1.57	
30	2,859	1.61	
31	2,936	1.42	1.49
31	2,936	1.56	

Table 4 (cont.).

Depth (cm)	Age (yrs BP)	$\delta^{13}C$ (‰)	Mean $\delta^{13}C$ (‰)
OCE205-2-100GGC			
32	3,017	1.20	1.25
32	3,017	1.29	
32	3,017	1.30	
33	3,097	1.17	1.26
33	3,097	1.35	
34	3,178	1.27	1.30
34	3,178	1.33	
35	3,258	1.35	1.46
35	3,258	1.42	
35	3,258	1.60	
36	3,339	1.40	1.50
36	3,339	1.44	
36	3,339	1.52	
36	3,339	1.63	
40	3,661	1.31	1.39
40	3,661	1.47	
45	4,064	1.37	1.46
45	4,064	1.42	
45	4,064	1.58	
46	4,145	1.20	1.33
46	4,145	1.36	
46	4,145	1.44	
48	4,306	1.34	1.39
48	4,306	1.44	
49	4,387	1.27	1.38
49	4,387	1.49	
50	4,467	1.27	1.39
50	4,467	1.35	
50	4,467	1.56	
51	4,548	1.31	1.33
51	4,548	1.35	
52	4,629	1.24	1.41
52	4,629	1.44	
52	4,629	1.56	
53	4,709	1.19	1.35
53	4,709	1.31	
53	4,709	1.40	
53	4,709	1.50	
54	4,790	1.41	1.53
54	4,790	1.54	
54	4,790	1.58	
54	4,790	1.60	
55	4,870	1.44	1.45
55	4,870	1.45	
55	4,870	1.47	
56	4,951	1.27	1.39

Table 4 (cont.).

Depth (cm)	Age (yrs BP)	$\delta^{13}C$ (‰)	Mean $\delta^{13}C$ (‰)
OCE205-2-100GGC			
56	4,951	1.41	
56	4,951	1.48	
57	5,031	1.33	1.37
57	5,031	1.41	
58	5,112	1.32	1.33
58	5,112	1.33	
60	5,273	1.09	1.36
60	5,273	1.28	
60	5,273	1.35	
60	5,273	1.38	
60	5,273	1.45	
60	5,273	1.47	
60	5,273	1.53	
61	5,354	1.33	1.47
61	5,354	1.36	
61	5,354	1.57	
61	5,354	1.60	
62	5,434	1.29	1.47
62	5,434	1.50	
62	5,434	1.55	
62	5,434	1.55	
63	5,515	1.33	1.43
63	5,515	1.53	
64	5,584	1.40	1.42
64	5,584	1.40	
64	5,584	1.41	
64	5,584	1.48	
65	5,652	1.35	1.38
65	5,652	1.35	
65	5,652	1.44	
66	5,721	1.35	1.42
66	5,721	1.49	
67	5,789	0.76	1.15
67	5,789	1.32	
67	5,789	1.36	
69	5,926	1.26	1.37
69	5,926	1.48	
70	5,995	1.38	1.39
70	5,995	1.40	
70	5,995	1.40	
71	6,063	1.37	1.40
71	6,063	1.42	
71	6,063	1.42	
72	6,132	1.40	1.41
72	6,132	1.41	
73	6,200	1.33	1.44

Table 4 (cont.).

Depth (cm)	Age (yrs BP)	$\delta^{13}C$ (‰)	Mean $\delta^{13}C$ (‰)
OCE205-2-100GGC			
73	6,200	1.44	
73	6,200	1.54	
74	6,310	1.31	1.44
74	6,310	1.56	
75	6,420	1.31	1.45
75	6,420	1.58	
76	6,530	1.27	1.34
76	6,530	1.32	
76	6,530	1.42	
77	6,640	1.34	1.41
77	6,640	1.38	
77	6,640	1.41	
77	6,640	1.51	
78	6,750	1.32	1.40
78	6,750	1.38	
78	6,750	1.49	
79	6,860	1.34	1.45
79	6,860	1.49	
79	6,860	1.52	
80	6,970	1.33	1.39
80	6,970	1.45	
81	7,144	1.22	1.55
81	7,144	1.45	
81	7,144	1.97	
82	7,318	1.29	1.43
82	7,318	1.37	
82	7,318	1.50	
82	7,318	1.54	
83	7,492	1.34	1.39
83	7,492	1.35	
83	7,492	1.48	
84	7,666	1.21	1.29
84	7,666	1.36	
85	7,840	1.35	1.43
85	7,840	1.38	
85	7,840	1.43	
85	7,840	1.55	
86	8,015	1.25	1.40
86	8,015	1.40	
86	8,015	1.42	
86	8,015	1.52	
87	8,189	1.23	1.32
87	8,189	1.30	
87	8,189	1.35	
87	8,189	1.38	
88	8,363	1.31	1.42

Table 4 (cont.).

Depth (cm)	Age (yrs BP)	$\delta^{13}C$ (‰)	Mean $\delta^{13}C$ (‰)
OCE205-2-100GGC			
88	8,363	1.33	
88	8,363	1.63	
89	8,537	1.20	1.35
89	8,537	1.30	
89	8,537	1.33	
89	8,537	1.40	
89	8,537	1.52	
90	8,711	1.18	1.27
90	8,711	1.23	
90	8,711	1.41	
91	8,885	1.20	1.28
91	8,885	1.26	
91	8,885	1.39	
92	9,059	1.30	1.37
92	9,059	1.32	
92	9,059	1.34	
92	9,059	1.35	
92	9,059	1.38	
92	9,059	1.39	
92	9,059	1.51	
93	9,117	1.06	1.35
93	9,117	1.41	
93	9,117	1.59	
94	9,176	1.27	1.38
94	9,176	1.31	
94	9,176	1.44	
94	9,176	1.50	
95	9,234	1.34	1.37
95	9,234	1.34	
95	9,234	1.37	
95	9,234	1.43	
96	9,292	1.27	1.32
96	9,292	1.27	
96	9,292	1.36	
96	9,292	1.36	
97	9,350	1.33	1.40
97	9,350	1.39	
97	9,350	1.40	
97	9,350	1.48	
98	9,409	1.28	1.35
98	9,409	1.36	
98	9,409	1.36	
98	9,409	1.39	
99	9,467	1.13	1.27
99	9,467	1.22	
99	9,467	1.22	

Table 4 (cont.).

Depth (cm)	Age (yrs BP)	$\delta^{13}C$ (‰)	Mean $\delta^{13}C$ (‰)
OCE205-2-100GGC			
99	9,467	1.49	
100	9,525	1.19	1.33
100	9,525	1.27	
100	9,525	1.32	
100	9,525	1.36	
100	9,525	1.39	
100	9,525	1.42	
101	9,741	1.36	1.39
101	9,741	1.37	
101	9,741	1.40	
101	9,741	1.43	
102	9,957	1.29	1.30
102	9,957	1.31	
103	10,173	1.13	1.15
103	10,173	1.14	
103	10,173	1.19	
104	10,389	1.23	1.25
104	10,389	1.26	
105	10,604	1.04	1.15
105	10,604	1.19	
105	10,604	1.21	
106	10,820	1.17	1.27
106	10,820	1.30	
106	10,820	1.30	
106	10,820	1.31	
107	11,036	1.20	1.24
107	11,036	1.28	
108	11,252	1.12	1.23
108	11,252	1.23	
108	11,252	1.24	
108	11,252	1.31	
109	11,468	1.04	1.16
109	11,468	1.17	
109	11,468	1.26	
110	11,718	1.00	1.15
110	11,718	1.08	
110	11,718	1.09	
110	11,718	1.11	
110	11,718	1.18	
110	11,718	1.22	
110	11,718	1.23	
110	11,718	1.29	
111	11,968	0.93	1.09
111	11,968	1.08	
111	11,968	1.10	
111	11,968	1.25	

Table 4 (cont.).

Depth (cm)	Age (yrs BP)	$\delta^{13}C$ (‰)	Mean $\delta^{13}C$ (‰)
OCE205-2-100GGC			
112	12,218	1.07	1.22
112	12,218	1.23	
112	12,218	1.36	
113	12,468	1.05	1.19
113	12,468	1.19	
113	12,468	1.32	
116	13,218	1.01	1.28
116	13,218	1.24	
116	13,218	1.25	
116	13,218	1.27	
116	13,218	1.37	
116	13,218	1.38	
116	13,218	1.41	
117	13,270	1.05	1.27
117	13,270	1.17	
117	13,270	1.19	
117	13,270	1.26	
117	13,270	1.26	
117	13,270	1.37	
117	13,270	1.59	
118	13,322	0.99	1.21
118	13,322	1.25	
118	13,322	1.29	
118	13,322	1.30	
119	13,375	0.94	1.03
119	13,375	1.12	
120	13,427	1.07	1.14
120	13,427	1.17	
120	13,427	1.19	
120	13,427	1.24	
123	14,548	1.16	1.21
123	14,548	1.20	
123	14,548	1.27	
127	15,905	0.88	0.99
127	15,905	1.09	
130	16,923	1.44	1.48
130	16,923	1.51	
133	17,940	1.31	1.35
133	17,940	1.38	
137	19,297	1.43	1.52
137	19,297	1.54	
137	19,297	1.59	
140	20,315	1.48	1.55
140	20,315	1.56	
140	20,315	1.61	
150	23,708	1.52	1.58

Table 4 (cont.).

Depth (cm)	Age (yrs BP)	$\delta^{13}C$ (‰)	Mean $\delta^{13}C$ (‰)
OCE205-2-100GGC			
150	23,708	1.64	
153	24,725	1.20	1.41
153	24,725	1.51	
153	24,725	1.53	
157	26,082	1.46	1.51
157	26,082	1.47	
157	26,082	1.50	
157	26,082	1.62	
160	27,100	1.53	1.56
160	27,100	1.53	
160	27,100	1.57	
160	27,100	1.62	

* Both previously published data [*Slowey and Curry,* 1995] and newly acquired data [this study].

Appendix 1. Zn/Ca data from KNR166-2-31JPC

Each *H. elegans* sample from sediment core KNR166-2-31JPC was simultaneously analyzed for Zn/Ca in addition to the element/Ca ratios presented in Chapters 4 and 5. Each sample consisted of approximately 2-3 individuals, which were crushed and cleaned according to the full trace metal protocol [*Boyle and Keigwin*, 1985/6] with a reversal of the oxidative and reductive steps [*Boyle and Rosenthal*, 1996; *Rosenthal*, 1994; *Rosenthal et al.*, 1995]. Samples were dissolved in trace metal clean HNO_3 to obtain samples of approximately 200 ppm Ca.

Element/calcium ratios were measured using a Thermo-Finnigan Element2 sector field single collector ICP-MS and an external standard. Converting ICP-MS intensity ratios to elemental ratios using an external standard requires similar [Ca] in both the sample and the standard due to a calcium matrix effect. To correct for samples with varying [Ca], a series of standards were run with identical element to Ca ratios, but with Ca concentrations that varied over the anticipated sample concentration range. The resulting matrix effect was calculated and the sample ratios were corrected.

In order to assess the precision of measurements on the ICP-MS, three consistency standards were treated as samples in each of the runs in which the data were generated. Mean Zn/Ca values for the three consistency standards were 5.42 μmol mol^{-1}, 8.70 μmol mol^{-1}, and 3.06 μmol mol^{-1}. Relative standard deviations were ±13.4% (n=5), ±2.0% (n=3), and ±14.6% (n=5), respectively. The large relative standard deviations for the consistency standards may be due, in part, to 1.) a poorly defined matrix correction, 2.) laboratory contamination, or 3.) a combination of the two.

The large standard deviations for the consistency standards prevent a reliable interpretation of the Zn/Ca record. However, the Zn/Ca results do lend some support for the conclusions of Chapter 5. As shown by Marchitto *et al.* [2000], Zn/Ca ratios in benthic foraminifera reflect the relative influences of northern versus southern source waters at a given location. The increase in Zn/Ca at ~18.5 ka (Figure 2), which occurred simultaneously with the increase in Cd_w, supports the conclusion that the influence of southern source waters in the Florida Strait began to increase at that time [Chapter 5]. However, there are considerable differences between the records as well. For example, Zn/Ca results for the Holocene are low relative to the earlier portion of the record, whereas Cd_w results for the

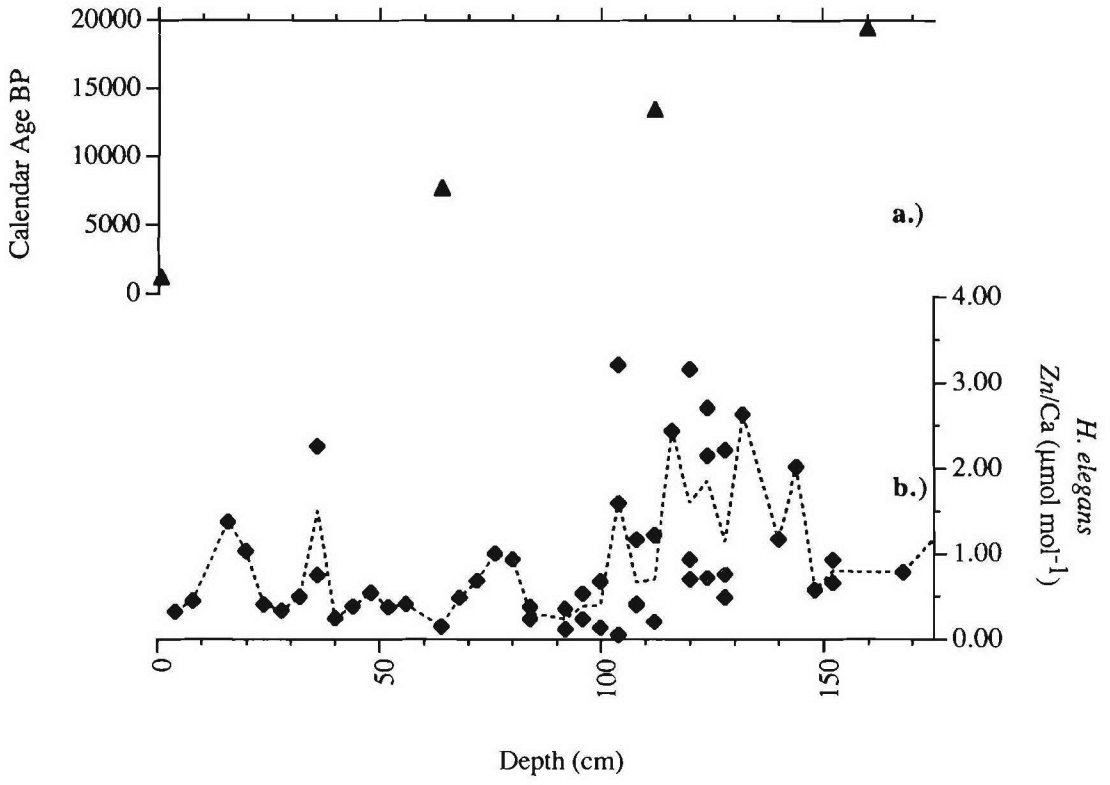

Figure 1. Benthic Zn/Ca data from KNR166-2-31JPC (24°13'N, 83°18'W, 751 m) *vs.* depth. **a.)** AMS radiocarbon dates [*Lynch-Stieglitz*, unpublished data] converted to calendar age using Calib 5.01 [*Stuiver and Reimer*, 1993], the calibration data set of Hughen *et al.* [2004], and a reservoir correction of 400 years; **b.)** all *H. elegans* Zn/Ca.

Holocene are relatively high. Again, interpretation of the Zn/Ca record is limited due to poor data quality.

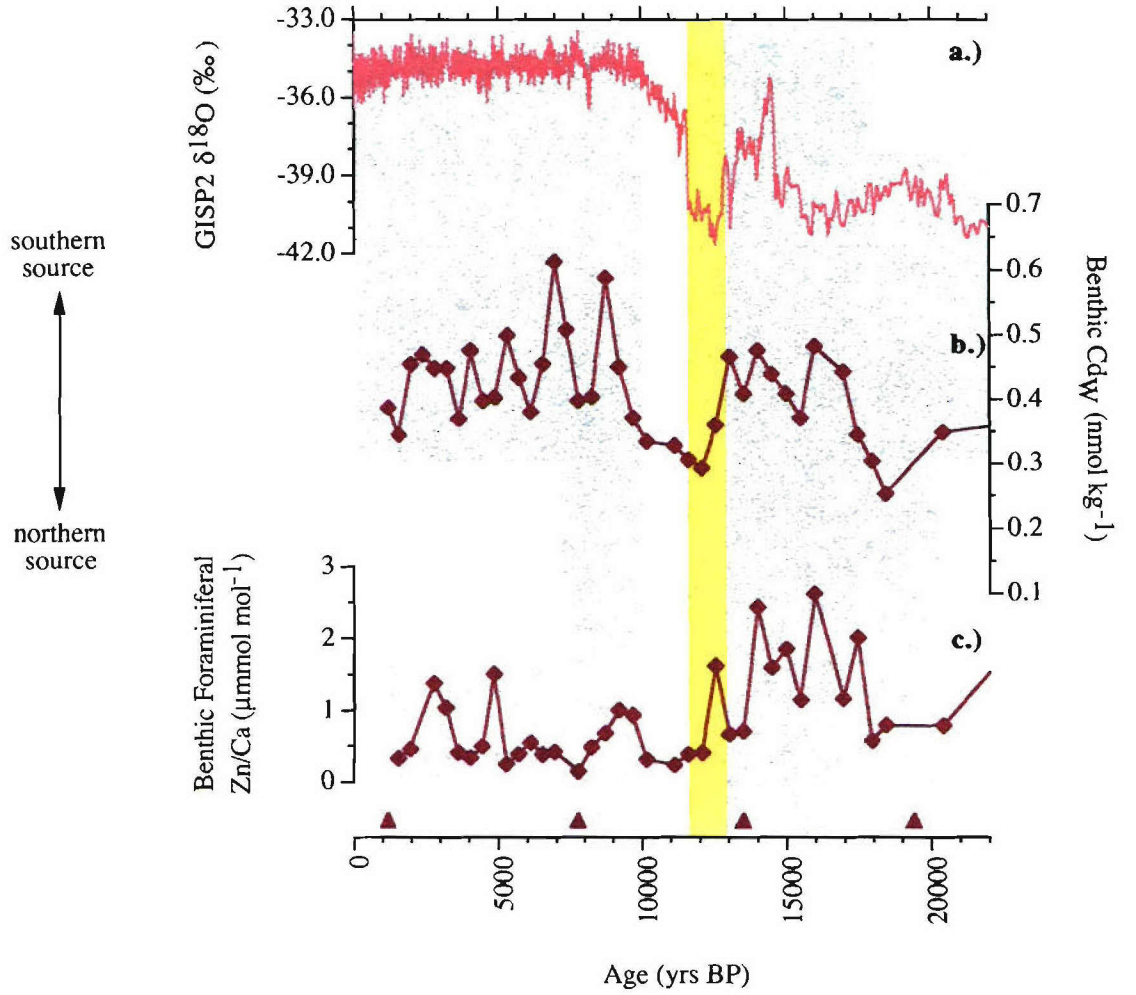

Figure 2. Benthic Cd_w and Zn/Ca data from KNR166-2-31JPC (24°13'N, 83°18'W, 751 m) *vs.* calendar age. **a.)** GISP2 $\delta^{18}O$ (pink) [*Grootes et al.*, 1993]; **b.)** average Cd_w from 31JPC; **c.)** average Zn/Ca from 31JPC. Triangles are AMS dates converted to calendar age. Yellow shading marks the Younger Dryas interval.

References

Boyle, E. A., and L. D. Keigwin (1985/6), Comparison of Atlantic and Pacific paleochemical records for the last 215,000 years: changes in deep ocean circulation and chemical inventories, *Earth Planet. Sci. Lett.*, *76*, 135-150.

Boyle, E. A., and Y. Rosenthal (1996), Chemical hydrography of the South Atlantic during the Last Glacial Maximum: Cd and $\delta^{13}C$, in *The South Atlantic: Present and Past Circulation*, edited by G. Wefer, pp. 423-443, Springer-Verlag, Berlin.

Grootes, P. M., M. Stuiver, J. W. C. White, S. J. Johnsen, and J. Jouzel (1993), Comparison of oxygen-isotope records from the GISP2 and GRIP Greenland ice cores, *Nature*, *366*, 552-554.

Hughen, K. A., et al. (2004), Marine04 marine radiocarbon age calibration, 0–26 cal kyr BP, *Radiocarbon*, *46*, 1059-1086.

Lynch-Stieglitz, J., unpublished data.

Marchitto, T. M., W. B. Curry, and D. W. Oppo (2000), Zinc concentrations in benthic foraminifera reflect seawater chemistry, *Paleoceanography*, *15*, 299-306.

Rosenthal, Y. (1994), Late quaternary paleochemistry of the Southern Ocean: evidence from cadmium variablity in sediments and foraminifera, Ph.D. thesis, 186 pp, Massachusetts Institute of Technology and Woods Hole Oceanographic Institution.

Rosenthal, Y., P. Lam, E. A. Boyle, and J. Thomson (1995), Authigenic cadmium enrichments in suboxic sediments: Precipitation and postdepositional mobility, *Earth Planet. Sci. Lett.*, *132*, 99-111.

Stuiver, M., and P. J. Reimer (1993), Extended ^{14}C database and revised CALIB radiocarbon calibration program, *Radiocarbon*, *35*, 215-230.

Tables

Table 1. KNR166-2-31JPC *H. elegans* Zn/Ca data.

Depth (cm)	Age (yrs BP)	[Ca] (ppm)	Mn/Ca (μmol mol^{-1})	Zn/Ca (μmol mol^{-1})	Mean Zn/Ca (μmol mol^{-1})
KNR166-2-31JPC					
4	1,566	192	0.21	0.33	0.33
8	1,980	268	0.95	0.46	0.46
16	2,808	284	0.25	1.38	1.38
20	3,221	271	0.39	1.04	1.04
24	3,635	188	0.37	0.41	0.41
28	4,049	262	0.43	0.34	0.34
32	4,463	210	0.40	0.50	0.50
36	4,876	85	0.61	2.26	1.51
36	4,876	257	0.46	0.75	
40	5,290	268	0.60	0.25	0.25
44	5,704	243	0.55	0.39	0.39
48	6,118	298	0.35	0.55	0.55
52	6,532	109	0.37	0.38	0.38
56	6,945	319	0.41	0.42	0.42
64	7,773	272	0.44	0.15	0.15
68	8,250	150	0.40	0.49	0.49
72	8,728	130	0.35	0.69	0.69
76	9,205	71	0.36	1.01	1.01
80	9,682	238	0.36	0.94	0.94
84	10,159	168	0.31	0.24	0.31
84	10,159	214	0.41	0.38	
92	11,114	217	0.27	0.12	0.24
92	11,114	81	0.36	0.36	
96	11,591	204	0.30	0.24	0.39
96	11,591	151	0.37	0.54	
100	12,068	135	0.32	0.14	0.41
100	12,068	237	0.28	0.68	
104	12,546	217	0.28	0.06	1.62
104	12,546	189	0.71	1.59	
104	12,546	130	0.43	3.21	
108	13,023	141	0.46	0.41	0.67
108	13,023	266	0.51	0.42	
108	13,023	162	0.42	1.17	
112	13,500	153	0.46	0.21	0.71
112	13,500	138	2.76	1.22	
116	13,991	181	0.61	2.44	2.44
116	13,991	187	0.40		
120	14,483	44	0.70	3.16	1.60
120	14,483	314	0.37	0.71	
120	14,483	200	0.69	0.94	
124	14,974	158	0.29	2.15	1.86

Table 1. KNR166-2-31JPC *H. elegans* Zn/Ca data.

Depth (cm)	Age (yrs BP)	[Ca] (ppm)	Mn/Ca (μmol mol^{-1})	Zn/Ca (μmol mol^{-1})	Mean Zn/Ca (μmol mol^{-1})
KNR166-2-31JPC					
124	14,974	217	0.57	2.71	
124	14,974	224	0.58	0.72	
128	15,465	309	0.23	2.21	1.15
128	15,465	252	0.25	0.49	
128	15,465	196	0.30	0.76	
132	15,957	177	0.55	2.63	2.63
140	16,940	255	0.26	1.17	1.17
144	17,431	260	0.33	2.02	2.02
148	17,923	272	0.30	0.58	0.58
152	18,414	265	0.46	0.66	0.80
152	18,414	242	0.44	0.93	
168	20,382	273	0.38	0.79	0.79
220	26,778	650	0.39	3.74	3.74
228	27,762	276	0.78	1.72	1.72
244	29,730	284	0.35	0.49	0.49
260	31,698	227	0.36	2.68	2.68
264	32,190	209	0.34	2.16	2.16
268	32,682	268	0.52	0.67	0.67

Appendix 2. Comparison of Cd_W data from OCE205-2-100GGC and OCE205-2-103GGC

Sediment cores OCE205-2-100GGC (26°04'N, 78°02'W, 1,057 m) and OCE205-2-103GGC (26°04'N, 78° 03'W; 965 m) were taken from similar locations and depths at the Little Bahama Bank, and should therefore record similar paleo-nutrient variability.

Comparison of the previously published Cd_W results from 103GGC [*Marchitto et al.*, 1998] and the newly acquired Cd_W results from 100GGC [Chapter 5] do reveal similar trends of increasing nutrients over the last 20,000 years (Figure 1). The new Cd_W results, therefore, suggest a good agreement between two analytical techniques: 103GGC data were obtained by atomic absorption spectrophotometry and 100GGC data were obtained by inductively-coupled plasma mass spectrometry.

In addition, the new Cd_W results support the conclusion of Marchitto *et al.* [1998], that nutrient contents in the North Atlantic subtropical gyre were lower during the last glacial than they are today. However, the Cd_W results for the Younger Dryas provide ambiguous information: 103GGC suggests a slight nutrient increase at the beginning of the Younger Dryas (~12.7 ka), whereas 100GGC suggests a slight nutrient increase just after the Younger Dryas (~11.6 ka). Therefore, it is difficult to draw conclusions about intermediate depth ventilation during the Younger Dryas interval. It is interesting to note, however, that both cores reveal Holocene Cd_W variability that was similar in magnitude to the Younger Dryas variability, perhaps suggesting similar intermediate depth ventilation changes during both the Younger Dryas and the Holocene.

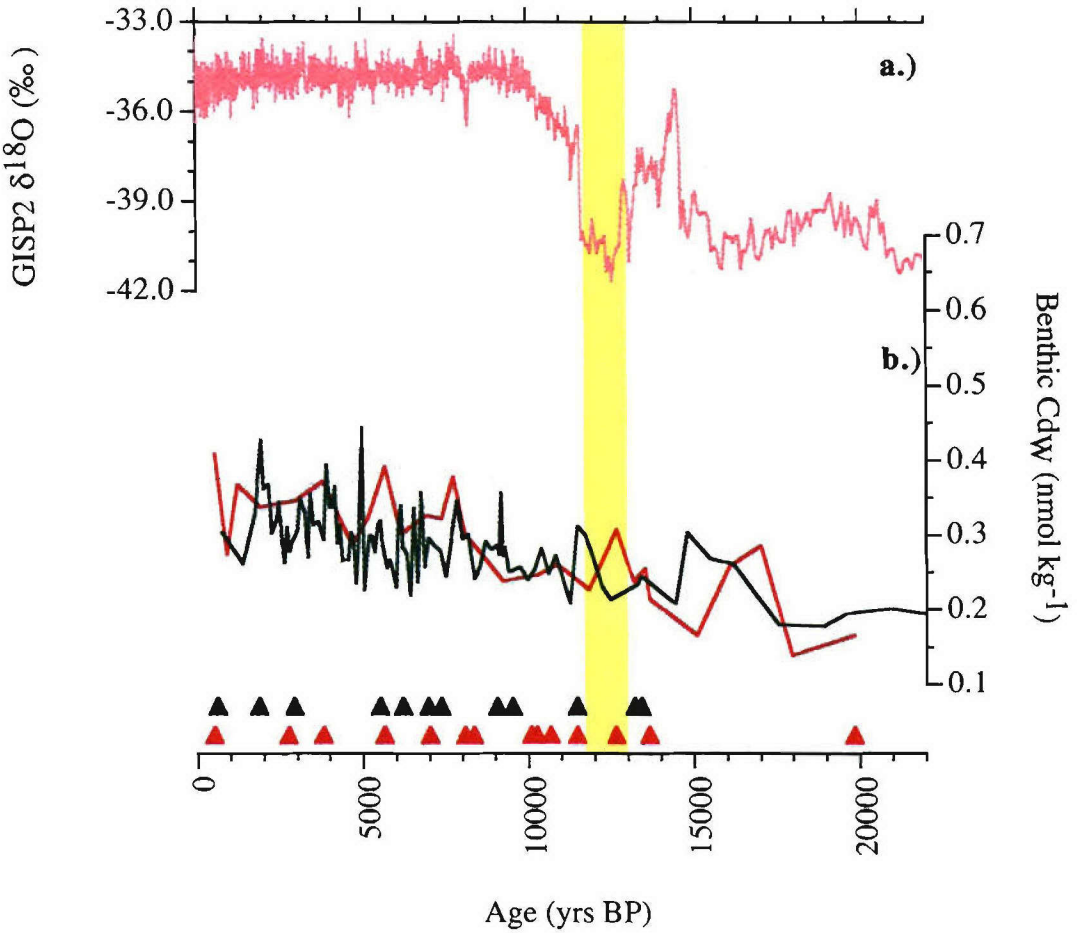

Figure 1. Benthic Cd_w data *vs.* calendar age. **a.)** GISP2 $\delta^{18}O$ (pink) [*Grootes et al.*, 1993]; **b.)** average Cd_w from OCE205-2-100GGC (26°04'N, 78°02'W, 1,057 m; green) and OCE205-2-103GGC (26°04'N, 78° 03'W; 965 m; red). Triangles are AMS dates converted to calendar age. Yellow shading marks the Younger Dryas interval.

References

Came, R. E., D. W. Oppo, and W. B. Curry (2003), Atlantic Ocean circulation during the Younger Dryas: Insights from a new Cd/Ca record from the western subtropical South Atlantic, *Paleoceanography*, *18*, 1086, doi:1010.1029/2003PA000888.

Curry, W. B., T. M. Marchitto, J. F. McManus, D. W. Oppo, and K. Laarkamp, Millennial-scale changes in ventilation of the thermocline, intermediate, and deep waters of the glacial North Atlantic, in *Mechanisms of Global Climate Change at Millennial Time Scales, Geophys. Monogr. Ser.*, vol. 112, edited by P. U. Clark, R. S. Webb, and L. D. Keigwin, pp. 59-76, AGU, Washington, D.C., 1999.

Grootes, P. M., M. Stuiver, J. W. C. White, S. J. Johnsen, and J. Jouzel (1993), Comparison of oxygen-isotope records from the GISP2 and GRIP Greenland ice cores, *Nature*, *366*, 552-554.

Hughen, K. A., et al. (2004), Marine04 marine radiocarbon age calibration, 0–26 cal kyr BP, *Radiocarbon*, *46*, 1059-1086.

Marchitto, T. M., W. B. Curry, and D. W. Oppo (1998), Millennial-scale changes in North Atlantic circulation since the last glaciation, *Nature*, *393*, 557-561.

McManus, J., unpublished data.

Stuiver, M., and P. J. Reimer (1993), Extended ^{14}C database and revised CALIB radiocarbon calibration program, *Radiocarbon*, *35*, 215-230.

Tables

Table 1. Previously published AMS dates and revised calendar ages*.

Depth (cm)	Species	NOSAMS ID	AMS Date	AMS Error	Age (yrs BP)	Reference
OC205-2-103GGC						
10	*G. sacculifer*	OS-10523	920	35	524	Marchitto *et al.* [1998]
28	*G. sacculifer*	OS-26154	2,970	50	2,748	Came *et al.* [2003]
42	*G. sacculifer*	OS-26155	3,850	35	3,808	Came *et al.* [2003]
61	*G. sacculifer*	OS-26785	5,280	45	5,639	Came *et al.* [2003]
62	*G. sacculifer*	OS-10524	5,290	45	5,648	Marchitto *et al.* [1998]
73	*G. sacculifer*	OS-26786	6,500	45	7,010	Came *et al.* [2003]
88	*G. sacculifer*	OS-15376	7,630	45	8,087	Curry *et al.* [1999]
90	*G. ruber*	OS-33629	7,890	45	8,356	McManus [unpubl.]
95.5	*G. ruber*	OS-33630	9,260	60	10,086	McManus [unpubl.]
99.5	*G. ruber*	OS-33631	9,800	60	10,667	McManus [unpubl.]
100	*G. sacculifer*	OS-26787	9,410	50	10,256	Came *et al.* [2003]
105.5	*G. ruber*	OS-33632	10,400	55	11,468	McManus [unpubl.]
113	*G. sacculifer*	OS-10526	11,000	50	12,661	Marchitto *et al.* [1998]
121	*G. sacculifer*	OS-10525	12,200	55	13,662	Marchitto *et al.* [1998]
134	*G. sacculifer*	OS-10527	17,100	100	19,841	Marchitto *et al.* [1998]

* AMS radiocarbon dates were converted to calendar age using CALIB 5.01 [*Stuiver and Reimer,* 1993], the Marine04 dataset [*Hughen et al.,* 2004], and a reservoir correction of 400 years.

50272-101

REPORT DOCUMENTATION PAGE	1. REPORT NO. MIT/WHOI 2005-18	2.	3. Recipient's Accession No.

4. Title and Subtitle
Abrupt Climate Change in the Atlantic Ocean During the Last 20,000 Years: Insights from Multi-Element Analyses of Benthic and Planktic Foraminifera and a Coupled OA-GCM

5. Report Date September 2005

6.

7. Author(s) Rosemarie Evangeline Came

8. Performing Organization Rept. No.

9. Performing Organization Name and Address
MIT/WHOI Joint Program in Oceanography/Applied Ocean Science & Engineering

10. Project/Task/Work Unit No. MIT/WHOI 2005-18

11. Contract(C) or Grant(G) No.
(C) OCE98-86748; OCE04-02565
OCE02-20776
(G) OCE96-33499; ATM05-01391

12. Sponsoring Organization Name and Address
National Science Foundation
John Lyons Fellowship
WHOI Ocean and Climate Change Institute

13. Type of Report & Period Covered Ph.D. Thesis

14.

15. Supplementary Notes
This thesis should be cited as: Rosemarie Evangeline Came, 2005. Abrupt Climate Change in the Atlantic Ocean During the Last 20,000 Years: Insights from Multi-Element Analyses of Benthic and Planktic Foraminifera and a Coupled OA-GCM. Ph.D. Thesis. MIT/WHOI, 2005-18.

16. Abstract (Limit: 200 words)

Minor and trace element records from planktic and benthic foraminifera from Atlantic sediment cores, as well as output from a coupled OA-GCM, were used to investigate the magnitude and distribution of the oceanic response to abrupt climate events of the past 20,000 years. The study addressed three major questions: 1) What is the magnitude of high-latitude sea surface temperature and salinity variability during abrupt climate events? 2) Does intermediate depth ventilation change in conjunction with high-latitude climate variability? 3) Are the paleoclimate data consistent with the response of a coupled OA-GCM to a freshwater perturbation? To address these questions, analytical methods were implemented for the simultaneous measurement of Mg/Ca, Zn/Ca, Cd/Ca, Mn/Ca and Al/Ca in foraminiferal samples using inductively-coupled plasma mass spectrometry.

Paired records of planktic foraminiferal $\delta^{18}O$ and Mg/Ca from the subpolar North Atlantic reveal trends of increasing temperatures (~3°C) and salinities over the course of the Holocene. The records provide the first evidence of open-ocean cooling (nearly 2°C) and freshening during the 8.2 kyr event, and suggest similar conditions at 9.3 ka.

Benthic foraminiferal Cd/Ca results from an intermediate depth, western South Atlantic core (1,268 m) are consistent with reduced export into the South Atlantic of North Atlantic Intermediate Water during the Younger Dryas.

Paired records of benthic foraminiferal Mg/Ca and $\delta^{18}O$ from two intermediate depth low latitude western Atlantic sites–one from the Florida Current (751 m) and one from the Little Bahama Bank (1,057 m)–provide insights into the spatial distribution of intermediate depth temperature and salinity variability during the Younger Dryas. The intermediate depth paleoceanographic temperature and salinity data are consistent with the results of a GFDL R30 freshwater forced model simulation, suggesting that freshwater forcing is a possible driver or amplifier for Bølling-Allerød to Younger Dryas climate variability.

Benthic foraminiferal Cd/Ca results from an intermediate depth Florida Current core (751 m) are consistent with a decrease in the northward penetration of southern source waters within the return flow of the Atlantic meridional overturning circulation (MOC) and an increase in the influence of intermediate depth northern source waters during the Younger Dryas.

17. Document Analysis **a. Descriptors**
geochemistry
paleoceanography
trace elements

b. Identifiers/Open-Ended Terms

c. COSATI Field/Group

18. Availability Statement
Approved for publication; distribution unlimited.

19. Security Class (This Report) UNCLASSIFIED

20. Security Class (This Page)

21. No. of Pages 152

22. Price

(See ANSI-Z39.18) *See Instructions on Reverse* OPTIONAL FORM 272 (4-77)
(Formerly NTIS-35)
Department of Commerce